Progress in Energy and Combustion Science 104 (2024) 101173

Contents lists available at ScienceDirect

Progress in Energy and Combustion Science

journal homepage: www.elsevier.com/locate/pecs

Review article

Potential of oxymethylene ethers as renewable diesel substitute

Heinz Pitsch [a,*], Dominik Goeb [a], Liming Cai [b], Werner Willems [c]

[a] Institute for Combustion Technology, RWTH Aachen University, Aachen, Germany
[b] School of Automotive Studies, Tongji University, Shanghai, China
[c] Ford Research and Innovation Center Aachen, Aachen, Germany

ARTICLE INFO

Keywords:
Oxymethylene ether
OMEx
Polyoxymethylene dimethyl ether
PODE
Dimethoxymethane
E-fuel

ABSTRACT

Oxymethylene ethers (OME_x), are a promising renewable replacement fuel for compression ignition engines. OME_x are largely compatible with current engines, can help to significantly reduce engine-out and tail-pipe emissions while simultaneously reducing the transport sector's net carbon emissions by gradually replacing fossil diesel fuel. This paper aims to compile and critically review recent research progress on OME_x, following the entire value chain from production to engine application. First, pathways for OME_x production are compiled and compared regarding energy efficiency, fuel production costs and life cycle CO_2 balance, showcasing advantages and disadvantages of more advanced production pathways with reduced hydrogen consumption. On the application side, chemical kinetics play a fundamental role in understanding OME_x combustion. Recent progress in understanding the decomposition and combustion of OME_x is discussed and resulting detailed chemical reaction mechanisms from the literature are investigated regarding their accuracy and capabilities. Furthermore, the liquid fuel properties of OME_x are presented and compared with conventional fossil diesel fuel as well as selected other renewable and surrogate fuels, pointing out possible issues and potentials for engine application. In particular, material compatibility is discussed, and suitable sealing materials are identified. Subsequently, the application of OME_x in CI engines is discussed in detail, including the fuel's potential for engine efficiency increase and significant decrease in engine-out particulate and NO_x emissions. Necessary and possible changes to engine design and control, such as longer injection duration or larger injector holes, are outlined. Finally, on a high level, the potential for large-scale application of e-fuels such as OME_x is discussed, and necessary political incentives are pointed out.

Contents

* Corresponding author.
E-mail address: h.pitsch@itv.rwth-aachen.de (H. Pitsch).

https://doi.org/10.1016/j.pecs.2024.101173
Received 22 August 2023; Received in revised form 20 June 2024; Accepted 23 June 2024
Available online 1 July 2024

1. Introduction

Worldwide, transport was responsible for around 24 % of total CO_2 emissions from fuel combustion in 2019, with road transport accounting for 74 % of those emissions [1]. Despite increasing efforts to improve fuel economy and increasingly stringent regulations, CO_2 emissions from the transport sector have grown continuously every year for the past two decades except during the economic crisis in 2009 and the COVID-19 pandemic in 2020. Growing populations and increasing mobility in developing countries combined with a trend towards larger and heavier vehicles in industrial countries counteracted the technical progress in engine efficiencies. The fuel economy improvement of light duty vehicles averaged 1.8 % per year between 2005 and 2016, but slowed down to 0.7 % already in 2017 [2], showcasing that the remaining potential for CO_2 reduction by engineering measures using established gasoline and diesel technology and fossil fuels is becoming smaller. Assuming that the worldwide mobility demand will keep increasing, the necessary reduction in CO_2 emissions from road transport to achieve the climate goals set in the Paris agreement can only be achieved by breaking the strong coupling between economic growth and transport fossil fuel consumption. This can be achieved by a significant increase in battery-electric vehicles (BEVs) or by replacing the fuel burnt in state-of-the-art internal combustion engine vehicles (ICEVs) with either biofuels or fuels synthesized using renewable energy (commonly called e-fuels), or, most likely, a combination of all three. The focus of this review is the e-fuel group of oxymethylene ethers (OME_x), which are oxygenated hydrocarbon molecules with repetitive ether functionalities that exist in different sizes. Fig. 1 visualizes the corresponding molecular structure. OME_x have major benefits as transportation fuels. While they are not carbon-free, they can be carbon-neutral if made from captured CO_2, and while their production from renewable electricity shows energetic efficiencies of only about 50 % [3–5], they are liquid with high energy densities and have combustion properties very suitable for compression-ignition engines. It will be shown below in Sections 6.1 and 6.2 that OMEx fuels can be competitive in cost and production energy efficiency to other liquid e-fuels suitable for CI engines.

Here, before discussing these molecules in more detail, we will first provide the context by discussing the major technological alternatives for future road transport, with their main advantages and disadvantages regarding emissions and greenhouse gas (GHG) reduction.

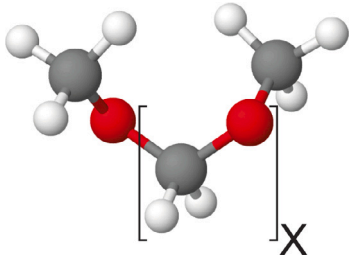

Fig. 1. OME_x molecular structure.

1.1. CO_2-neutral transport

A multitude of technologies, ranging from BEVs and fuel cell electric vehicles (FCEVs) over conventional ICEVs burning renewable gaseous or liquid fuels to hybrid vehicles of different kinds, exists to transform the transport sector towards sustainable, renewable energy utilization. However, all of them have their own advantages and challenges, and as of today, it is unlikely that there will be a single one-fits-all technological solution. Apart from the different vehicle engine concepts, also the energy supply and energy storage in the supply chain need to be considered.

BEVs have the strong advantages of a very high energy efficiency as well as zero local emissions, excluding PM emissions from tire and brake wear, and their net CO_2 driving emissions are directly coupled to the increasing share of renewable power in the electrical grid. However, battery production is both resource- and energy-intensive [6], and due to the much lower energy densities compared to common liquid fuels, batteries add significant weight to vehicles [7]. The achievable range of BEVs is therefore practically limited by economically and ecologically sensible battery sizes, and refueling requires significantly more time compared to established ICEVs [8]. This makes them unattractive for certain fields of application, as for example long-haul transport [9], although this could change with increasingly competitive battery prices [10]. Additionally, long-distance transmission of electrical energy is difficult, raising the need for significant renewable power-generation expansion in regions with high consumption such as Central Europe. However, these regions often also have high population density and relatively low solar potential, resulting in limited potential for renewable power generation. For example, for Germany in 2050, with an assumed 67 % market share of BEV in the light vehicle fleet only, the additional electricity demand for these vehicles would already correspond to 10 % of the total electricity production [11]. Almost all of this additional demand would have to be covered by renewable sources for a net climate benefit. Hybrid vehicles with a combustion engine and a smaller battery can bring together the advantages of both ICEVs and BEVs and increase the overall efficiency of operation by recuperation (among other things).

A wide range of options exist in terms of fuels for ICEVs and FCEVs. All of them have in common that energy is stored chemically, and therefore with much higher energy density compared to BEVs. Particularly liquid fuels have the advantage of an extremely high energy density, enabling long-distance transport with negligible losses, geographically decoupling the fuel production from consumption and enabling global trade. Renewable liquid fuels can thus be produced and exported by countries with beneficial conditions, i.e. large agricultural potential for biofuels or high potential for solar and wind power.

Biofuels are produced either from dedicated food crops (first generation biofuels) or from lignocellulosic or waste biomass (second generation biofuels). The resulting fuel can be burnt in common ICEVs and is often used in fuel blends with regular fossil fuel, e.g. ethanol in gasoline, or biodiesel (fatty acid methyl ester, FAME) or hydrotreated vegetable oil (HVO) in diesel fuel. An overview of biofuel application in CI engines can be found in Agarwal et al. [12]. First generation biofuels came under scrutiny due to competition with food production [13], and the potential for second generation biofuels is limited by the availability of biomass. A study by the IEA suggests that only between 4.1 % and 14.8 % of transport fuel demand can be covered by second generation biofuels in 2030 [14].

E-fuels are produced using electrolysis to break down water into oxygen and hydrogen. If renewable power is used, the resulting hydrogen is also considered as a renewable fuel. Problems arise in direct usage of hydrogen for road transport in either ICEVs or fuel cell electric vehicles (FCEVs): due to its very low boiling point and small volumetric energy content, it is difficult to transport and store. Thus, high-pressure or cryogenic systems are required, incurring significant losses. Additionally, hydrogen has extremely wide flammability limits and is hence more challenging in terms of safety. However, by activating CO_2, more easily handled renewable hydrocarbon fuels such as methane can be synthesized. If longer-chained, liquid fuels are produced, and then the advantages of liquid fuels in terms of transportation, storage, and order of energy density are retained. Additionally, they can, unlike hydrogen, be distributed using the existing fuel infrastructure and, in the best case, unlike methane, be utilized in already existing, mature ICEVs with no or small modifications. This would allow to also reduce CO_2 emissions of the existing vehicle fleet, while it would take significant time for BEVs to make up a large fraction of the vehicle fleet and achieve a corresponding CO_2-emission reduction even if they made up the majority of sales in the near future, considering the average life time of a passenger vehicle of around 16 years [15]. With wrong political incentives, a premature exchange of the current vehicle fleet towards BEV could lead to even larger total CO_2 emissions compared to a baseline scenario. Emissions arising from vehicle production and shifting of emissions from the transport sector to the power generation sector [16] need to be considered, thus making renewable liquid fuels for the existing fleet and ICEVs sold in the upcoming years an important aspect for reaching the transport sector emission targets. A combination of BEVs with liquid renewable fuel is likely also the most beneficial solution of heavy-duty transport [17]. Additionally, the synthesis of the liquid fuel from basic components enables tailor-made fuels with advantageous properties compared to fossil fuels. Fuels containing significant amounts of oxygen, for example, lead to a significant reduction of engine-out particulate emissions [18], and can thereby also contribute to cleaner air in urban areas and cheaper aftertreatment systems.

1.2. Oxymethylene ethers

The range of possible e-fuel or biofuel molecules for internal combustion engines is nearly endless, and the selection of promising candidates is a significant challenge in itself [19]. On a high level, alcohols, esters and ethers appear as the three major categories for internal combustion engines. Methanol and ethanol as alcohols are already widely used as gasoline substitute, e.g. ethanol in E10 fuel. The most common esters are Fatty Acid Methyl Esters (FAMEs), which exhibit a high cetane number, making them suitable for CI engines. FAMEs are also referred to as biodiesel. The currently least established fuel group are the ethers, of which the most commonly considered molecules are characterized by a very high oxygen content compared to FAMEs. One particular fuel group among the ethers which has received increasing attention in recent years is that of oxymethylene ethers (OME_x) with the molecular structure $CH_3\left(OCH_2\right)_x OCH_3$ and a chain length of $1 \leq x \leq 5$.

This group of fuels, as shown in Fig. 1, is also known under the names polyoxymethylene dimethyl ethers (POMDME or PODE) and oxymethylene dimethyl ethers (OMDME). In particular, OME_1 is also known under various chemical names, mainly methylal and dimethoxymethane (DMM), with DMM_n sometimes also being used for longer chain lengths. OME_x are liquid fuels that can be blended with fossil diesel fuels and used in existing diesel engines with small

modifications. OME_0 corresponds to dimethyl ether (DME), which is a gaseous fuel, while longer chain lengths ($x > 5$) are solid under standard conditions. OME_1 is also used as a chemical solvent as well as in the perfume and plastics industries [20]. OME_x share a repetition of the unit CH_2O with the engineering thermoplastic polyoxymethylene (POM), which is widely used as injection molding material.

Oxygenated fuels have been investigated for their soot reduction potential in CI engines already the in 1990s and early 2000s [21–23]. Oxymethylene ethers show very promising soot suppression, even among other oxygenates [24]. For OME_x with $x \geq 2$, the cetane number is larger than that of conventional diesel fuel, leading to improved combustion behavior [25]. OME_x can theoretically be blended with conventional diesel fuel and achieve highly super-linear soot reduction in such fuel blends [26]. This blending option enables a continuous transition towards a full replacement of fossil fuels until the point when sufficient renewable electricity is available. However, some fuel properties which differ significantly between different chain lengths and compared to conventional diesel fuel [25] lead to challenges regarding engine design and operation. Additionally, material compatibility with sealings and fuel lines is a challenge [27].

Overall, OME_x can be considered as being compatible with current CI engine technology, similar to, e.g., biodiesel or Fischer–Tropsch diesel. Compared to other possible renewable fuels such as methanol or hydrogen, which lack the high Cetane numbers necessary for CI-engines and hence require significant engine modifications, such as dual-fuel operation, the required changes for OME_x application appear relatively minor.

OME_x, more specifically OME_1, was first mentioned by Romano et al. [28] in 1986 as engine fuel in the context of gasoil extension to satisfy increased gasoil demand in the patent application covering a large group of dioxygenated methane derivates. Molton and Naegli [29] were the first to describe OME_x with a chain length of $1 < x < 10$ as component of a diesel fuel blend with reduced smoke formation, and gave several synthesis pathways in 1998. In the following years, BP from 1999 to 2001 and later BASF from 2006 to 2008 investigated and patented various OME_x synthesis routes from different feeds. Fleisch and Sills [30] described the advantages of an OME_{3-8} blend as diesel additive in terms of soot and NO_x reduction. However, this work was still in the context of a fossil gas-to-liquid production motivated by an increase in global methanol availability. Finally, with increased focus on coal-to-liquid, interest rose in China with various production patents, research papers and pilot plants from 2010 onwards [31]. In the last decade, Germany was a second driver of OME_x research, now based on renewable P2X production. There, the two research projects Kopernikus Power-to-X [32] and Namosyn [33] funded significant OME_x production and utilization research on a larger scale.

1.3. Objective and structure of this paper

This work aims to critically review research conducted on OME_x with $1 \leq x \leq 5$. This excludes DME, as it is already extensively covered in literature on its own [34,35], as well as oxymethylene ethers with other chain terminating groups. For the latter, Bartholet et al. [36] and Lucas et al. [37] highlight the impact of the different end groups on combustion and material compatibility. Substantial work on different end groups for oxymethylene ethers was done in the U.S. Department of Energy funded Co-Optima research program, tackling, for example, the water solubility and heating value issues of OME_x [38,39].

We will critically assess the potential of OME_x as diesel replacement fuel, also considering different aspects related to production and usage as a fuel. Concluding each major section, we also provide possible research directions. First, in Section 2, several production pathways for OME_x are given. This section concludes with results of life cycle assessments. Research regarding chemical reaction kinetics of OME_x is presented in Section 3. In particular, important reaction channels during auto-ignition are discussed. On the fuel side, differences in fuel properties such as viscosity, surface tension, energy content, and cetane number compared to conventional Diesel fuel are found for different OME_x chain lengths. In Section 4, these properties and the consequential opportunities and challenges, including, e.g., material compatibility and lubrication, are discussed. The resulting spray behavior under engine conditions is analyzed based on spray chamber measurements. Spray and ignition behavior are then combined in Section 5, where a large amount of experimental engine measurements and simulation data for both neat OME_x and various blends is gathered and analyzed regarding impact on engine efficiency, engine design, as well as, among others, particulate and NO_x emissions. A special focus lies on the non-linear blend behavior. The paper finishes with a discussion of production efficiency, cost and life cycle assessments, as well as a concluding outlook on the short- and long-term potential of the large-scale application of OME_x in Section 6.

2. Fuel production

In the competition between various bio- and e-fuels as well as other alternatives such as BEV, the production efficiencies as well as the associated production costs are probably deciding factors. For OME_x, various production pathways based on different reactants exist, resulting in a wide spread of predicted production efficiencies and costs. To enable a better understanding, the first part of this chapter is thus dedicated to a brief, high-level overview of the various production pathways with their corresponding process engineering advantages and disadvantages. First, the chemical processes necessary to produce the base chemicals for further OME_x synthesis are outlined in Section 2.1, focusing on production from renewable H_2 and CO_2. Second, in Sections 2.2 and 2.3, the production of OME_1, and based on that also of $OME_{x\geq2}$ is discussed. Where available, technology readiness level (TRL) assessments from literature, ranking from 1 to 9 using the TRL definitions of the European Union for the Horizon 2020 program [40], are also given. All pathways discussed here are summarized in Fig. 2.

It was shown by Peters et al. [41] that production of $OME_{x\geq2}$ directly from H_2 and CO_2 without intermediates is thermodynamically nearly impossible. For OME_1, such synthesis is possible at high pressures and low temperatures, but catalysts are necessary to suppress the strongly favored production of DME. Thus, so far, all production routes discussed in literature are based on methanol as base reactant, even though formation of methanol from H_2 and CO_2 already involves oxidizing part of the hydrogen, as discussed in Section 2.1, resulting in an overall reduction of production efficiency compared to an idealized one-step process.

As OME_1 sees widespread use as chemical solvent, some production pathways for OME_1 are well-documented and on a very high TRL. Production of longer-chain liquid OME_x, on the other hand, has only recently started to gather research attention and only some pilot plants exist outside of China, where OME_x production was pushed towards an industrial scale. An overview of known Chinese plants with the corresponding base reactants used and the plant capacities can be found in a review by Hackbarth et al. [42].

2.1. Base chemical production

All practical OME_x synthesis pathways are based on methanol (CH_3OH) as base reactant. Methanol is a versatile precursor for various chemical products and one of the most-produced chemicals world-wide with around 100 million tons in 2017 [43], resulting in a TRL of this sub-process of 9 [4]. It has also gathered attention as fuel for spark ignition engines [44]. Methanol production is usually based on syngas mainly consisting of H_2, CO, and CO_2 following

$$CO + 2H_2 \leftrightarrow CH_3OH, \quad (1)$$

$$CO_2 + 3H_2 \leftrightarrow CH_3OH + H_2O. \quad (2)$$

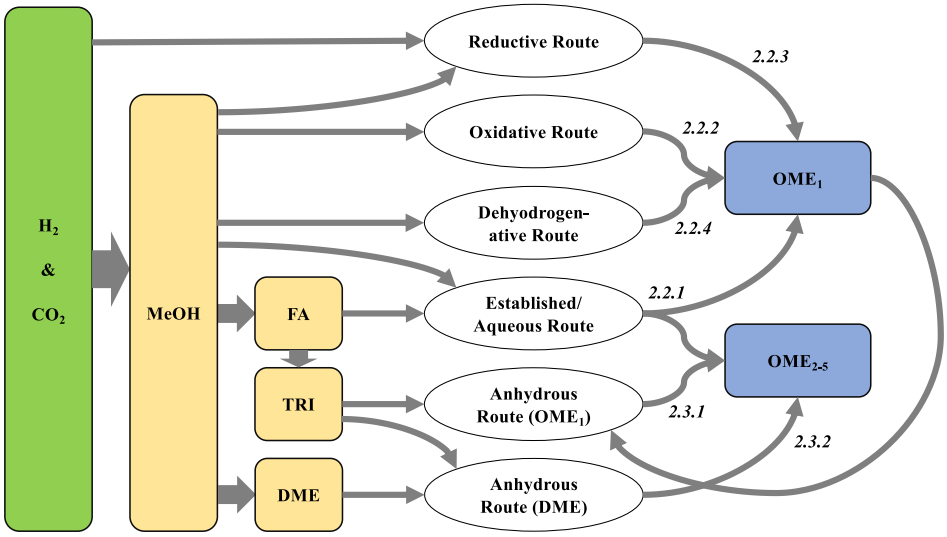

Fig. 2. OME_x production pathway overview with major reactants and products with the corresponding chapter numbers in this review paper in italic.

Conventionally, the syngas is produced from methane steam reforming or coal gasification [45]. However, production from hydrogen produced by electrolysis of water and CO_2 from direct air capture according to Eq. (2) is also possible, enabling renewable production of methanol [45]. In the context of methanol as reactant for OME_x production, especially the latter methanol production pathway - making OME_x an e-fuel - has garnered research attention in recent years, e.g., in the German research initiative Kopernikus Power-to-X [32]. On the other hand, the focus of Chinese OME_x research was mainly based on their coal gasification-based methanol industry [46]. Finally, production of syngas is also possible from biomass [47,48], so that production of OME_x from biomass follows the same subsequent production steps.

The synthesis of OME_x can follow different routes based on different intermediates produced from methanol. In general, an oxymethylene monomer source and a methyl end group capping source need to be provided. Capping sources can be methanol, DME, or OME_1 (for higher OME_x), while the monomer source is usually formaldehyde (CH_2O), which is highly unstable in monomeric form and is mostly provided either in an aqueous solution (formalin), as trioxane (TRI, $C_3H_6O_3$). or as paraformaldehyde (PFA_n, $HO(CH_2O)_nH$) [49].

Formaldehyde and subsequently trioxane and paraformaldehyde can be produced from methanol via oxy-dehydrogenation of methanol to formaldehyde on a silver catalyst (BASF process) or via the Formox process, both with a TRL of 9 and according to the global reaction

$$CH_3OH + 0.5O_2 \rightarrow CH_2O + H_2O \tag{3}$$

followed by synthesis of trioxane according to

$$3CH_2O \leftrightarrow TRI, \tag{4}$$

with a TRL of 5 [4], or to paraformaldehyde

$$CH_2O + H_2O \leftrightarrow PFA_1, \tag{5}$$

$$CH_2O + PFA_n \leftrightarrow PFA_{n+1} \tag{6}$$

with a TRL of 5 as well [4].

DME can be produced via methanol dehydration according to

$$2CH_3OH \leftrightarrow CH_3OCH_3 + H_2O, \tag{7}$$

with a TRL of 9 [4]. Advanced pathways with a direct DME synthesis from syngas and thus improved efficiency are also available [50].

2.2. OME_1 production

OME_1 is both a potential product as well as a possible reactant for further OME_x synthesis. Four promising pathways for OME_1 production are presented here in detail with their respective advantages and challenges.

2.2.1. OME_1 and OME_x production via established/aqueous route

The established production route corresponds to the route currently already used on the large scale for commercial OME_1 production. It is based on methanol and formaldehyde (likely also produced from methanol as discussed above) as base reactants, and takes place in an aqueous solution using an acidic catalyst. The same reaction system can also be used to produce longer-chain OME_x with the formaldehyde concentration in the reactant feed mainly driving the tendency to longer chain lengths. Therefore, $OME_{x\geq 2}$ synthesis via this pathway is also included here. The TRL of this pathway is assessed to be relatively high with 5 to 9 for OME_1 [4,5], and 3–4 for OME_{3-5} [4,5].

In this pathway, methanol is used as capping source and formaldehyde is provided in an aqueous solution (formalin) as monomer source. The aqueous solution contains only very low amounts of monomeric formaldehyde. Formaldehyde quickly reacts with water, forming methylene glycols (MG_x, $HO(CH_2O)_xH$, longer chains also known as paraformaldehydes) via

$$CH_2O + H_2O \leftrightarrow MG_1, \tag{8}$$

$$CH_2O + MG_x \leftrightarrow MG_{x+1}, \tag{9}$$

and with methanol, forming hemiformals (HF_x, $CH3O-(CH_2O)_xH$) via

$$CH_2O + CH_3OH \leftrightarrow HF_1, \tag{10}$$

$$CH_2O + HF_x \leftrightarrow HF_{x+1}. \tag{11}$$

The reaction equilibria for these formation reactions are far on the product side [51]. OME_x is formed from HF_x and methanol by the acetalization reaction

$$HF_x + CH_3OH \leftrightarrow OME_x + H_2O \tag{12}$$

on an acidic catalyst [52]. Sequential growth of OME_x can then also occur by insertion of monomeric formaldehyde [53] following

$$OME_x + CH_2O \leftrightarrow OME_{x+1}. \tag{13}$$

In the absence of OME_1, $OME_{x\geq 2}$ are formed mainly via reactions of hemiformals with methanol, not via sequential growth based on

monomeric formaldehyde. In the presence of OME_1, both pathways become relevant [53].

Additional side products are trioxane and methyl formate formed from monomeric formaldehyde [54]. This results in a reaction system of competing reactions with the product composition depending on reaction conditions, reactant feed composition, and catalysts. For a low concentration of formaldehyde, there is no observable formation of longer-chained OME_x, and only OME_1 is found in the product feed [52]. An increased ratio of formaldehyde to methanol increases the yield of longer chain OME_x compared to OME_1, while a higher water content reduces the overall OME_x yield because water is a product of the OME_x synthesis from HF_x, Eq. (12).

Instead of aqueous formaldehyde, paraformaldehyde can be utilized as monomer source. In this case, the first step is the dissociation of PFA as

$$PFA_n \leftrightarrow PFA_{n-1} + CH_2O. \tag{14}$$

Finally, trioxane can be utilized as monomer source instead of formaldehyde. Here, trioxane is dissociated via an acidic catalyst into formaldehyde by the reversal of the reaction in Eq. (4) first. Due to using methanol as capping group source, water is produced in this synthesis and the remaining process is similar to the aqueous route described above. Trioxane is, however, an expensive reactant compared to aqueous formaldehyde.

The practical challenge for this production route lies in the separation of the desired OME_x from water, side products, and reactants routed back into the feed. This is achieved by a reactive distillation in multiple columns. The yields are lower compared to other reaction pathways [55]. Burre et al. [56] estimate the achievable carbon yield, defined by the carbon mass in the desired product compared to the carbon mass in the initial reactants, to 90 %. On the other hand, the costly synthesis of intermediates such as trioxane and also OME_1 for products $OME_{x\geq 2}$ can be avoided [54].

For production of OME_1 from H_2 and CO_2, the overall reaction balance assuming no side product formation is given by

$$9H_2 + 3CO_2 + 0.5O_2 \leftrightarrow OME_1 + 5H_2O, \tag{15}$$

i.e., five molecules of hydrogen are oxidized to water during the production process. Considering that H_2 consumption is likely the driver of the overall production costs as well as exergetic efficiency, most development on more advanced routes tries to partially avoid these oxidative reaction pathways.

2.2.2. OME_1 production via oxidative route

In this pathway, the first step of formaldehyde synthesis from methanol on a silver catalyst in a different reactor is skipped. Instead, methanol can be partially oxidized to formaldehyde according to Eq. (16), which then directly reacts with methanol to OME_1 according to

$$CH_3OH + 0.5\ O_2 \leftrightarrow CH_2O + H_2O, \tag{16}$$

$$2CH_3OH + CH_2O \leftrightarrow OME_1 + H_2O, \tag{17}$$

requiring a catalyst with both redox sites and acidic sites of appropriate strength. A review of this method with an extensive overview of different suitable catalysts can be found in Thavornprasert et al. [57]. As in the established route, water is found in the product stream. However, as formaldehyde instantly reacts to the desired product, it is not bound to water, which thus can be separated more easily as it contains less side products. As less side products are formed, yields are also higher. Carbon yields are estimated to about 94 % [56]. Less heating of the reactor itself is required compared to the established route, but the product removal from the highly diluted gaseous product stream is energy intensive [56].

For production of OME_1 from H_2 and CO_2, the overall reaction balance assuming no side product formation is given by

$$9H_2 + 3CO_2 + 0.5O_2 \leftrightarrow OME_1 + 5H_2O, \tag{18}$$

which is identical to the established route. The oxidative route does not improve the hydrogen utilization. Its advantages and disadvantages in comparison lie in different process engineering alone.

2.2.3. OME_1 production via reductive route

To improve the utilization of hydrogen, a pathway that avoids the partial oxidation of methanol to form formaldehyde has been formulated by Thenert et al. [58]. This pathway is of particular interest when considering OME_x as an e-fuel due to the resulting improved exergetic efficiency of production and the fact that CO_2 and H_2 feedstocks are already available, if the methanol synthesis from hydrogen and CO_2 is located in the same plant. CO_2 is catalytically reduced with H_2 in the presence of methanol. Via the two intermediates methylformate and then methoxymethanol, OME_1 is formed. The resulting overall reaction is described by

$$2CH_3OH + CO_2 + 2H_2 \leftrightarrow OME_1 + 2H_2O. \tag{19}$$

Schieweck et al. [59] were able to achieve the same reaction pathway using a cobalt-based catalyst instead of the ruthenium-based catalyst proposed by Thenert et al. [58], eliminating the need for rare earth catalyst materials.

The overall carbon yield of the reductive process is estimated to be very high with about 97 % [56]. However, the most relevant downside is the large heat demand for product separation due to low methanol conversion rates in the reactor, significantly impacting the efficiency. Moreover, with H_2 and CO_2, two additional reactants are required also in the OME_1 production step.

For production of OME_1 from H_2 and CO_2, the overall reaction balance assuming no side product formation is given by

$$8H_2 + 3CO_2 \leftrightarrow OME_1 + 4H_2O, \tag{20}$$

showing the advantage of the reductive route compared to the two routes previously discussed.

2.2.4. OME_x production via methanol-dehydrogenation route

Another alternative pathway, which improves the overall hydrogen balance, is based on methanol dehydrogenation,

$$CH_3OH \leftrightarrow CH_2O + H_2. \tag{21}$$

Here, hydrogen is not directly oxidized to water, can be separated from the product stream and routed back into the methanol synthesis. The challenge in this step lies in the instability of molecular formaldehyde, which quickly reacts to various undesired side products and intermediates. Two different ways to avoid this have been discussed in the literature.

The first was described by Ouda et al. [55,60,61]. It utilizes endothermic dehydrogenation of methanol at high temperatures (above 650 °C) on a selective catalyst to produce formaldehyde and hydrogen followed by rapidly cooling down the mixture to avoid formation of side products and then by separation of hydrogen. The second step, the formation of OME_1 or $OME_{x\geq 2}$, is the same as in the established route including all side product reactions. Advantages of this method are the improved H_2 balance as well as higher product yields in the OME_x reactor, as no water is contained in the reactant feed and thus the overall water concentration is lower. The TRL of the dehydrogenation process is assessed to be 3 [5].

The second way was published by Sun et al. [62]. Here, similar to the oxidative route, a one-pot process on a single catalyst is used. On different sites, first methanol is dehydrogenated to formaldehyde following Eq. (21), which then on a different site immediately reacts with more methanol to OME_1 according to

$$2CH_3OH + CH_2O \leftrightarrow OME_1 + H_2O. \tag{22}$$

This process heavily relies on high catalyst selectivity to avoid the formation of side products, which include methyl-formates and DME.

With the currently available catalyst, the carbon yield is relatively low at about 77 % [56]. Additionally, the conversion rate of methanol is low, leading to large separation energy demand. On the other hand, the side products are valuable, and again the hydrogen extracted during the methanol dehydrogenation can be routed back to methanol production, improving the overall hydrogen utilization.

Consequently, for both alternatives, the overall reaction balance for production of OME_1 from H_2 and CO_2, including the side product H_2 from the methanol dehydrogenation given in Eq. (21) and assuming no other side product formation, is given by

$$9H_2 + 3CO_2 \leftrightarrow OME_1 + 4H_2O + H_2. \tag{23}$$

For $OME_{x\geq 2}$ production based on the Ouda process, the advantageous non-oxidative formaldehyde provision without water side product formation also leads to significant improvements on overall hydrogen utilization compared to all other pathways.

2.3. $OME_{x\geq 2}$ production

The most common production process for $OME_{x\geq 2}$ is the aqueous, established route already discussed in detail in the previous Section 2.2.1. However, also anhydrous production is possible, as described in the following subsections. Typical for all production pathways is that the end product is not a single chain length, but a mixture of chain lengths depending on the process parameters. A common composition for diesel fuel substitution called OME_{3-5} typically consists of ~40–50 % OME_3, ~25–40 % OME_4, ~10–25 % OME_5 and ~0–15 % other OME_x [3,5,63,64]. The exact composition of such a fuel mixture has impact on its fuel properties, discussed in Section 4, and consequently also on its combustion as discussed in Section 5.

2.3.1. $OME_{x\geq 2}$ production via anhydrous route from trioxane and OME_1

When OME_1 is produced in a first step and then used as end group provider, chain growth via insertion of formaldehyde from trioxane is a way to synthesize higher OME_x. The TRL of this pathway is assessed to be about 5 [4]. The main reactions are given by

$$TRI \leftrightarrow 3CH_2O, \tag{24}$$

$$OME_1 + CH_2O \leftrightarrow OME_2, \tag{25}$$

$$OME_x + CH_2O \leftrightarrow OME_{x+1}. \tag{26}$$

Trioxane dissociates into monomeric formaldehyde, e.g. on an H_SO_4 catalyst, which then in turn is inserted into existing OME_x leading to sequential chain growth[1]. As all reactions are equilibrium reactions, a mixture of reactants and OME_{2-10} constitute the reactor products [65,66]. As water is not part of the reactant stream and not formed during the process, this constitutes an anhydrous route. Burger et al. [65] investigated the process in more detail and gave a technical production process capable of producing 1 million tonnes per year in a single train plant.

A slightly different variant of this reaction pathway is the utilization of paraformaldehyde as formaldehyde source. Only reaction Eq. (24) is replaced by the dissociation of PFA, Eq. (27).

$$PFA_n \leftrightarrow PFA_{n-1} + CH_2O \tag{27}$$

The product yields for the anhydrous route are very high [46] and the product work-up through distillation much easier compared to the aqueous route, as no water is contained in the product feed. On the other hand, the reactants OME_1 and trioxane are significantly more expensive. No additional oxidation reactions appear in the synthesis steps described here, so that the overall hydrogen conversion rate depends entirely on the processes utilized to produce the reactants OME_1 and trioxane, as discussed above. A combination of either the reductive pathway or the dehydrogenation pathway with the anhydrous $OME_{x\geq 2}$ process results in slightly less hydrogen consumption overall compared to the aqueous route, but as those savings can be attributed to the OME_1 end group production, the relative effect on total hydrogen consumption is lower for $OME_{x\geq 2}$ than for OME_1.

2.3.2. $OME_{x\geq 2}$ production via anhydrous route from trioxane and DME

Using DME instead of OME_1 as a capping source and the same zeolite catalyst, trioxane is directly incorporated into DME forming OME_3[2], resulting in the overall reaction

$$DME + TRI \leftrightarrow OME_3. \tag{28}$$

Subsequently, transacetalization reactions lead to a mixture of different chain lengths,

$$OME_n + OME_m \leftrightarrow OME_{n+1} + OME_{m-1}. \tag{29}$$

The advantage of this production path is the usage of cheaper DME instead of OME_1 compared to the other anhydrous reaction pathway. However, it still relies on the costly trioxane. Major disadvantages are the necessary very long residence times and significant formation of methylformate as side product, which cannot be easily recycled [68]. The TRL of this pathway is assessed to be about 4 [4].

2.4. Future research perspectives

The development of alternative, advantageous production pathways has received a lot of research attention in the recent years, as evident in the number of publications discussed above. The results from the production cost and efficiency as well as life cycle assessments, which are all closely related to each other and presented in Sections 6.1 to 6.3, show how significant the advantages of these production pathways can become in comparison to the established pathway when it comes to competitiveness with other e-fuels. However, most studies of the corresponding reaction systems were entirely theoretical or limited to lab-scale experiments, and the corresponding technology readiness levels are thus still low, as also pointed out by many authors. If a favorable political framework is created, collaboration between academia and industry will be necessary to move towards small and mid-scale production plants to gather valuable practical information about the underlying processes. At the same time, recent research achievements have shown that there is still room for improvement regarding, e.g., catalyst choice, so continued fundamental research in that area is still desirable.

3. Combustion reaction kinetics

Combustion characteristics of OME_x depend on the details of chemical kinetics. For instance, the auto-ignition characteristics of OME_x are of particular importance for their CI engine applications. In Fig. 3, it is interesting to observe a non-linear behavior of ignition delay times of OME_x when going from small to large molecules. This is also reflected in their cetane numbers. Detailed knowledge about these auto-ignition characteristics and other combustion behaviors of OME_s are thus prerequisite to understand their engine performance and to assess their application potential as diesel substitutes. Therefore, the fundamental combustion behaviors of OME_x are evaluated and their underlying chemical kinetics are explored here, which is greatly facilitated by a series of recently published studies on OME_1 [69–75] and larger OMEs [70,76,77].

[1] An alternative mechanism, in which trioxane does not fully dissociate into formaldehyde, but just breaks open and is inserted into OME_x is unlikely, as this would lead to a selective favorisation of $OME_{4,7,10,\ldots}$, which was not experimentally observed [65].

[2] This was also confirmed by species measurements, which showed a substantial peak of OME_3 in the product stream [67].

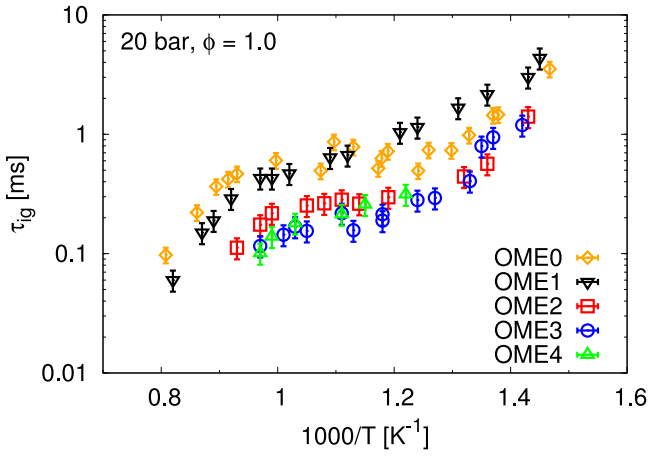

Fig. 3. Measured ignition delay times of OME_{0-4}. Ignition delay times of OME_0 were determined at 25 atm [78] and scaled to 20 bar following a linear function. Ignition delay times of OME_1 and OME_{2-4} at 20 bar were reported by Jacobs et al. [71] and Cai et al. [77], respectively.

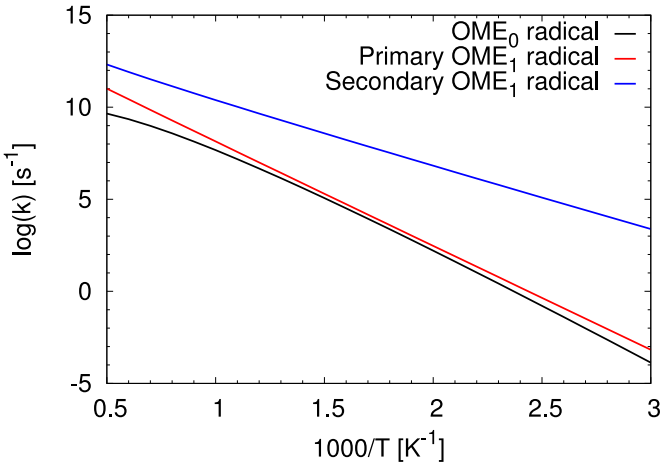

Fig. 4. High-pressure limiting rate constants of β-scission reactions of OME_0 [78] and OME_1 [83] radicals..

3.1. Kinetic modeling

3.1.1. OME_1

With the significantly increased interest in the application of OME_x, OME_1 as the smallest OME_x fuel, has received extensive research attention. Based on the analogies drawn to structurally similar fuels, a number of studies have developed chemical mechanisms for OME_1. Daly et al. [79] developed the first mechanism in 2001. It includes the detailed reaction channels of fuel decomposition, H-abstraction of the fuel, and fuel radical decomposition as well as global reactions for the sequences of $R + O_2 \rightarrow RO_2 \rightarrow QOOH \rightarrow$ decomposition products. The rate coefficients of these reactions were estimated according to analogous reactions of DME, DEE, and small normal alkanes. Based on this mechanism, Dias et al. [80] and Marrodán et al. [81,82] proposed updated reaction mechanisms of OME_1, which also only include the simplified low-temperature oxidation pathways from Daly et al. [79].

A number of studies became available recently, reporting theoretically and experimentally determined rate constants for elementary reactions taking place in the oxidation of OME_1. Vermeire et al. [69] explored the fate of the peroxy (RO_2) and peroxy hydroperoxide (O_{2QOOH}) radicals of OME_1 by calculating their potential energy surfaces (PESs) and consequently estimated the thermochemical properties of species and rate constants of reactions present on the PESs. In the same year, He et al. [70] used quantum chemistry methods as well to calculate the rate constants of the H-atom abstraction reactions of OME_1 by OH, the β-scission reactions of OME_1 radicals (R), the isomerization reactions of peroxy radicals, and the decomposition reactions of hydroperoxide radicals (QOOH) in the oxidation of OME_1. The rate coefficients of the β-scission reactions of secondary hydroperoxide radicals were recalculated later by Jacobs et al. [71] at high level of theory, motivated by their high impacts on the prediction of ignition delay times at low and intermediate temperatures. The rate constants of H-abstraction reactions of OME_1 by H and CH_3 were determined by Kopp et al. [83] based on *ab initio* calculations at the same level, in conjunction with those of the β-scission and isomerization reactions of OME_1 radicals. Fig. 4 shows the comparison of high-pressure limiting rate constants of β-scission reactions of OME_1 radicals [83] with those of OME_0 radicals calculated by Burke et al. [78]. It is apparent from Fig. 4 that the rate constants of secondary OME_1 radicals are much larger than others over the entire temperature range, indicating a rapid β-scission of secondary OME_1 radicals even at low and intermediate temperatures. This favored β-scission reaction is attributed to the significantly lower dissociation energy of the corresponding C-O bond, as discussed by Jacobs et al. [71], and has a strong impact on the ignition propensity of OME_1, which will be discussed later in more detail. The unimolecular decomposition reactions of OME_1 were studied theoretically [72,74,84] and experimentally [72–74,85]. Moreover, Golka et al. [73] carried out shock tube experiments to measure the rate constants of the H-abstraction reaction by H radical.

These investigations on elementary reactions have greatly promoted the development of the chemical mechanisms for the oxidation of OME_1 in recent years. Vermeire et al. [69], He et al. [70], Jacobs et al. [71], Shrestha et al. [86], and Li et al. [75] have constructed detailed chemical mechanisms of OME_1, respectively, by applying the concept of reaction classes and rate rules [87–89]. Recently reported rate constants were incorporated in these mechanisms, which were validated against different sets of experimental measurements covering a range of conditions.

3.1.2. *Larger* OME_x

While extensive research efforts have been dedicated to the reaction kinetics of OME_1, studies on larger OME_x are still scarce in the literature.

Sun et al. [76] measured the laminar burning velocities of OME_3 in a combustion vessel and the species profiles in a low-pressure premixed flame with synchrotron vacuum ultraviolet photoionization mass spectrometry. These datasets provide an initial insight into the high-temperature reaction kinetics of large OME_x and, in addition, serve as validation targets for a proposed chemical mechanism [76]. This mechanism was developed by incorporating only high-temperature reactions. The rate coefficients of analogous reactions of DME and DEE were employed as consistent rate rules for these three fuels, as theoretical calculations of C-H and C-O bond dissociation energies confirmed the similarity between the same bond types of OME_{1-3} [76]. In both experimental and numerical investigations, it was found that the formation of C_2 species is strongly inhibited, while the emissions of formaldehyde is increased, owing to the replacement of C–C by C-O bonds in the molecule structure.

A comprehensive kinetic mechanism for the oxidation of OME_{1-3} was derived afterwards by He et al. [70], which includes both low- and high-temperature chemistry. This model was also constructed based on the concept of reaction classes and rate rules [87–89] and its rate rules were adopted from the theoretically calculated rate constants for analogous reactions of OME_1 or structurally similar smaller molecules. The mechanism has been validated against the ignition delay times of diluted OME_3/air mixtures measured in an RCM for the temperature range of 640–865 K as well as cylinder pressure and rate of heat release

profiles of HCCI engine experiments [70]. Nevertheless, it is worth mentioning that non-reactive volume profiles were not reported for these RCM experiments. This can lead to large uncertainties in model prediction, when using results of constant-volume reactor simulations for comparison with these RCM experiments [78]. While the mechanisms of Sun et al. [76] and He et al. [70] were derived with a hierarchical structure by including the relevant reaction schemes of OME_1 and OME_2 as well, these respective submechanisms were not validated, partly due to the missing experimental data at that time. Lately, Drost et al. [90] measured ignition delay times of stoichiometric OME_2/air and OME_3/air mixtures in an RCM at pressures of 3-10 bar and temperatures of 570–690 K.

A new detailed chemical mechanism of OME_{2-4} was developed by Cai et al. [77] based on the OME_1 mechanism of Jacobs et al. [71] taking advantage of the improved kinetic knowledge on OME_1. The fuel-specific mechanism was derived by using an automatic reaction-class-based mechanism generator, which adopted the reaction classes and rate rules from the OME_1 mechanism of Jacobs et al. [71] and then applied them consistently for larger OME_x. This approach ensures the chemical consistency of the proposed reaction mechanism. In order to minimize its prediction uncertainty, the model was subjected subsequently to an automatic model optimization process by calibrating some rate rules within their uncertainty limits [91,92] against the ignition delay times of OME_{2-4} reported also by that study [77]. Fig. 5 compares the ignition delay times of OME_3 calculated by using the detailed mechanisms from Cai et al. [77] and He et al. [70]. While the differences between models are minor in the high-temperature range, the model of Cai et al. [77] predicts the ignition delay times at low and intermediate temperatures with improved accuracy. A high-temperature chemical mechanism was proposed by Kathrotia et al. [93] for the oxidation of OME_{1-5}. The model was validated successfully against the ignition delay times and laminar flame speeds of OME_1 as well as the species profiles of laminar flames of OME_1 and OME_3.

A chemical mechanism of OME_2 was also developed by De Ras et al. [94], who also investigated the pyrolysis and oxidation chemistry of OME_2 in a quartz reactor and in a rapid compression machine, respectively. The chemical mechanism was generated by using the automatic kinetic model generator Genesys [95] based on reaction families extracted from the OME_1 mechanism [69]. The model incorporates theoretically calculated parameters for species and reactions, mostly available on PESs of peroxy radicals. Nevertheless, it is notable that, for the sake of the reduction of computational costs, this mechanism excludes O_2 addition reactions to hydroperoxide radicals and their subsequent reaction pathways. This may lead to large model prediction uncertainties for the ignition delay times at lean conditions as shown in Fig. 6 and mentioned by De Ras et al. [94]. It is also found that this model [94] gives more satisfactory results at high temperatures than the model of Cai et al. [77].

Very recently, Shrestha et al. [96] proposed a new chemical mechanism for the oxidation of OME_{1-3} based on the model of He et al. [70]. The rate parameters of a number of important reactions, such as H-abstraction of fuel by HO_2, CH_2, and CH_3O, were updated by taking values from literature studies [77]. The information of all mechanisms mentioned above is summarized in Table 1. An overview of validation experiments can be found in Fenard and Vanhove [97] and Shrestha et al. [96]. Performance comparisons between various models can be found in Fig. 6 and in literature works [94,96]. Note that the mechanism of Cai et al. [77] was applied in the present work for further kinetic analysis, as it is the only one including consistent and comprehensive reaction chemistry of OME_{0-4}.

3.1.3. Reduced chemical models

In addition to the detailed chemical models for the oxidation of larger OME_x, several studies focused on the development of reduced chemical mechanisms, including those from He et al. [100], Ren et al. [101], Huang et al. [102], Lin et al. [103], Jing et al. [104],

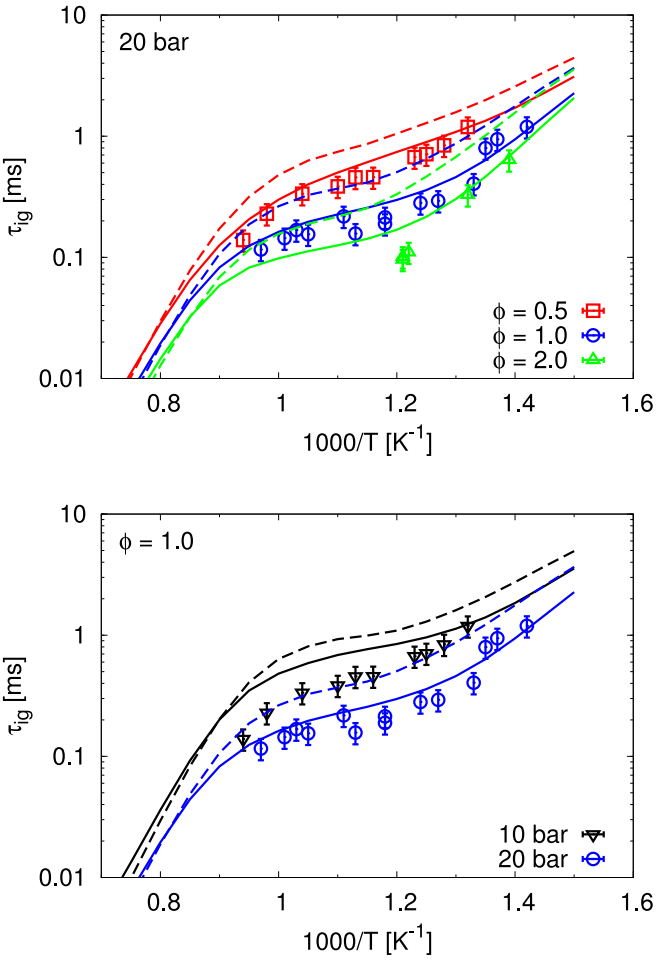

Fig. 5. Ignition delay times of OME_3. Symbols denote data from Cai et al. [77]. Solid and dashed lines show the computed results with the mechanisms from Cai et al. [77] and He et al. [70], respectively.

Niu et al. [105], and Bai et al. [106]. These reduced mechanisms were generated based on the detailed mechanisms mentioned above by using various reduction techniques, such as direct relation graph with error propagation (DRGEP) [107], isomer lumping [107], sensitivity analysis [108], and decoupling method [105]. Some of them were additionally optimized automatically for good model performance [105,106]. Due to their compact sizes, these mechanisms of larger OME_x can reduce the computational cost in CFD simulations.

3.2. Auto-ignition characteristics

Ignition delay times of neat OME_1 were determined experimentally in a rapid compression machine (RCM) [71], a flow reactor [71], and shock tubes [71,109]. A comprehensive dataset of ignition delay times of OME_{2-4} measured in a shock tube at engine-relevant conditions was reported in the recent past by Cai et al. [77] at pressures of 10 and 20 bar for equivalence ratios of 0.5, 1.0, and 2.0 covering the temperature range of 663–1112 K. That work facilitates a direct comparison of the ignition delay times of OME_{2-4} over a wide range of initial temperatures and also allows for their comparison with the data of OME_1 [71] at identical conditions, as demonstrated in Fig. 3. It is seen that the ignition delay times of larger OME_x are smaller than those of OME_1, while the temperature dependence follows a similar trend for all OME_x.

By using the optimized model of Cai et al. [77], the reaction pathways of OME_{1-4} were explored and compared consistently, which

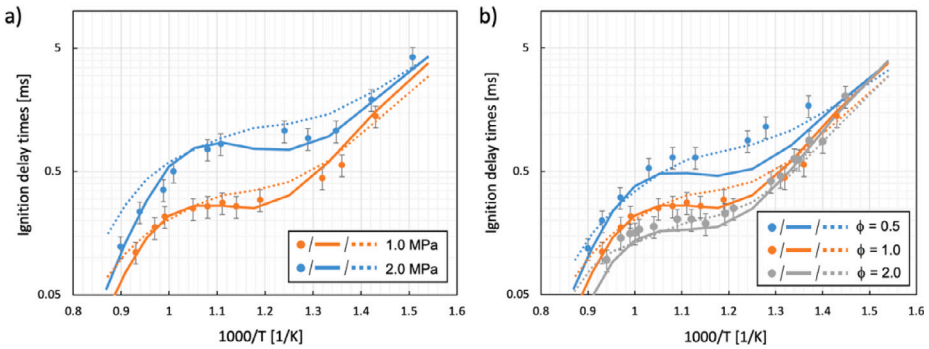

Fig. 6. Ignition delay times of OME_2. Symbols denote data from Cai et al. [77]. Solid and dotted lines show the computed results with the mechanisms from De Ras et al. [94] and Cai et al. [77], respectively.
Source: Reprint from De Ras et al. [94] with the permission from Elsevier.

Table 1
Summary of all OME_x kinetic models.

Fuel	Validation	Condition	Reference
OME_1	Species profiles of JSR	800 – 1200 K, 5.07 bar, ϕ = 0.444, 0.889, and 1.778	Daly et al. [79]
OME_1	Species profiles of premixed flame	50 mbar, ϕ = 0.24 and 1.72	Dias et al. [80]
OME_1	Species profiles of flow reactor	373 – 1073 K, 20 – 60 bar, air excess ratios = 0.7, 1.0, and 20	Marrodán et al. [81]
OME_1	Species profiles of flow reactor	573 – 1373 K, atmospheric pressure, air/fuel ratios = 0, 0.4, 0.7, 1, and 35	Marrodán et al. [82]
OME_1	Species profiles of JSR	500 – 1100 K, 1.07 bar, ϕ = 0.25, 1.0, 2.0, and ∞	Vermeire et al. [69]
	Species profiles of flow reactor	20 – 60 bar, air excess ratios = 0.7 – 20	
OME_1	Ignition delay times of shock tube, RCM, and laminar flow reactor	590 – 1215 K, 1 – 40 bar, ϕ = 1.0	Jacobs et al. [71]
	Laminar burning velocities	298, 328, and 358K, atmospheric pressure, ϕ = 0.6 – 1.85	
	Species profiles of JSR	600 – 1100 K, 1.07 bar	
	Species profiles of flow reactor	373 – 1373 K, 1 – 60 bar, air excess ratios = 0 – 35	
OME_1	Ignition delay times of RCM	600 – 1250 K, 10, 20, and 40 bar, ϕ = 1.0	Shrestha et al. [86]
	Laminar burning velocities	298 and 373 K, 1, 3, and 5 bar, ϕ = 0.6 – 1.8	
	Species profiles of JSR	4 kPa, ϕ = 2.0	
OME_1	Ignition delay times of shock tube and RCM	590 – 1450 K, 1, 4, 10, 20, and 40 atm, ϕ = 0.5, 1.0, and 2.0	Li et al. [75]
	Laminar burning velocities	298 and 373 K, 1, 3 and 5 bar, ϕ = 0.6 – 1.8	
	Species profiles of JSR	500 – 1200 K, 1.07 and 10 bar, ϕ = 0.5 and 2.0	
	Species profiles of premixed flame	40 mbar, ϕ = 2.0	
	Species profiles of flow reactor	800 – 1400 K	
OME_2	Ignition delay times of RCM	600 – 715 K, 0.5 and 1 MPa, ϕ = 0.5	De Ras et al. [94]
	Species profiles of flow reactor	373 – 1150 K, 0.34 MPa	
OME_2	Species profiles of flow reactor	850 – 1150 K, 0.15 MPa	De Ras et al. [98]
OME_{1-3}	Laminar burning velocities	408 K, atmospheric pressure, ϕ = 0.7 – 1.6	Sun et al. [76]
OME_{1-3}	Ignition delay times of RCM	640 – 865 K, 10 and 15 bar, ϕ = 0.5, 1.0, and 1.5	He et al. [70]
OME_{1-3}	Species profiles of JSR	450 – 1080 K, 1.03 atm	Zhong et al. [99]
OME_{1-3}	Ignition delay times of RCM	550 – 680 K, 10 and 15 bar, ϕ = 0.5 – 2.0	Shrestha et al. [96]
	Laminar burning velocities	393 and 443 K, 1 – 5 bar, ϕ = 0.8 – 1.6	
	Species profiles of flow reactor	700 – 1300 K, 1 atm, ϕ = 1.2	
	Species profiles of JSR	500 – 1000 K, 1 atm, ϕ = 1.2	
	Species profiles of premixed flame	33.3 mbar, ϕ = 1.0	
OME_{1-4}	Ignition delay times of shock tube	663 – 1137 K, 10 and 20 bar, ϕ = 0.5, 1.0, and 2.0	Cai et al. [77]
OME_{1-5}	Laminar burning velocities	473 K, 1, 3, and 6 bar, ϕ = 0.6 – 1.8	Kathrotia et al. [93]
	Species profiles of premixed flame	33.3 mbar, ϕ = 1.0	

provided deeper insights into the ignition kinetics of OME_x. While, as shown in [97], the various recently developed models [69,71,86] still provide different numerical results, for instance for ignition delay times and species mole fraction profiles in JSR, the major reaction pathways of OME_1 predicted by the different models are similar. As shown in Fig. 7, primary and secondary radicals are formed in the oxidation of OME_1 after the H-abstraction of fuel by small radicals, such as OH and HO_2. The consumption pathways of primary fuel radicals follow the conventional reaction channels of alkane radicals, which decompose via β-scission at high temperatures and are oxidized via oxygen addition at low temperatures. A notable difference is, however, observed in the reactions of secondary radicals. As mentioned earlier, the β-scission of secondary radicals is very favorable. Over the entire temperature range, rather than being subject to oxygen addition and subsequent low-temperature reactions at low and intermediate temperatures, as in the case of secondary alkane radicals, the mechanism of the secondary OME_1 radical is governed by its decomposition, leading to methyl radical and methyl formate. This reaction channel inhibits the chain-branching pathway of the secondary radical almost completely. As a consequence, the ignition propensity of OME_1 at low and intermediate temperatures is substantially reduced compared with OME_0, which is seen in Fig. 3 and, in addition, expressed in its small cetane number.

It is seen in Fig. 7 that, for larger OME_x, the β-scission reaction is the dominant consumption path for the secondary fuel radicals with the radical site β to the primary carbon over the entire temperature range with more than 90%, while the primary and other secondary fuel radicals are mainly oxidized by undergoing the conventional chain-branching pathways at low and intermediate temperatures. This is consistent with the findings for OME_1. As mentioned earlier, this decomposition reaction decelerates auto-ignition by inhibiting the chain propagation in the low- and intermediate-temperature ranges. Owing to the decreased branching ratio of β fuel radical production in the

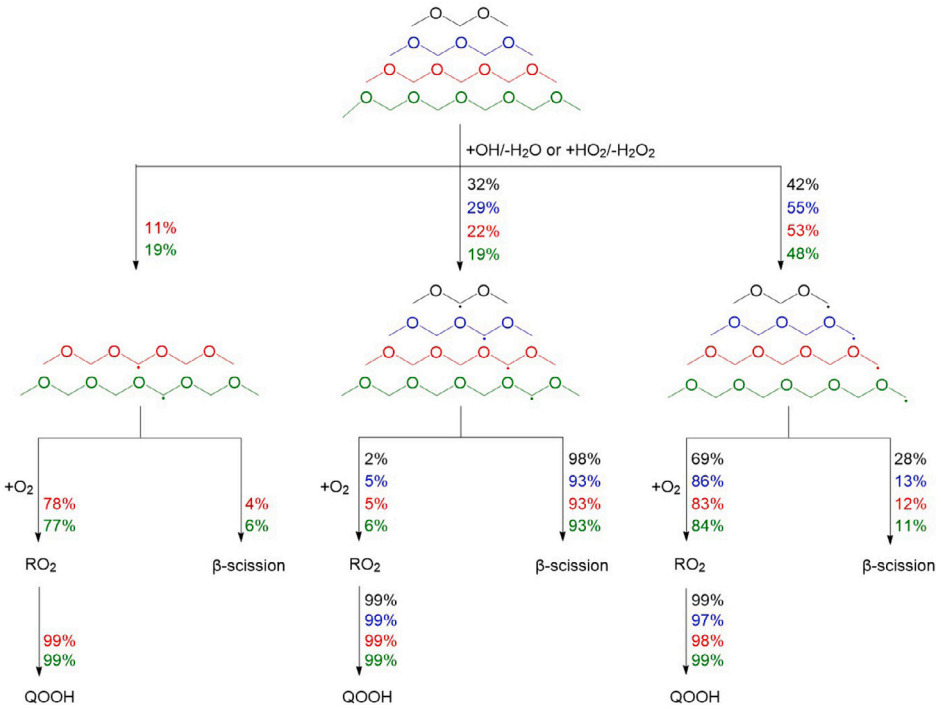

Fig. 7. Reaction channels during the auto-ignition of stoichiometric mixtures of OME_x in air at 20 bar, 825 K, and 20% fuel consumption, predicted by using the model of Cai et al. [77].

oxidation of OME_{2-4}, which decreases from 29% for OME_2 to 19% for OME_4, the ignition propensity of larger OME_x is promoted in comparison with OME_1.

In comparison to the reaction pathways of long-chain normal alkanes, such as n-heptane and n-dodecane, which are typical surrogate components of conventional petroleum fuels, the polyoxymethylene structure introduces two major features. First, the H-abstraction reactivity is strongly promoted by the decreased C-H bond dissociation energies. Second, the β-scission reactions of fuel radicals are facilitated at low temperatures as well, which is not observed for alkanes. Both impacts compensate each other in part leading to similar cetane numbers between OME_x and their alkane counterparts with identical numbers of heavy atoms.

3.3. Pyrolysis and combustion characteristics

A large number of datasets can be found in the literature for the combustion and pyrolysis of OME_1. Laminar flame speeds were measured by Shrestha et al. [86] and Eckart et al. [110]. Speciation experiments were conducted in various laboratory configurations, including premixed flames [80,110,111], diffusion flames [112], jet stirred reactors (JSRs) [79,113,114], and flow reactors [62,71,82]. Detailed information on these measurements was summarized in a recently published mini-review by Fenard and Vanhove [97] and are thus not repeated here. The latest studies include those by Li et al. [115], Nativel et al. [116], and Ngugi et al. [117], who investigated the impact of blending with OME_1.

Eckart et al. [110] applied a heat flux burner to measure the laminar burning velocities and exhaust gas compositions of OME_1 and OME_2 at atmospheric pressure and initial temperatures of 383–401 K for equivalence ratios of 0.6–1.9. As demonstrated by vom Lehn et al. [118], OME_x have faster laminar burning velocities than typical petroleum-derived fuels, such as *n*-heptane and iso-octane. This can be attributed to the large amount of reactive formaldehyde produced via the β-scission of primary fuel radicals [76].

Efforts have been also dedicated to investigating the oxidation of OME_3 in a jet stirred reactor [119], in flow reactors [120], in low-pressure flames [121], and in cool flames [122]. Qiu et al. [119] obtained the concentration profiles of fuel, oxygen, products, and some stable intermediate species of OME_3 oxidation from JSR experiments at atmospheric pressure. Reasonable agreements were observed between the experimental data and the numerical results with the chemical mechanisms from He et al. [70] and Cai et al. [77]. However, notable differences were found in the reaction pathways predicted by the two models in terms of the branching ratios of β-scission reactions of fuel radicals. Very recently, a systematic study was carried out by Gaiser et al. [120] to measure the speciation data of OME_{0-5} oxidation in laminar flow reactors with mass spectrometry and photoelectron photoion coincidence spectroscopy. It was found that methyl formate is the oxygenate intermediate with the highest fraction formed in the oxidation of OME_{1-5}. Speciation measurements were performed by Gaiser et al. [121] for premixed low-pressure flames of rich OME_{0-3}/air mixtures. The results demonstrated the enhanced reactivity for larger OME_x. Soot precursors were not detected in experiments, which indicates good application potential of OMEs in engines in terms of soot reduction. Experiments were performed by De Ras et al. [122] for stabilized, ozone-seeded OME_2/DME/O_2 premixed cool flames in a heated stagnation plate burner at lean conditions. The quantified reaction products were methoxymethyl formate, methyl formate, methanol, formaldehyde, CO, and CO_2.

Due to its importance, the pyrolysis chemistry of OME_x was investigated in the literature as well. Pyrolysis experiments of OME_2 were performed in a quartz reactor over a broad temperature range to gain insights into the primary and secondary pyrolysis chemistry [94,98]. Major products and intermediate species were identified and it was found that the elimination of formaldehyde is the dominant reaction for the decomposition of OME_2. In addition, both studies highlight the importance of the radical chemistry in the pyrolysis of OME_2 at high temperatures, which is driven by the decomposition of carbenes. The highly unstable methoxycarbene is formed via the unimolecular decomposition of OME_2 and decomposes quickly to form methyl and formyl radicals. As reported in [98], while carbenes cannot be detected during the experiments, the byproduct of the carbene formation, methoxymethanol, was measured in significant concentrations. It was also observed that, with the increased initial reactor temperatures,

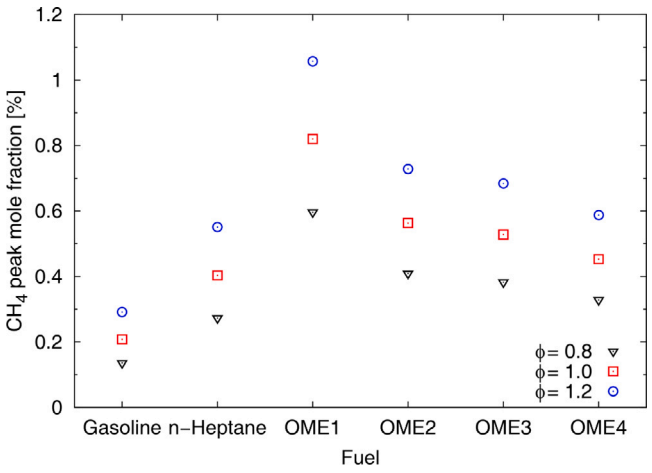

Fig. 8. Peak mole fractions of CH_4 during the auto-ignition of OME_{1-4} and gasoline at 20 bar and 825 K..

more radicals are generated via the decomposition of carbenes, and their chemistry becomes of increasing importance. Thus, the formation of radicals via carbenes is identified as a characteristic feature in the pyrolysis of OME_x [94,98]. The pyrolysis of OME_{1-3} was studied by Zhong et al. [99] in a jet-stirred reactor with gas chromatography/mass spectrometry methods. Again, formaldehyde was detected as major intermediate species along with methyl formate. With the increased chain length, the fuel reactivity increases significantly, which is evidenced by the decreased initial pyrolysis temperature. It was also found that the fuel-specific chain initiation reactions are important in the unimolecular decomposition of OME_{1-3} by providing the initial methyl and hydrogen radicals. These reactions have a significant influence on the production and consumption of methyl formate.

3.4. Unburnt hydrocarbon formation

The unburnt hydrocarbon formation of the oxidation of OME_x is of high research interest. As illustrated previously, the β-scission of secondary fuel radicals, which eliminates a methyl radical, is an important reaction channel in the oxidation of OME_x. Owing to this, methane is supposed to be a major chemical component in combustion emissions of OMEs, which is a very important issue for practical applications as it is difficult to reduce methane in exhaust gas aftertreatment systems. To gain a first insight into this, a numerical analysis was performed here to assess methane formation during the oxidation of OMEs. The computation was carried out for the auto-ignition of OME_{1-4} at a pressure of 20 bar and an initial temperature of 825 K for three different equivalence ratios by using the optimized model [77]. The peak mole fractions of methane formed during the oxidation are shown in Fig. 8. For comparison, the computed results for the auto-ignition of conventional petroleum fuel are depicted in Fig. 8 as well. The calculation was performed with a surrogate mixture of a characterized research grade gasoline, RON95E10 [123] and n-heptane as a single-component diesel surrogate fuel. The chemical mechanism from [123] was used in the simulations. It is seen that the formation of methane is promoted significantly in the oxidation of OME_{1-4} at the investigated conditions. With the increase in chain length and the number of oxymethylene groups, the maximum concentration of methane consequently decreases. Nevertheless, compared with gasoline, more methane is emitted from the combustion of OME_x, which deserves particular attention when applying OME_x as renewable substitutes. This aspect will be discussed in Section 5.5.

3.5. Future research perspectives

The recently published research has greatly deepened our understanding on the reaction kinetics of OME_1. The theoretical calculations reported thermochemical properties for species and rate constants for important elementary reactions. Datasets were obtained in various experimental configurations covering a very wide range of initial conditions. Detailed mechanisms were proposed to describe the oxidation of OME_1 and were validated successfully. Further insights were provided into the consumption pathways of OME_1. Nevertheless, there are still remaining limitations motivating further investigations. First, the H-abstraction reaction of OME_1 by the HO_2 radical has not been studied, which is, however, one of the most important reactions for the OME_1 oxidation at intermediate and high temperatures, as identified by various studies [71,75,97]. Second, remarkable differences were observed in the prediction results with different chemical reaction mechanisms [97], which are mostly attributed to the differently assigned rate constants for sensitive reactions. While several theoretical and experimental studies have reported rate constants for the same reactions, differences can be observed between their respective values, for instance for the H-abstraction reactions of fuel by the H radical [97], which points to considerable remaining uncertainties. This motivates a careful evaluation of these results, the calculation of rate constants at higher levels of theory, or the automatic model optimization and uncertainty quantification [91,92] to minimize model prediction uncertainties. Third, additional research efforts should be dedicated to understand the blending impact of OME_1. The blending behaviors of OME_1 with components, such as *n*-heptane [124], NO [125], and diesel surrogate [126], have been investigated in the past. However, as found by Zhang et al. [125], the available mechanisms failed to predict the measurements of OME_1/NO mixtures, which implied that the chemical interactions between OME_1 and NO are not well understood [125].

In comparison to OME_1, the knowledge on the combustion kinetics of higher OMEs is still very limited, despite the significantly increased interests in their application. As the larger OMEs are fuel candidates for compression-ignition engine application, the available experimental works mostly focused on their auto-ignition behaviors. Therefore, extensive efforts are required to gain more data with well-quantified uncertainties from various fundamental configurations over a wide range of conditions for the different OMEs to allow for a thorough assessment of their fundamental combustion characteristics and to provide a comprehensive database of experimental targets for model development and validation.

The available chemical mechanisms for larger OMEs were developed with a hierarchical structure based on the model of OME_1. The rate constants of elementary reactions were specified by using rate rules adopted from analogous reactions of OME_1. While the rate constants of some OME_1 reactions were well-estimated and studies confirmed the similarity between the corresponding C-H and C-O BDEs of OME_1 and larger OMEs, this approach still inevitably introduces model uncertainties. Moreover, rate parameters are often tuned for a particular large OME fuel. Figs. 9 and 10 compare the rate constants of the H-abstraction reactions of OME_2 by OH and HO_2 radicals used in different chemical mechanisms, respectively. Particularly interesting here is the fact that strong variations are observed in these rate parameters, even though some of them were determined by modifying the same original values [70,77,94] and important combustion targets are found to be very sensitive towards them [94]. As a consequence, various models yield significantly different results, for instance for ignition delay times, as demonstrated in Figs. 5 and 6. Therefore, it is desirable, on the one hand, to obtain accurate rate constants for the reactions of larger OMEs from calculations and experiments directly and, on the other hand, to explore the kinetic similarity between the analogous reactions of OME_1 and larger OMEs in depth. The advanced model optimization and uncertainty quantification methods [91] can also be applied to calibrate rate parameters and to minimize model prediction uncertainties.

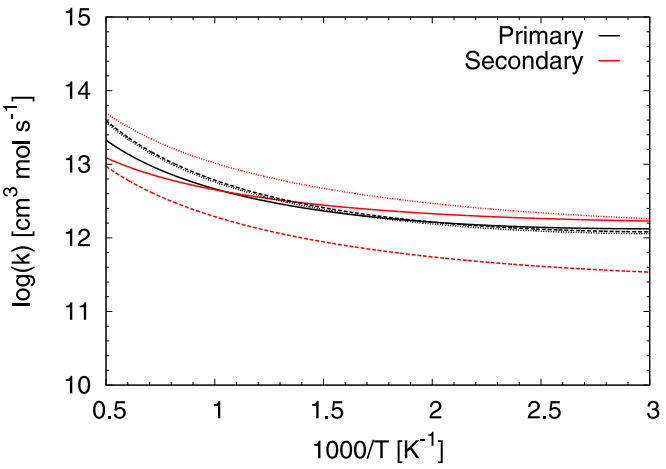

Fig. 9. Rate constants of the H-abstraction of OME_2 by OH. Solid, dashed, and denoted lines show the values used in the mechanisms from De Ras et al. [94], Cai et al. [77], and He et al. [70], respectively.

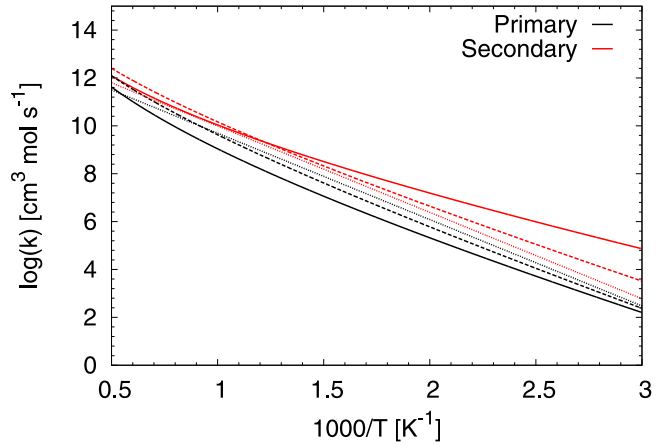

Fig. 10. Rate constants of the H-abstraction of OME_2 by HO_2. Solid, dashed, and denoted lines show the values used in the mechanisms from De Ras et al. [94], Cai et al. [77], and He et al. [70], respectively.

Furthermore, theoretical investigations are expected to reveal potential novel pathways initiated by the increased chain length, which are not considered in the present mechanisms.

Finally, for practical applications in industry, development of heavily reduced, yet still accurate kinetic reaction mechanisms both for neat OME_x as well as blends with common diesel surrogates are desirable. Fuel blends are the most likely first step in the transition phase to a fully renewable fuel. This makes seamless transition to a fully renewable drivetrain possible, which is a major advantages for e-fuels such as OME_x compared with other technologies. Reduced mechanisms for neat OME_x and relevant fuel blends can substantially support the necessary parameter optimization of engine design and control based on CFD methods.

4. Fuel properties and spray behavior

A renewable drop-in diesel fuel that meets the requirements of existing standards would be desirable to assist the defossilization of in-service diesel vehicles. However, depending on the chain-length, some properties of pure OME_x are outside the scope of the EN590 diesel fuel standard and present challenges for engine design and control. Some of them impact spray behavior, mixture preparation, or combustion and are important for efficiency and pollutant emissions. Others such as melting points, material compatibility and toxicity are relevant for operability, fuel handling and environment. If a drop-in fuel fulfilling existing fuel standards (i.e., EN590 in Europe for diesel fuel) would be desired for applications in future and existing vehicles, only a very limited amount of the OME_x component could be blended into diesel fuel. To increase the blending rate of OME_x into diesel fuel, the EN590 specification would have to be modified or a new standard developed, as the chemical properties of OME_x (higher cetane number than diesel ≥65, higher density and maximum boiling temperature) would violate the EN590 limits. For this reason, new standardization activities have been initiated, e.g. the German DIN standard 51699 for OME_{3-5} as a fuel for CI engines is currently under preparation [127]. In the meantime, a technical specification DIN/TS 51699 has been published as a first step. Following the suggested specifications, the largest differences to EN590 will be an increase of the minimum cetane number to 70 as well as an increase of the maximum density and a decrease of the maximum boiling temperature. This way, OME fuels could be used even in the existing fleet, if vehicles would be adapted for their use, for instance, in terms of engine control system and material compatibility.

Here, we will first discuss the most interesting properties together with their qualitative impact on engine utilization in Section 4.1. In Section 4.2, the impact of some of these properties on liquid spray behavior is investigated based on experimental measurements and simulation data. For quantitative discussions about the impact of the different fuel properties on real engine operation, the reader is referred to the subsequent Section 5.

4.1. Liquid fuel properties

In the following, data for various fuel properties of OME_x are collected, compared, and discussed. As reference, values for the range defined by EN590 [128] for conventional diesel fuel, values for DME, and typical values for HVO as renewable alternative, and for *n*-dodecane and *n*-heptane as common single-component diesel surrogates are given. Table 2 gives an overview of the fuel properties. Finally, the OME_x-specific issue of sealing and fuel system degradation as well as the miscibility with conventional diesel fuel are discussed.

4.1.1. Density

The liquid density of OME_x is generally higher than the range given by EN590 for conventional fossil diesel fuel, and increases with the chain length. This partly counteracts the lower heating value of OME_x as discussed in Section 4.1.6. Injection rate measurements performed for OME_{3-5} showed that for a given injection pressure, the fuel density is governing the total injected mass [144], with minor contributions from other fuel properties. A higher liquid density at constant injection pressure typically also leads to longer liquid spray penetration [145, 146].

4.1.2. Viscosity

The liquid viscosity of OME_x increases strongly with the chain length. Only OME_5 has a viscosity that lies within the EN590 range, while OME_1 is an order of magnitude lower. Low fuel viscosity can lead to issues in the fuel system, e.g. due to seal leakage, but even the low viscosity of OME_1 seems to be high enough to avoid these issues [147], while uncontrolled fuel leakage was encountered with DME, which has an even lower viscosity [148]. Fuel viscosity also plays a significant role in fuel spray breakup, with a higher viscosity slowing down spray breakup by suppressing surface instabilities and increasing the resulting Sauter mean diameter (SMD) of spray droplets [146,149]. Finally, fuel viscosity is closely related to the fuel's lubricating properties, which are discussed in Section 4.1.4.

Table 2
Liquid fuel properties of OME_x and selected reference fuels.

	Density at 20 °C [kg/m³]	Viscosity at 25 °C [mm²/s]	Lubricity at 60 °C [µm]	Surface Tension at 25 °C [mN/m]
Diesel EN590	820.0–845.0	2.00–4.50[a]	<460	~ 26.0 [25]
n-heptane	685.8 [129]	0.57 [130]	981 [131]	19.8 [129]
n-dodecane	749.5 [130]	1.89 [129]	787 [131]	24.9 [129]
HVO	775.8 [132]	2.65[a]	727 [132]	24.8 [133]
DME	661.0[b] [35]	0.23[b] [129]	900 [134]	11.2 [129]
OME_1	859.3 [130]	0.36 [25]	759 [26]	20.8 [129]
OME_2	977.5 [25]	0.64[a] [135]	545[c] [136]	27.0 [136]
OME_3	1030.5 [25]	1.08 [25]	534 [25]	28.8 [25]
OME_4	1073.7 [25]	1.72 [25]	465 [25]	30.7 [25]
OME_5	1105.7 [25]	2.63 [25]	437 [25]	32.6 [25]

	Melting Point [°C]	Boiling Point [°C]	Flash Point [°C]	Autoignition Point [°C]
Diesel EN590	−20.0–0.0[d]	~ 170.0[e]	> 55	~ 220 [25]
n-heptane	−90.6 [129]	98.4 [129]	−4 [129]	204 [129]
n-dodecane	−9.6 [129]	216.3[129]	74 [129]	203 [129]
HVO	−2.0[d][132]	~ 42.0[e] [132]	99 [137]	204 [138]
DME	−141.5 [129]	−24.8 [129]	−41.1 [129]	350 [129]
OME_1	−104.8 [129]	41.9 [129]	−32 to −18 [129,130]	237 [129]
OME_2	−69.7 [139]	105.0 [139]	12 [63]	230 [136]
OME_3	−42.5 [139]	155.9 [139]	51–54 [25,63]	235 [25]
OME_4	−9.8 [139]	201.8 [139]	84–88 [25,63]	235 [25]
OME_5	18.3 [139]	242.3 [139]	112–115 [25,63]	240 [25]

	Mol. Weight [g/mol]	Oxygen [wt%]	LHV [MJ/kg]	LHV[c] [MJ/l]	DCN [–]
Diesel EN590	~ 200 [140]	–	42.6 [25]	36.0	>51
n-heptane	100.2	0	44.6 [129]	30.6	54 [141]
n-dodecane	170.3	0	44.1 [129]	33.1	73 [141]
HVO	~ 216 [132]	0	43.9 [132]	34.1	82 (CN) [132]
DME	46.1	34.7 [134]	28.8 [129]	19.0[b]	55–68 [142,143]
OME_1	76.1	42.1 [25]	23.4 [25,63]	20.1	24–28 [25,63]
OME_2	106.1	45.2 [25]	20.6 [63]	20.5	64–68 [25,63]
OME_3	136.1	47.0 [25]	19.6 [25,63]	20.2	71–72 [25,63]
OME_4	166.1	48.1 [25]	19.0 [25,63]	20.4	82–84 [25,63]
OME_5	196.1	48.9 [25]	18.5 [25,63]	20.5	93–95 [25,63]

[a] At 40 °C.
[b] At −25 °C.
[c] At 20 °C.
[d] Cold filter plugging point (CFPP).
[e] Initial boiling point (IBP).

4.1.3. Surface tension

The surface tension of OME_x is of the same magnitude as fossil diesel fuel, about twice to thrice the surface tension of DME, and, similar to the viscosity, increases with chain length. Surface tension influences spray breakup, with higher surface tension delaying droplet breakup [149]. However, the effect of surface tension was found to be substantially smaller than that of viscosity [146], so no significant impact of the difference in surface tension between different OME_x and fossil diesel fuel is expected. Furthermore, in the Weber number, which is relevant for droplet breakup, the increased surface tension for the larger OME_x is at least partly compensated by the increased density.

4.1.4. Lubricity

In diesel engines, the fuel itself must lubricate the moving parts of the high-pressure injection system. Fossil diesel fuel contains polar compounds, which are mainly responsible for forming a protective layer on metal surfaces and preventing excessive wear. As the process of hydrotreating, commonly performed on modern diesel fuel to reduce sulfur levels, also destroys some of these compounds, lubricity additives were developed and are commonly employed to reach the necessary minimum lubricity as defined by EN590 [150]. Among the group of OME_x, only OME_5 reaches this level without additives, while with decreasing chain length, lubricity deteriorates. However, it was shown that with appropriate additives, the necessary lubricity can be achieved. Härtl et al. [24] used 6 %(m/m) of a mixture of 50 %(m/m) polyethylene glycol dimethyl ether and 50 %(m/m) SYNALOXTM40-D700 as an additive in neat OME_x to simultaneously improve lubricity and cetane number, and reported an improvement of lubricity from 759 µm to 297 µm measured on a standardized high-frequency reciprocating rig (HFFR). In a follow-up study, Härtl et al. [151] added 300 ppm di-n-decyl ether to a blend of OME_{3-6}. Pélerin et al. [152] used 300 ppm of di-n-decyl ether in OME_1 to achieve a lubricity of 543 µm.

4.1.5. Freezing temperatures, boiling temperatures, and vapor pressure

The freezing point of all OME_x except OME_5 is low enough to be used even in cold climates. Even the high freezing point of OME_5 is not an issue when it is used in a blend with other short-chain OME_x. For example, a cold filter plugging point (CFPP) of −18 °C was measured for a commercial blend of OME_{3-5} containing up to 30 weight% OME_5 [63]. The freezing point of a typical mass-produced mixture containing 42.7 weight% OME_3, 33.2 weight% OME_4 and 24.1 weight% OME_5 is −23.3 °C, and of a blend of 20 weight% OME_{3-8} in fossil diesel still −7.8 °C [153]. As comparison, DIN EN590 requires a CFFP ranging from −20 °C during winter to 0 °C during summer for conventional fossil diesel fuel [128]. These results confirm that long-chain OME_{5-8} with very high freezing points can be used in practical fuel blends up to a certain content. Issues with the miscibility of fuel blends at low temperatures are discussed in Section 4.1.10.

The boiling point and the corresponding vapor pressure are likely the most important difference between OME_1 and longer chain OME_x. While OME_{3-5} exhibit boiling points in a similar range to the initial boiling point of fossil diesel fuel, particularly OME_1 has a boiling point close to ambient temperature, similar to gasoline, and thus must be treated similarly when it comes to the fuel supply system.

4.1.6. Heating value

The heating value of all OME_x is significantly lower than that of diesel fuel by about a factor of two and decreases with increasing chain length. The simultaneous increase in density with increasing chain length counteracts this, resulting in almost constant volumetric heating value for all chain lengths. For a similar range compared to fossil diesel, the fuel tank of a vehicle to be operated with any OME_x must hold a larger volume, also increasing vehicle weight. The heating value has significant impact on engine operation, as it directly correlates with engine power, and changes to the injection system in terms of injection duration, injection pressure, or injector nozzle diameter are necessary when utilizing OME_x to achieve similar engine power as with conventional diesel fuel. The detrimental effects of the reduced heating value are discussed in detail in Sections 5.1 and 5.2.

4.1.7. Cetane number

The cetane number is a measure for the ignitability of a fuel in compression ignition engines. The lower the cetane number, the longer the ignition delay after start of injection, affecting the ratio between premixed and diffusion controlled combustion and thereby engine noise, efficiency, and emissions. A higher cetane number was found to improve engine efficiency and reduce engine-out emissions [154]. For OME_{2-5}, the derived cetane number (DCN) is above the minimum cetane number of 51 specified in EN590 for diesel fuel. In the case of OME_1, the DCN is 28 and hence significantly lower, which might lead to issues if used in unaltered diesel engines. The low DCN and its consequences on the suitability of OME_1 in a fuel blend are discussed in more detail in Goeb et al. [155].

4.1.8. Safety and toxicity

The flash point of a fuel determines the temperature above which fuel vapor ignites when exposed to an ignition source. For safety reasons, a high flash point is desirable. For example, gasoline has a flash point significantly below 0 °C, an initial boiling point below 35 °C and is classified as extremely flammable liquid and vapor (category 1 flammable liquid) under the globally harmonized system of classification and labeling of chemicals (GHS), while Diesel with a much higher flash point is classified as flammable liquid and vapor (category 3 flammable liquid). OME_{3-5} have the advantage that they retain the GHS flammability safety classification of diesel fuel due to their flash point above 23 °C, while OME_{1-2} are classified as highly flammable liquid and vapor (category 2 flammable liquid). ASTM D975 requires diesel fuel #1 to have a flash point above 38 °C, and diesel fuel #2 to have a flash point above 52 °C. The former can be met by OME_{3-5}, the latter by OME_{4-5} or blends of OME_x with high enough OME_{4-5} content. Vertin et al. [147] investigated the flammability of OME_1 and blends with diesel fuel in a fuel tank, and found that for neat OME_1 the flammability range is −32 °C to −4 °C. Above the latter temperature, the air-vapor mixture in the tank is above the rich flammability limit, below the former temperature it is below the lean limit. In cold climates, addition of an even more volatile component might be benefital for safety reasons to decrease the upper flammability limit.

OME_1 is used as solvent in various chemical products ranging from adhesives to cosmetic products and therefore has a well-documented toxicological profile. Unlike conventional diesel fuel, it is not acutely toxic and not hazardous to the aquatic environment. OME_x with longer chain lengths are not as commonly used, but it is generally assumed that these are also non-toxic [24,49,135].

For OME_1, a relatively low reactivity and corresponding long atmospheric life time of 2–4 days was found [156], so that it can be assumed that most OME_1 emissions into the atmosphere, e.g. from incomplete combustion or evaporation, will be deposited by rainout before they undergo photochemical reactions forming ozone [147].

One significant shortcoming of OME_x is their high water solubility, which is multiple orders of magnitude higher than the water solubility for diesel fuel (283–481 g/kg compared to less than 0.1 g/kg for diesel) [37]. This makes separation of spilled OME_x from water much more difficult and might thus hinder the market introduction due to environmental concerns. The water solubility also impacts storage, in particular in fuel blends, which is discussed in Section 4.1.10.

4.1.9. Material compatibility

OME_x are generally not corrosive to metals, with a copper strip corrosion grade 1, the lowest category and the same as fossil diesel fuel [27,147,157], whereas for, e.g., methanol and ethanol, steel corrosion has been reported in the past [158].

However, as OME_x are powerful solvents, they are chemically incompatible with some common elastomers used in fuel systems, e.g., in sealings. While the hydrocarbons constituting fossil diesel fuel are non-polar, the presence of oxygen in the chain of OME_x and the corresponding dipole moment make OME_x strongly polar molecules [159]. Typical polar elastomer sealings swell up and, worst case, lose function when encountering a polar fuel such as OME_x. Non-polar elastomers on the other hand are resistant to polar OME_x, but will be susceptible to non-polar conventional diesel fuel.

Subjected to neat OME_x, fluorocarbon (FKM) and nitrile rubbers (NBR) can exhibit volume increases in the range of 100 % [27], corresponding to unacceptable increases of thickness and elongation in the range of 25 % [147]. Swelling is less severe with lower OME_x content, but still significant [27,147]. Ethylene propylene diene monomer rubber (EPDM) shows significantly better behavior with neat OME_x, but in turn swells in paraffinic diesel fuel [152]. Only perfluoroelastomer (FFKM) and polytetrafluorethylen (PTFE) are suitable for operation with both OME_x as well as diesel fuel and blends of the two [152]. Fig. 11 shows the change of weight for a range of sealing materials after exposure to different OME_x as well as paraffinic diesel fuel, showcasing the issues with standard FKM and NBR sealings as well as the advantageous behavior of FFKM and PTFE. The viability of the latter materials for operation with blends of OME_x with diesel fuel was also shown in practice. Replacement of all sealings by FFKM [151] or PTFE [63] allowed for extensive engine operation without any reported sealing issues. EPDM was reportedly suitable for neat OME_x, but not for diesel fuel [151].

4.1.10. Storage and miscibility

OME_x exhibit very good storage properties. A mixture of OME_{2-6} showed no residue and no property changes after being stored for 24 weeks [27]. Also with neat OME_1 as well as blends of it with fossil diesel fuel, no peroxides and no increase in gum was found after five months at 40 °C [147].

There is large interest in using OME_x as a component in blends with either fossil diesel fuel, or synthetic renewable diesel such as Fischer–Tropsch (FT) diesel or HVO. This allows for utilizing its emission reduction potential as discussed in Section 5 and to balance its fuel properties to fulfill EN590. Fortunately, OME_x generally exhibit good solubility in diesel fuel and diesel fuel substitutes. OME_1 is soluble in fossil diesel throughout the blending range [26,147]. This is generally also true for longer-chain OME_x [24,65]. However, it was found that blends containing significant fractions of $OME_{x>2}$ have a cloud point higher than acceptable for common diesel fuel, effectively limiting the blending range for practical applications [63]. The cloud point increases for higher contents of OME_{3-5} in both fossil diesel and HVO, indicating blend component separation [63]. This is much more pronounced for HVO, where all of the prepared OME_{3-5} blends with

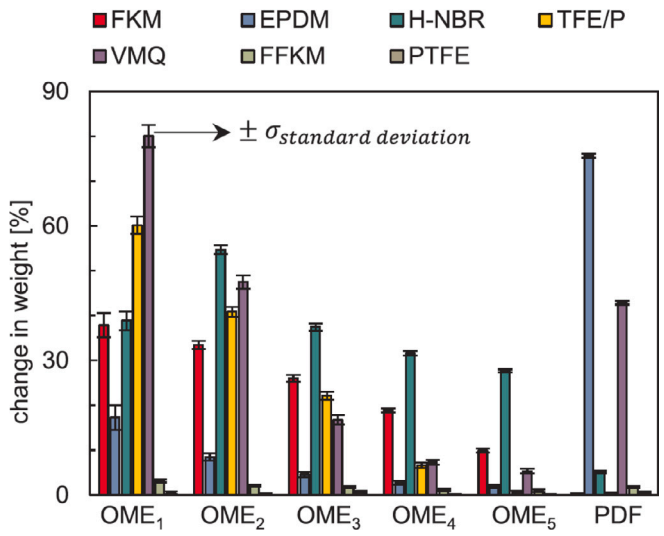

Fig. 11. Change in weight of several sealing materials after 100 h dipping in paraffinic diesel fuel (PDF) and OME_x.
Source: Reproduced from Pélerin et al. [152] with permission by Elsevier.

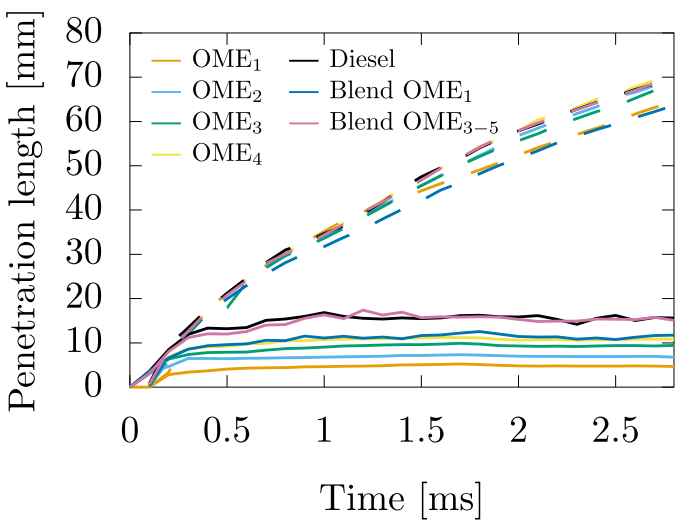

Fig. 12. Liquid (solid lines) and vapor penetration lengths (dashed lines) in spray chamber experiments. Neat OME_1 to OME_4, fossil diesel fuel and two blends of fossil diesel with 35 vol% OME_1 and 26 vol% OME_{3-5}, respectively. 3-hole piezo injector with 109 µm nozzle diameter. Injection pressure 1000 bar, fuel temperature 323 K, chamber pressure 100 bar, chamber temperature 850 K, ambient medium air [166–168].

an OME_x volume fraction of 35 vol% exhibit a cloud point above 0 °C, which makes such blends unsuitable for practical usage, even though the cloud point of the examined neat HVO was much lower than that of fossil diesel [63]. Addition of OME_2 to the OME_x mixture improved solubility and reduced the cloud point to −10 °C [63].

Theoretical calculations were able to confirm these practical findings. According to calculations of the liquid–liquid equilibrium, the miscibility of OME_x decreases with the chain length, and increases with the aromatics content of the other blend component [160,161]. Most common diesel additives improve the miscibility of OME_x in diesel fuel, with the notable exception of a pour point depressant [160].

Lastly, OME_x and HVO separate when stored for a longer time. This is rooted in small amounts of ambient water taken up by the mixture which brings an inherent incompatibility between the components into play, resulting in a split where the OME_x fraction contains almost all of the water and the HVO fraction almost none of it [162]. This means that for storing blends of OME_x and HVO, either the humidity of the gas phase must be reduced or a solubilizer must be employed [162].

4.2. Spray behavior

Due to their different liquid fuel properties, also a significantly different spray behavior of OME_x compared to fossil diesel fuel and common diesel fuel surrogates can be expected. However, while various studies on the overall engine performance and emissions of OME_x exist, which are in the focus of Section 5, detailed investigations of the liquid fuel spray are sparse.

Nozzle-internal flow simulation results suggest that OME_1 does not exhibit more cavitation inside the nozzle compared to the diesel surrogate *n*-dodecane despite the significantly different vapor pressure [163]. For $OME_{x>1}$, flash boiling is not relevant under typical engine conditions. Only at low ambient pressure, flash boiling significantly impacts the fuel spray [164]. The macroscopic liquid spray, far from the nozzle, also looks very similar to diesel fuel for high ambient pressures, with the spray cone being very slightly wider for OME_1 [163] and OME_{3-5} [31,165] compared to diesel fuel. The penetration length of the liquid fuel spray, however, is significantly lower for the low boiling point fuel OME_1 compared to the longer chained OME_4 and diesel fuel as shown by Ottenwälder et al. [166] and Goeb et al. [167]. Within their work, spray chamber measurements were performed with OME_1 to OME_4 as well as with diesel fuel and blends of OME_1 with diesel fuel and a mixture of OME_{3-5} with diesel fuel. In Fig. 12, the resulting liquid penetration lengths (LPL) and vapor penetration lengths (VPL) are shown together with other OME_x as well as the fuel blends.

The vapor penetration is mainly driven by the injection momentum, which is the same for all fuels. Thus, also the VPL of all fuels is very similar, with the exception of the OME_1-diesel blend. The increasing vapor pressure (as represented by the boiling point in Table 2) and viscosity for longer OME_x chain length lead to significant increases in LPL, more than doubling from OME_1 to OME_4. Even though the initial boiling point of fossil diesel is in the same range as the boiling point of OME_{3-4}, the final boiling point of fossil diesel is larger than 300 °C, and these higher boiling components likely contribute to the longer liquid penetration in comparison. Other spray chamber measurements performed by various groups using different injectors and operating conditions largely confirm the VPL and GPL trends discussed above [165,169,170]. Pastor et al. [169] also found that under reactive conditions, the VPL of the fuel differs more strongly, with fuels igniting earlier also penetrating deeper. The impact of the nozzle hole diameter on the droplet diameter distribution is negligible, but the VPL increases with increasing diameter [170].

The impact of the nozzle diameter on the fuel spray is generally similar with OME_x fuels compared to common diesel fuel, *n*-dodecane or HVO. With a larger diameter, liquid penetration increases due to higher momentum flux [171].

In their work, Goeb et al. [167] also performed large-eddy simulations (LES) with state-of-the-art spray breakup models, and stated that despite the significantly different properties, the proven models for diesel spray simulations can also be applied to OME_x with reasonable results even without recalibration of model parameters. Parameter studies performed as part of that work have shown that, at least in the utilized modeling framework, vapor pressure is the dominant driver for the different LPLs, while viscosity and surface tension play a minor role.

Overall, the available detailed spray investigations largely confirm the expectations based on the liquid fuel properties. For OME_{3-5}, the liquid spray behavior is very similar to that of diesel fuel when the same nozzle is utilized, likely also resulting in very similar mixing as well as wall impingement. Based on these findings, no mandatory engine geometry modifications for the utilization of OME_{3-5} or blends with diesel fuel are to be expected. This assessment, however, no longer holds when the significantly lower heating value is considered.

If the injector nozzle diameter is increased to achieve similar energy density flow, LPL as well as VPL change, so that differences in mixture formation as well as spray-wall-interaction compared to the baseline engine can be expected and additional optimization might be required. For example, with an injector nozzle with doubled volume flow for OME_{3-5}, a reduced cone angle and thus stronger wall impingement of the liquid spray onto the piston bowl was found [172]. This might contribute to the higher wall heat losses, which were found in this case. For OME_1, as expected, the liquid penetration is significantly shorter. However, for relevant blends with diesel fuel, the properties become again similar enough to neat diesel that the assessment above likely holds.

4.3. Future research perspectives

The discussion of fuel properties in Section 4.1 highlighted the main differences between OME_x and diesel fuel, such as liquid density, heating value, and cetane number.

For predictive simulations of fuel sprays, accurate temperature-dependent fuel properties are required. For OME_1, such properties are well documented in the literature. However, for $OME_{x>1}$, only data under standard conditions can be found. It would be highly desirable to have such data from measurements available for accurate fuel spray simulations. For validation of typically used mixing rules, also some measurements of fuel blends, e.g., with common diesel surrogates, would be helpful.

In recent years, lab experiments have significantly improved the understanding of the material compatibility of OME_x with common sealing materials, and suggestions for suitable materials have been made. An appropriate next step would now be to perform long term studies of the durability of the suggested sealings in engine operation in actual vehicles to rule out any undesirable effects before possibly a large number of vehicles is retro-fitted or manufactured using OME_x-compatible seals and piping.

Some studies have recently been published which investigated the spray formation with OME_x under engine-relevant conditions, but still more research will be necessary to fully understand the differences in mixture formation and flame characteristics arising from the different fuel properties of OME_x compared to fossil diesel. Finally, more research on the nozzle-internal flow behavior as well as, in the case of OME_1, flash boiling would be helpful to improve nozzle designs for OME_1-containing fuels.

5. Engine application and emissions

OME_x can be utilized as neat fuel in state-of-the-art compression ignition engines after few modifications. However, due to the possibly advantageous blending properties, blends of OME_x with other fuels, like, e.g., fossil diesel fuel, have also gathered considerable research attention. Overall, a large amount of experimental and some numerical work regarding engine operation and emissions have been published for various OME_x and OME_x blends. This section aims to condense, compare, analyze, and consolidate these data. The focus lies on the impact of the particularly interesting properties of OME_x, such as their potential for soot reduction, possibly breaking the soot-NO_x trade-off by allowing for more EGR, and thus overall significantly lowered engine-out emissions, and their chain-length dependent cetane number.

First, in Section 5.1, necessary and optional modifications for utilizing OME_x fuels compared to existing conventional diesel engine designs and control strategies are outlined. In Section 5.2, the impact of OME_x in fuel blends on the combustion process and thus on the engine efficiency is discussed. Engine-out emissions as well as aftertreatment options are then compared and analyzed in Sections 5.3 to 5.6. This work focuses on conventional CI engine combustion modes using blends of OME_x with fossil diesel or similar fuels. For a review of advanced combustion modes such as homogeneous charge compression ignition or partially premixed compression ignition, as well as for an overview of work conducted on blends including gasoline fuel, the reader is referred to the review by Liu et al. [173].

5.1. Modifications to engine control and design

OME_x has two properties which necessarily require changes to engine design and control. First, as described in Section 4.1.9, OME_x are incompatible with certain sealing and piping materials, which have to be replaced before safe long-term engine operation is possible. Second, the reduced heating value of fuels containing OME_x necessitates counter measures to achieve the same indicated mean effective pressure (IMEP), since without adaption the engine power output reduces significantly [174,175]. In addition to the necessary changes due to material compatibility and heating value, as well as the vapor pressure in case of OME_1, other optional changes are possible to reap the full benefit of OME_x fuels. Some possible changes are discussed in the following as well.

5.1.1. Injection duration and nozzle modifications

The required increase in injected mass can be achieved easiest by increasing the injection duration, up to almost double for neat OME_1 [24]. This, however, has an impact on mixing and thus emissions. The injection duration for OME_x is longer, thus the maximum nozzle flow rate is already reached at low load points. Therefore, any increase in load directly relates to a similar increase in injection duration. In contrast, for diesel fuel, the mass flow has not yet reached its steady maximum during the shorter necessary injection duration at part load, as the transient run-in phase of the nozzle is not completed. Thus, any further increase of the opening duration of the injector leads to a doubled effect of an increased injection duration as well as of a higher maximum mass flow. As a consequence, in contrast to OME, only moderate increases in injection duration are required for diesel fuel. These still increasing nozzle flow rates under increasing load in case of diesel fuel lead to improved mixing because of higher droplet velocities and faster break-up with load increase. This results in a significant increase in maximum rate of heat release for diesel fuel, and a corresponding increase of NO_x and decrease of PM and unburned hydrocarbon emissions, as discussed by Pélerin et al. [152]. Contrary to this, there is almost no change in peak heat release for OME_x, as the nozzle mass flow rate has already reached its maximum at lower loads [152]. Due to the increase in maximum temperature accompanied with a higher peak heat release, the combustion duration also reduces for diesel fuel under higher loads. For OME_x, the combustion duration is governed by the injection duration, which increases with higher loads [152]. This effect reduces and, at worst, reverses the efficiency advantage of OME_x compared to diesel fuel at high loads and indicates that higher nozzle mass flow rates are desirable for OME_x.

Alternatively, the injector nozzle mass flow rates can be changed, e.g., by increasing the nozzle diameters. While such change requires higher effort, advantages in terms of engine efficiency are expected [152,174,176–178]. This was shown, e.g., by Härtl et al. [178] in a single cylinder engine using three different nozzle diameters, a base nozzle, a nozzle with increased diameter corresponding to the same energy flow rate as with diesel fuel, and a nozzle with further increased diameter to allow for reduced rail pressure while maintaining energy density flow. With OME_1, additivized to increase the cetane number significantly, they showed lower efficiency by about 2 percentage points throughout the engine map with the unmodified nozzle, but improved efficiency by about 1 percentage point for the largest nozzle with reduced rail pressure. Soot mass remained negligible for all nozzles. When the nozzle diameter is increased, ignition delay increases slightly as well due to worse mixing, as shown in a comparison of the ECN Spray A and D nozzles [171]. This effect is however not very pronounced for OME_{3-5} and actually reverses for OME_1, where the resulting richer mixtures promote ignition [171,179]. Parravicini et al. [180] followed a different approach and used injectors with an increasing number of nozzle holes for increasing OME_{3-4} content in a blend with diesel fuel, keeping rail pressure, duration of injection, and injected energy constant. The higher number of nozzles leads to earlier interaction of

the spray cones, resulting in a limitation of the diffusion-controlled combustion phase by oxygen availability in case of diesel fuel. With OME_{3-4} blends, thus containing oxygen in the fuel, this effect was much less pronounced, and a simultaneous increase of number of holes and OME_{3-4} fraction in the fuel only resulted in an increase of the premixed combustion heat release peak, but relatively similar diffusion combustion heat release peak.

The typical disadvantages of lower rail pressure, which for diesel fuel are mainly a rise in particulate emissions and CO because of poorer mixing, are not present with neat OME_x. Thus, the rail pressures could be decreased to improve engine efficiency and reduce component cost [177]. This, however, requires adapted nozzle geometries to allow for large enough injection rates as already discussed. This improved behavior with OME_x at low rail pressure is also relevant under transient conditions, where a load step can be immediately realized by extended injection duration without the necessity to wait for rail pressure build-up, if the total injection duration does not become too long to reduce engine efficiency significantly [152].

A third option to achieve the desired injected mass, conversely, is increasing the rail pressure to increase the mass flow through the nozzle [48]. This is, however, accompanied by increased cost and decreased engine efficiency.

5.1.2. OME_1-specific changes due to vapor pressure

For OME_1 in particular, the low vapor pressure poses an additional challenge, which might prevent its use as a fuel component. For any application, OME_1 would have to be handled like gasoline fuel. The fuel tank must be sealed and requires an evaporative emission control system (EVAP) [63]. Vertin et al. [147] additionally suggest that a quick-disconnect type dispensing nozzle equipped with a vapor recovery system would be required to prevent sudden release of fugitive emissions while refueling, which would pose a flammability hazard. They reported a vapor pressure of up to 2.75 bar at 71 °C, temperatures which can be reached in almost empty fuel tanks due to the way diesel engines use fuel to cool the fuel systems. Omari et al. [26] additionally pressurized the fuel tank when operating with OME_1 to eliminate the risk of cavitation in the fuel pump, and Härtl et al. [24] pressurized the fuel back flow to 10 bar to avoid vapor bubbles. Zhu et al. [181] report vapor lock in the fuel supply pump, resulting in significant power drop, with a blend containing 50 vol% OME_1.

5.1.3. Shift of injection timing and multi-injection

The injection timing may be shifted to achieve constant combustion timing, i.e., crank angle of 50 % of fuel mass burned (MFB50 or CA50), for different OME_x and OME_x blends, counteracting the different ignition delays and combustion durations [26,152]. Without adaption of the injection timing for OME_x-containing blends, the lower heating value and corresponding longer injection duration lead to a delayed MFB50 and thereby efficiency loss [144]. This was also confirmed in a passenger vehicle study, where without changes to engine control, engine efficiency dropped with increasing OME_x content in the diesel fuel [174]. An ad-hoc engine control calibration by a closed loop system or a blend detection system might be very beneficial if largely varying fuel blends are to be burnt in the same engine.

For OME_1 without cetane enhancing additives, the very long ignition delay particularly at low loads can lead to an unusually large share of premixed combustion, leading to a very high peak in heat release rate and high mechanical stress on the engine [152,181,182]. This effect is stronger with higher EGR, which further increases ignition delay times [182]. To avoid this, a pilot injection can be used, which completely removes this effect and smoothens the heat release curve similar to OME_{3-5} [152].

Also for more enhanced multi-injection strategies, the reduced heating value of OME_x compared to diesel fuel should be taken into account. If the injected mass of the pilot injection, for example, is not appropriately increased, the effect of the pilot injection on the main ignition might be reduced due to its lower heat release [183]. On the other side, the necessity of a pilot injection itself might be questioned when the highly reactive OME_{3-5} is used as fuel, as negligible differences for the main ignition delay as well as the maximum rate of heat release were found for a range of engine loads [152].

5.1.4. Increase of EGR and simplification of aftertreatment

In state-of-the-art CI engines fueled with fossil diesel, PM and NO_x emissions are closely coupled through the EGR rate, with increased EGR reducing NO emissions and increasing PM emissions. OME_x-containing fuels produce significantly less soot, and thus the EGR rate can be significantly increased to also reduce engine-out NO_x emissions. The EGR variation impact is discussed in detail in the sections focusing on soot emissions (Section 5.3) and nitric oxide emissions (Section 5.4), but generally, the range of possible EGR rates increases significantly when OME_x is part of the fuel. For fuel blends not leading to fully soot-free combustion, the OME_x content in the blend still allows for smaller increases of EGR due to the lower sooting tendency, without changing the engine operation strategy entirely. The combined reduction of both NO_x and PM emissions allows for simplified after-treatment systems while still maintaining or exceeding current emission regulations. Regeneration intervals of a diesel particulate filter (DPF) can be increased, reducing fuel consumption [184], and a diesel oxidation catalyst (DOC) combined with a lean NO_x trap might be sufficient for NO_x reduction. Existing older vehicles can potentially achieve compliance with newer emission regulations without the installation of costly after-treatment when operated with a fuel blend containing significant fractions of OME_x and corresponding changes to the engine map are made.

5.1.5. Stoichiometric CI operating strategy

The advantageous properties of OME_x, in particular breaking the NO_x-soot tradeoff, allow for entirely different engine operation and emission aftertreatment strategies, some of which are not possible with conventional diesel fuel in common CI engines. For neat OME_x or blends with very high OME_x content, operation at stoichiometric conditions achieved by high amounts of exhaust gas recirculation (EGR) is possible, as soot emissions remain negligible, see Section 5.3. The high EGR also reduces NO_x to extremely low values as shown in Section 5.4. The aftertreatment can then be significantly simplified by employing a three-way catalyst as utilized in SI engines. Operating under such high EGR at stoichiometric conditions, however, massively increases CO and unburnt hydrocarbon emissions, mainly methane which is difficult to convert in aftertreatment, as discussed in Sections 5.5 and 5.6. This also results in a measurable drop in thermal efficiency, making fully stoichiometric operation throughout the engine map unattractive. Operation in a high EGR range, but under still lean conditions above an air fuel equivalence ratio of $\lambda = 1.1$, similar to the strategy published by Upatnieks et al. [185], prohibits the use of a three-way catalyst, but it also eliminates the increased CO, the unburnt hydrocarbon emissions, and the corresponding drops in engine efficiency, but also disables the possibility of NO_x reduction in a three-way catalyst. Limiting the engine to high EGR, lean operation also reduces maximum power output significantly. A combined operating strategy was suggested by Ogawa et al. [182]. They combined a high EGR lean operating strategy for low loads with a stoichiometric operation and a three-way catalyst at high loads to achieve very low NO_x throughout the engine operating range. For the stoichiometric operation at higher loads, further load increases necessitate a reduction of the EGR rates to maintain the air-fuel-ratio. However, due to stoichiometric operation, the three-way catalyst was able to simultaneously reduce the resulting NO_x, CO, and hydrocarbon emissions very effectively. At low to medium loads, EGR was kept at 30 % under lean λ-controlled combustion to avoid excessive emissions of partially oxidized combustion products and achieve high thermal efficiency. The catalyst was effective at converting remaining CO and hydrocarbon emissions, while NO_x emissions remained low without after-treatment due to the high EGR rate.

5.1.6. Engine geometry modifications

Besides the injection system, also the piston geometry holds potential for optimization and, especially for operation with neat OME_x, adjustments might be beneficial. The different liquid fuel properties affect fuel break-up, and so does a larger injection nozzle to accommodate for the reduced heating value compared to diesel fuel. Thus, piston bowl designs for diesel fuel might be less optimal for neat OME_x. For instance, Gaukel et al. [186] have performed an optimization of the piston bowl shape for the highly volatile OME_1 using numerical simulations and experiments. They suggest a step-shaped bowl for OME_1 due to better mixture formation at high EGR rates.

5.2. Combustion process and engine efficiency

Sections 5.1 and 5.1.5 discussed how in particular injection timings and durations as well as EGR rates are subject to changes when operating a CI engine designed for diesel fuel with a fuel containing OME_x. The resulting consequences for the combustion process as well as the impact on overall engine efficiency will be discussed in more detail in the following.

The theoretical maximum engine power output is higher with neat OME_x, as no smoke limit approaching stoichiometric operation exists [182]. In practice, operation near stoichiometric conditions without EGR, however, leads to excessive NO_x emissions

When trying to approach $\lambda < 1.1$ with significant EGR rates to limit NO_x, thermal efficiency with OME_x drops significantly due to higher fresh gas temperature because of high EGR, extended burn duration, worse process gas heat capacities, and incomplete combustion [151,177,187]. This drop, however, appears at significantly lower air-fuel-ratio compared to, e.g., HVO, thus still allowing for a much wider operating range of the engine [187].

Utilization of pure OME_x or addition of OME_x to diesel fuel under typical CI engine operation generally improves engine efficiency due to changes to the heat release rate. Fig. 13 shows a typical heat release profile of OME_x compared to diesel fuel.

The necessary longer injection duration due to the lower heating value leads to a lower rate of maximum heat release and a longer main burning phase [63,151,152,187]. However, the heat is released closer to TDC leading to a shorter burn-out phase [24,26,63,151,152,176,187,188]. As the latter effect is more important than the former, overall this results in a shorter, more isochoric total combustion phase and thus in higher efficiency. Quantitatively, engine efficiency improvements in the range of 1–5 % were reported for neat OME_x [24,63,152] or blends with high OME_x content above 35 vol% [26,180,181]. Without modified injector geometry, this efficiency benefit is smaller or vanishes entirely for high loads and high OME_x content due to the long necessary injection durations, i.e., the maximum rate of heat release is limited by the maximum nozzle flow rate resulting in a longer combustion duration than desired [26,63,151,152,177]. With an injector diameter optimized for OME_x instead of for diesel fuel, the efficiency advantage possibly widens to up to 6 % [189]. Increasing the injection pressure can also help to counteract the lower energy density of neat OME_x, improving the efficiency [48]. Comparing different OME_x chain lengths, the efficiency benefit decreases slightly with increasing chain length [63,187,190] due to a slightly longer combustion duration and lower peak heat release. As the volumetric heating value is roughly the same between the fuels and the cetane number increases with the chain length, which should theoretically improve engine efficiency, one possible explanation for this could be the higher volatility of smaller OME_x chain lengths [187]. This could lead to better mixing in the diffusion-controlled combustion phase, resulting in higher rate of heat release.

When blending OME_{3-5} into diesel fuel without optimizing the injector nozzle diameter, thermal efficiency first drops with increasing OME_{3-5} content, but then increases again towards neat OME_{3-5} [144,191]. At high OME_{3-5} contents, the advantageous cetane number and fast burn-out over-compensate for the long necessary injection duration [144,191].

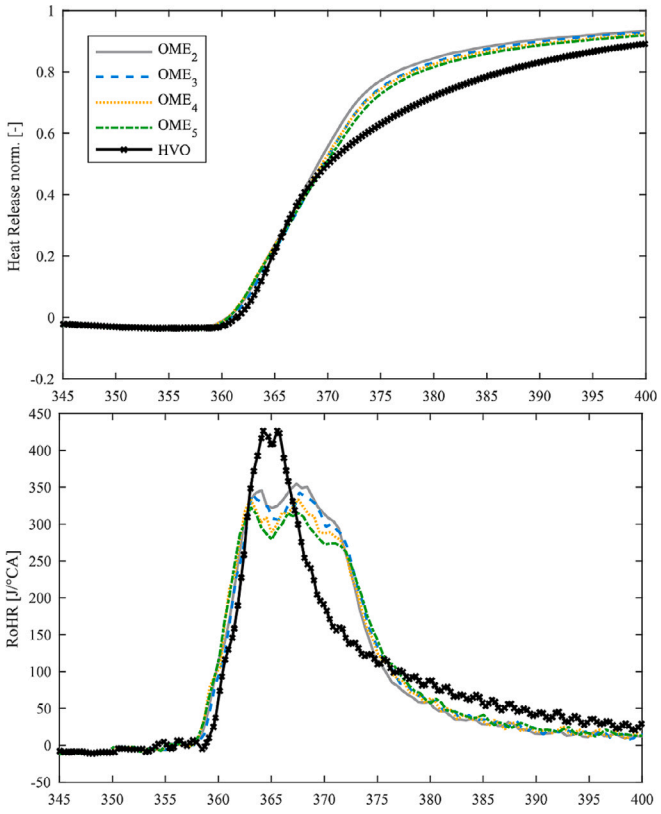

Fig. 13. Normalized heat release (top) and rate of heat release (bottom) at IMEP = 13 bar, 1200 rpm, no EGR, AFR = 1.8 in a single cylinder optical engine.
Source: Reproduced from Dworschak et al. [187] with permission by SAE.

The reason for the overall shorter combustion duration and thus higher thermal efficiency with OME_x despite the possibly much longer injection durations lie in the significantly faster diffusion-controlled second combustion phase roughly between MFB50 to MFB90, resulting in less remaining fuel to be inefficiently burned in the late burning phase. The molecular oxygen content and thus the reduced demand for air entrainment and mixing is commonly seen as main contributor to this effect [152,187,189]. This can be corroborated by OH* chemiluminescence images and engine simulations, which show a larger combustion zone with OME_x [183,192]. Fig. 14 shows OH* chemiluminescence during engine operation, comparing OME_x with diesel fuel. Around peak heat release at about 9 CAD aTDC, there are significantly smaller dark blue areas, corresponding to regions without combustion, for OME_x. Please note that the absence of OH* chemiluminescence in the piston bowl in case of diesel fuel at this time is likely due to shielding of the radiation by soot [183,192].

Additional contributors could be the higher volatility, resulting in faster evaporation, and the lower soot formation, resulting in less soot oxidation in the late combustion phase [187]. The assumption that the diffusion combustion process with OME_x is faster because it happens closer to the nozzle due to the intramolecular oxygen [189] can however be disproved by spray chamber experiments under engine-relevant conditions. In these experiments, the flame lift-off length (FLOL) with OME_x was consistently similarly long or longer than with *n*-dodecane, a diesel surrogate which has a similarly high cetane number, but no fuel oxygen [166,167,169,193].

The FLOL increases with increasing OME_x fraction. This effect is stronger at lower ambient temperatures. Here, the lower LHV of OME_x and the resulting lower flame temperatures, which lead to a longer

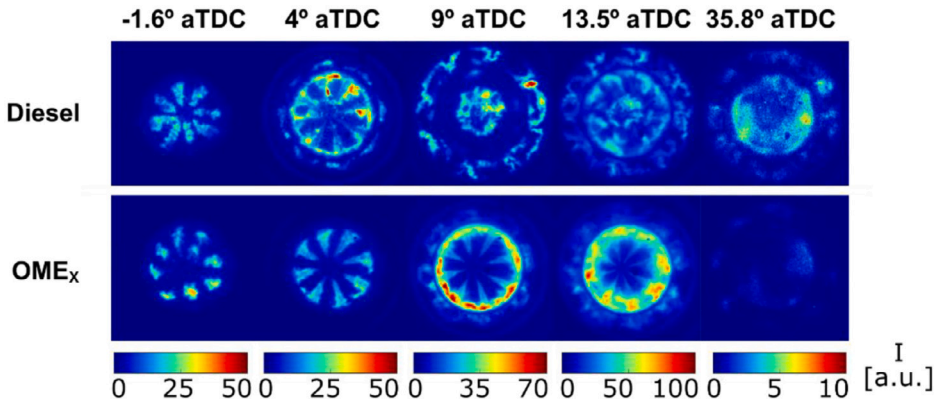

Fig. 14. OH* chemiluminescence images at different CAD comparing diesel fuel with an OME_x blend at 7.5 bar IMEP in a single cylinder optical engine.
Source: Reproduced from García-Oliver et al. [192] with permission by SAGE, original data by Pastor et al. [183].

FLOL, dominate over the improved ignitability of OME_x at these temperatures, which on its own would lead to a smaller FLOL [193]. This is supported by the increased fuel composition effect on ignition delay at higher ambient temperatures, i.e., at higher temperatures, the higher cetane number of OME_x is better able to compensate for the smaller heating value [193].

All investigated fuels stabilize downstream of the nozzle under rich local conditions, except OME_1, where the extremely long ignition delay leads to an FLOL at roughly stoichiometric conditions [169]. A side effect of the longer FLOL and thus a longer distance between liquid fuel spray and flame is expected to be an improved mixing and thus lower sooting tendency [166]. It was also found that the maximum stationary flame length is lower with OME_x, which is explained based on the much lower stoichiometric air-fuel-ratio [169].

5.3. Particulate matter emissions

As all oxygenated fuels, OME_x show significantly reduced particulate matter (PM) emissions. In a screening of a large range of oxygenated fuels blended with diesel fuel such that all blends had the same oxygen content, Härtl et al. [24] found that OME_1 led to the highest soot reduction. The work of Cheng et al. [194] on an older engine, however, came to the opposite conclusion, with OME_1 blends exhibiting slightly higher soot emissions than other oxygenates with similar oxygen content by mass. As the discrepancies are relatively small, this might be a difference in operating and/or injection conditions, which will have a large impact on the volatile low-cetane OME_1. Under controlled, engine-relevant conditions in a spray chamber, both OME_1 and a mixture of OME_{3-5} showed no measurable soot luminosity [169], indicating a very good potential of OME_x for soot reduction. The following subsection summarizes and reviews various soot measurements in engines, while reasons for the superlinear soot reduction are analyzed and discussed in more detail in Section 5.3.2.

5.3.1. Engine measurements

For all neat OME_x, PM emissions are close to the detection limit under normal engine operation conditions, even for extremely high EGR rates [63,151,152,174,182,195]. While a reduction of soot formation from fuel combustion to almost zero can be expected, engine-out or tailpipe PM emissions do not reduce to zero, as other sources of PM such as combustion of engine oil remain. This almost full PM emission reduction also holds for blends with diesel fuel down to 80 vol% OME_1 [26]. Lower OME_x content leads to increasing PM emissions with decreasing OME_x content and with increasing EGR rate, so that the common soot-NO_x tradeoff is weakened, but not entirely broken. Fig. 15 shows this exemplary for different OME_1-diesel blends in two different load points [26].

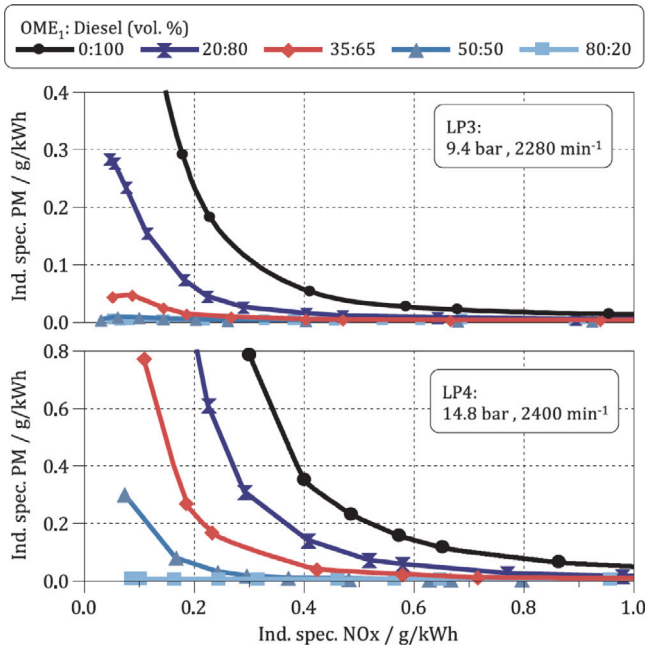

Fig. 15. Particulate matter emissions at higher loads for OME_1-diesel blends, varying EGR to achieve different NO_x levels in a single cylinder research engine.
Source: Reproduced from Omari et al. [26] with permission by Elsevier.

Some published data from engine measurements of fuel blends are collected in Fig. 16, showing the reduction of PM emissions compared to a fossil diesel reference over the volumetric content of OME_x in the blend with fossil diesel. The figure covers a wide range of engines, from single cylinder research engines over older Euro II production engines to modern Euro VI engines with particulate filter, and a range of load points or driving cycles.

The spread of the data exemplary given in Fig. 16 is obvious. The quantitative amount of PM emission reduction is, among other aspects, highly dependent on the engine and injector design, the chosen engine map, and the operating conditions, i.e., load and speed. For the last point, the general trend seems to suggest that the PM reduction is more pronounced at lower loads [26,135,191]. This might be a mixture formation effect due to the higher required injection duration for OME_x. At low loads, OME_x-containing fuels show improved mixing due to higher peak mass flow rates caused by the generally longer injection durations as already discussed in Section 5.1.1. With increasing load, diesel mixing still improves due to increasing maximum mass flow rates through the nozzle, but for OME_x, mixing quality does not further

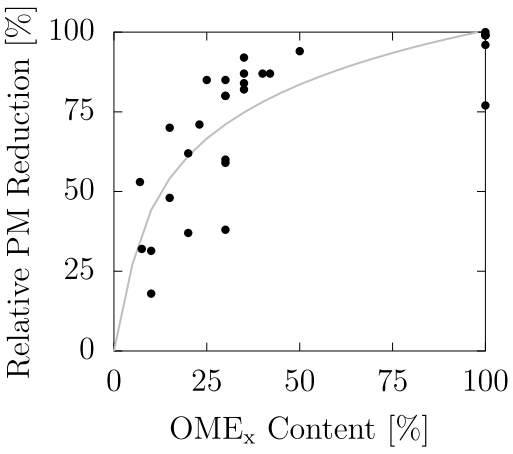

Fig. 16. Measured particulate matter emission reduction over volumetric OME_x content (points), compiled from literature [24,48,63,151,152,174,175,180,181,187,191,196–198] and logarithmic regression curve, extrapolated to zero (line).

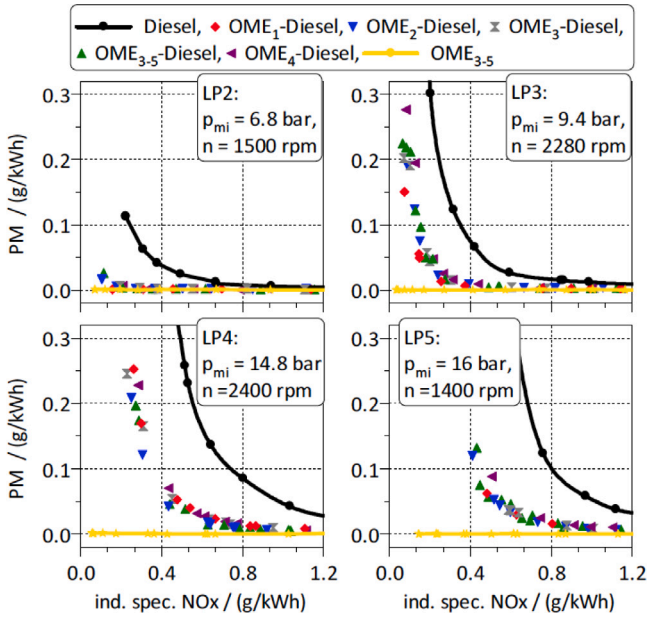

Fig. 17. Particulate matter emissions at different loads for various blends of 35 vol% OME_x in diesel fuel, varying EGR to achieve different NO_x levels, in a single cylinder research engine.
Source: Reproduced from Omari et al. [63] with permission by Elsevier.

change. Interestingly, the soot reduction is almost independent of the OME_x chain length, as with increasing chain length, the increased soot production due to increasing cetane numbers (and thus reduced ignition delay and poorer mixing) and the reduced soot production and increased oxidation due to slightly increasing oxygen contents counteract each other [63]. This is also shown in Fig. 17, where a strong but very similar PM reduction at constant NO_x emissions for all different chain lengths is apparent.

Overall though, a clear trend can be extracted from the available data: The PM emission reduction is very high even for low amounts of OME_x in diesel fuel, and the absolute change reduces asymptotically with larger amounts of OME_x, in line with findings for other oxygenated fuels since the 1990s. Thus, the identification of an optimal blend ratio for commercial introduction of such a fuel blend is an important and challenging task. For example, Omari et al. [63] suggest a blend content of 35 vol% OME_x in diesel fuel as compromise between very high pollutant reduction on one side and low fuel costs and high heating value of the fuel on the other side. The possible combined PM and NO_x emissions achievable with such a blend by choosing appropriate EGR rates can be seen in Fig. 17. Chen et al. [199] recommend a maximum of 20 vol% OME_x in diesel fuel in their review on the assumption that no changes are made to engine control and injector to limit the negative effects of the reduced lower heating value on efficiency and engine power.

As PM are still formed and emitted, even a vehicle fueled with a blend containing more OME_x would still require a particulate filter to fulfill the current emission regulations [63], so that the main advantage of the engine-out PM emission reduction is the corresponding possibility to reduce NO_x emissions due to the eliminated or weakened soot-NO_x tradeoff while still maintaining extended active regeneration intervals of the filter. Alternatively, an open channel particulate filter could be employed, offering higher thermodynamic efficiency due to lower exhaust back pressure [200]. If an engine is also supposed to be operated on neat diesel fuel (flex-fuel engine), the full aftertreatment system needs to remain in place.

Introduction of OME_x into a blend with diesel fuel also reduces the soot particle number [63,176,198], and leads to a shift of the mean particle size to smaller values [63,174,175,198]. This is surprising, as investigations for other oxygenates such as biodiesel often showed the opposite effect of increased PN at decreased total PM [201]. Particularly for neat OME_{3-5}, a significant reduction of the mean diameter was found, with these particles probably largely resulting from combustion of evaporating motor oil and not from fuel-induced soot [63], as also indicated by a large volatile organic fraction originating from engine lube in the PM emissions [174]. An electron microscope analysis combined with energy dispersive X-ray analysis showed that the small soot particles below 20 nm formed in OME_x combustion contain or are made of mostly metal particles, likely partly contained in the fuel, partly from the injection system and the lube oil [202]. The very smallest particles below 10 nm, on the other hand, seem to consist mostly of volatile components, as proven by measurements with a catalytic stripper [200]. For fuel blends of OME_{2-6} in diesel fuel in a stationary diesel engine, a smooth shift towards smaller mean diameters, but no second peak at very small diameters was detected for increasing OME_x content [198]. In a different engine under medium load, just a reduction in number but no shift in particle size distribution was found for neat OME_x compared to HVO as diesel substitute [187], possibly because of a different engine lubrication or wear status. The particle number increases with increased load [152]. The small particles are still efficiently filtered by a diesel particulate filter [184,203], in contrast to assumptions made by Omari et al. [63], but the filtering efficiency can suffer slightly [204]. In addition, the filter loading is decreased, resulting in lower pressure loss and longer regeneration intervals, and the required regeneration temperature is lower due to higher particle reactivity, all in all leading to lower fuel consumption, when even small amounts of OME_x are blended into diesel fuel [184,204–206]. It was also speculated that the small particles could maybe be converted in an efficient diesel oxidation catalyst [174,207]. This was, however, not confirmed by studies with DOC, where soot particle number and mass remained unchanged [176]. As shown in premixed ethylene flames doped with OME_{2-4}, the resulting soot particles contain slightly more oxygenated functionalities, in particular C=O, making them more reactive in both after-treatment systems as well as possibly more toxic [208,209].

Exhaust gas recirculation is a frequently applied measure to reduce combustion temperature and thereby NO_x emissions [210], as discussed in Section 5.4. However, particulate emissions lead to fouling of EGR components, such as cooler, valves, and pipes. A significant reduction of the heat transfer in the EGR cooler or even blockage of the EGR line can be the consequence, leading to a strong rise in NO_x emissions [211]. Without soot emissions and, in case of neat OME_x, no sulfur in the fuel, fouling is less of a concern and high EGR rates are also possible from a durability point of view. In general, smaller PM diameters and higher

volatile content, as encountered with OME_x blends, increase EGR fouling as they seem to be more likely to deposit at cold walls [211], thereby possibly counteracting the overall reduction in PM emissions in terms of EGR fouling. However, tests with blends of OME_{2-6} in diesel fuel in a stationary combined heat and power unit showed decreased EGR fouling and thereby reduced maintenance downtimes and cost [198].

5.3.2. *Analysis of soot reduction potential of* OME_x

The soot reduction potential of OME_x in particular, and oxygenated fuels in general, is not straightforward and still a topic of ongoing research. While some authors report almost linear soot reduction with oxygen mass fraction in the fuel, regardless of molecular composition and other fuel properties [212,213], others come to a different conclusion [24,214,215]. Most studies agree that above around 30 % to 40 % oxygen mass fraction in the fuel, soot production is completely suppressed [212,216]. González et al. [217] report similar total PM levels for the same oxygen mass content with different oxygenates, but different dry PM levels indicating that while total PM emissions mainly depend on total oxygen content, the ratio between volatile PM fraction and dry soot PM fraction changes with the fuel structure, which impacts aftertreatment possibilities.

Multiple different reasons exist for the total engine-out PM reduction with OME_x, and the final reduction of soot emissions is a combination of these with different contributions depending on the conditions. These reasons are listed next.

Shift of equivalence ratio for given fuel-to-air mass ratio due to fuel oxygen: Leaner flames are known to produce less soot. In case of oxygenated fuels such as OME_x, the stoichiometric mixture fraction increases, as less air or more fuel mass is required for complete combustion. This means that production of major soot precursors, such as acetylene or polycyclic aromatic hydrocarbons (PAHs), also shifts towards higher mixture fractions. Assuming similar injector nozzle mass flow rates, the local distribution of mixture fractions in the reacting vapor phase will be somewhat similar though, resulting in an overall significant reduction in the production of soot precursors. This was shown by Goeb et al. [155] based on a combination of LES and 1D flamelet computations. Fig. 18 shows this based on the acetylene production comparing *n*-dodecane as reference fuel and a blend of *n*-dodecane with OME_1. While the peak acetylene production reduces in 1D flamelet space for the blend compared to neat *n*-dodecane, this effect is not responsible for the observed reduction by an order of magnitude of integral acetylene production in the LES domain. The local mixture fraction distribution in the LES does not show significant differences at higher mixture fractions, and thus the most important factor in the overall reduced acetylene production in the LES is the shift of acetylene production to higher mixture fraction values. This shift is thus likely the most important contributor to the super-linear soot reduction with OME_x. Engine simulations were able to reproduce this effect of significantly lower local fuel-air equivalence ratios with neat OME_x [192] and with OME_x blended with *n*-heptane [218], resulting in qualitatively significantly lowered soot formation.

Molecular structure - lack of carbon–carbon bonds: Without carbon–carbon bonds, formation of soot precursors such as acetylene is less likely. Carbon atoms bonded to an oxygen atom tend to keep that bond, so that they likely do not participate in formation of soot precursors [18,194,216]. OME_x, just like DME, do not contain any C–C-bonds, but as discussed in Section 3.1, the beta-scission of the beta-fuel radical is a dominant fuel-consumption pathway and leads to formation of methyl radicals. These can recombine to form C2 species. Consequently, soot formation by OME_x fuel is not entirely suppressed by its molecular structure. More importantly, this fuel effect cannot be responsible for the superlinear reduction of soot found with OME_x in diesel fuel, as it only affects the OME_x fraction of the blend. Thus, it likely plays a role when comparing different oxygenates with similar oxygen content, but is not the main driver for the overall superlinear soot reduction in fuel blends.

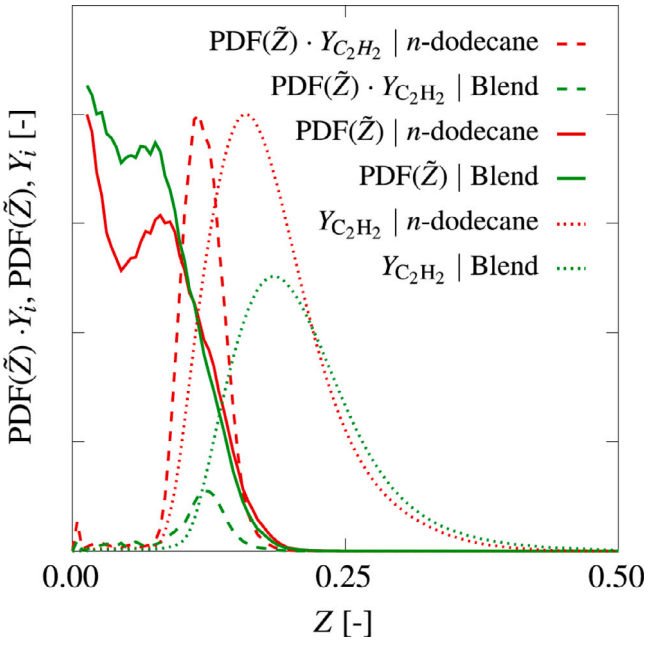

Fig. 18. Normalized mass fractions of acetylene for *n*-dodecane and a blend in 1D flamelet mixture fraction space, averaged over all realizations and flamelets, together with the PDFs of mixture fraction in the LES at 0.4 ms after start of injection, and the resulting normalized convolutions.
Source: Reproduced from Goeb et al. [155] with permission by Elsevier.

Increased air entrainment upstream of the flame: If more air is entrained into the fuel jet before combustion, local equivalence ratios are lower and soot formation is reduced. A higher FLOL likely also means higher air entrainment up to the flame and thereby lower local equivalence ratios, leading to less rich combustion and thereby less soot formation [215]. The stationary FLOL of OME_x and blends of OME_x with diesel fuel are generally longer compared to neat diesel fuel or diesel surrogates [155,166,167,193]. This should correspond to a slight increase in air entrainment, and thus reduced soot formation. This effect can be quantified by the overlap number [219], which describes the normalized distance between liquid spray and flame. A small or negative overlap number will likely be associated with higher soot formation, as not all liquid droplets are evaporated in the region of the flame and thus local rich regions can be expected. Based on the results by Goeb et al. [167] under the spray chamber conditions also shown in Fig. 12, the overlap number in the stationary spray duration is consistently around zero for OME_4, indicating no significant interaction between liquid spray and flame. On the other hand, for diesel fuel, the overlap number is significantly negative, reaching below −0.5 in the early combustion phase and only going towards zero in the later combustion phase.

Changes in combustion mode: Similar to the longer FLOL, longer ignition delay times also cause a shift in the shares of premixed- and diffusion-controlled combustion, which changes sooting behavior. Longer ignition delays lead to better mixing, a higher share of premixed combustion and thus reduced soot formation. Only for OME_1 there is a clear trend towards a higher share of premixed combustion due to the extremely low cetane number, which might contribute to its slightly advantageous soot reduction compared to other OME_x. For OME_{2-5}, there is no clear trend towards more [24,180] or less [152,189] premixed combustion, as for example a changed injector with higher mass flow or an altered ignition timing will have significant impact on this. Considering that the changes in combustion mode seem to be minor, it

can be assumed that this effect only plays a minor role in overall soot reduction with OME_x.

Changes in Temperature: Fuels containing OME_x generally exhibit slightly higher cylinder-average temperatures [63,144,198], most likely due to the more efficient diffusion phase of combustion. In general, higher temperatures promote both soot formation as well as soot oxidation. However the general consensus is that the latter effect is more pronounced, thus likely leading to an overall reduction of soot emissions [187].

Spray and fuel properties: Fuel properties impact mixture formation and temperature. The high vapor pressure especially of OME_1 leads to faster evaporation and mixture formation, thus decreasing the occurrence of rich pockets and hence soot formation. However, considering the minor differences in soot emissions between the different OME_x compared to the significant differences in vapor pressure or boiling temperature, this effect cannot play a major role.

Increased oxidation of soot precursors and soot: Even if soot precursors or soot are formed, an increased rate of oxidation can lead to lower engine-out soot emissions. There is still some, even though very low, flame luminosity with OME_1, indicating that at least some soot is formed even for neat OME_x during combustion, but likely fully oxidized again [182]. Two effects with OME_x could promote soot oxidation: First, fuel oxygen promotes the formation of OH, which is important for soot and soot precursor oxidation particularly in rich regions [213,220]. Second, a faster mixing rate during the late combustion phase could lead to increased soot oxidation. For OME_x blends, significant contribution of increased soot oxidation to the overall soot emission reduction is reported, with some authors attributing the engine-out PM reduction almost entirely to increased oxidation [144,196]. However, while some increase of OH radical concentration is found with OME_x in the fuel [167,193,221], it is likely not significant enough to be solely responsible for the reduced engine-out emissions. On the other hand, the mixing rate with neat OME_x and blends containing significant OME_x is much higher compared to diesel fuel, at least for the majority of the combustion phase [180,189]. This could significantly contribute to increased soot oxidation under certain operating conditions, and is consistent with the stoichiometry effect discussed as first point above for soot formation, as it is also related to locally leaner mixtures.

5.4. Nitric oxide emissions

It is generally assumed that the thermal NO_x formation pathway is dominant under typical CI engine operating conditions. Both a higher peak combustion temperature as well as longer residence time of the burnt gas at high temperatures are the leading influencing factors for thermal NO_x. Following the assumption that NO_x formation is dominated by the thermal pathway, utilization of OME_x in place of fossil diesel fuel leads to competing effects for in-cylinder NO_x production. First, the more complete combustion close to TDC observed with OME_x results in a higher maximum temperature in the cylinder, leading to slightly more NO_x production for most load points [26,144,181,198]. Second, the higher mixing rates with OME_x due its oxygen content [180] together with a shorter main combustion phase [152] can lead to overall lower residence times at high temperatures, reducing thermal NO_x formation, possibly outweighing the first effect. Specifically for OME_1 with its very low cetane number, a high blend content at very low engine loads additionally leads to a mostly lean premixed fuel-air mixture at ignition. Thus, combustion becomes largely lean premixed with a reduction of NO_x emissions due to the low resulting temperatures [26]. With increasing chain length, the combustion duration as well as the peak temperature decrease, the latter due to increased heat capacity of the combustion products because of higher CO_2 content, overall resulting in slightly decreasing NO_x emissions [187,190]. Overall, no clear trend for NO_x emissions compared to diesel fuel for unchanged EGR rates can be stated from literature data. However, emissions generally seem to remain in the same order of magnitude.

Increasing exhaust gas recirculation (EGR) is a common way to decrease engine-out NO_x emissions. To achieve similar NO_x levels with OME_x-containing fuels as for fossil diesel fuel, EGR needs to be raised slightly in most load points. However, the significant reduction in PM emissions as discussed in Section 5.3, and the elimination of the soot-NO_x tradeoff for neat OME_x and high blend ratios of OME_x in diesel fuel allow for a further significant increase of EGR rate, potentially even up to a globally stoichiometric air-fuel ratio [24,152,176,182,187]. The impact of different blend ratios on the range of possible EGR rates can also be seen in Figs. 15 and 17, where the soot-NO_x-tradeoff is shown for different fuel blends with the strong increase of soot emissions limiting the maximum EGR rate. Such increased EGR allows significant reduction of engine-out NO_x emissions due to lower combustion temperatures, down to below 0.2 g/kWh without aftertreatment, half of the Euro VI level, for stoichiometric operation [152]. For neat OME_x and high blend contents, the increase of EGR is only limited by the drop in engine efficiency below $\lambda = 1.1$ [152], as discussed also in Section 5.2. For higher EGR rates, the effect of chain length on NO_x emissions vanishes [190].

Some apparent discrepancy exists between the moderate increase of NO_x engine-out emissions measured in lab experiments, as discussed above, and more pronounced increases of tail pipe emissions with modern vehicles. In a Euro VI vehicle performing an RDE drive, a strong increase of NO_x emissions by 60 % for a blend of 30 vol% OME_{3-5} in diesel fuel and up to 26 % for a blend of 15 vol% OME_{3-5} in diesel fuel was detected [197]. In a Euro VI engine performing a WLTC test, an increase of tailpipe NO_x emissions by about 100 % was measured for a blend of 30 vol% OME_{3-5} in diesel fuel [191]. A comparison between engine-out and tailpipe emissions after aftertreatment with the fuel blend relative to neat diesel fuel additionally revealed a much lower relative increase in engine-out NO_x emissions compared to tailpipe, indicating non-proper function of the aftertreatment system with OME_x in the fuel [191,197]. These stark increases can be attributed to the non-adapted engine control in these particular cases though, leading to operation in a perceived higher load point with less EGR due to the lower heating value of OME_x, resulting in higher engine-out NO_x emissions as well as lower exhaust gas temperature [191,197,222]. The exhaust temperatures in turn might be too low for the oxidation catalyst to convert NO to NO_2 to be stored in the lean NO_x trap of the Euro VI vehicles. This would explain the discrepancy between the relative increases of engine-out and tailpipe emissions [191,195]. In fact, after optimization of the engine control map for a fuel blend containing 15 vol% OME_{3-5} in diesel fuel to achieve the same engine-out NO_x emissions, also the tailpipe emissions dropped accordingly [223]. Similarly, also the efficiency of an active SCR is reduced with lower exhaust gas temperatures when OME_x is burnt [200]. Despite that, taking advantage of the increased EGR range, tail pipe NO_x emissions with neat OME_x and an advanced, twin-dosing SCR system under real driving conditions could still be reduced to below 10 mg/kWh, more than an order below the Euro VI limit [200].

To achieve low tailpipe NO_x emissions with OME_x in the fuel, even for relatively low OME_x content, an adaptation of the engine map and/or of the injector geometry to account for the lower heating value of the fuel is inevitable, as shown above. This is a limitation for OME_x as drop-in fuel, as a rough estimate of the content in the fuel must be made available to the engine control at all times. Then again, due to significantly lowered PM emissions as discussed in Section 5.3, the upper limit for EGR increases significantly and extremely low engine-out NO_x emissions are thus achievable, potentially significantly reducing aftertreatment efforts and cost.

5.5. Unburnt hydrocarbon emissions

Unburnt hydrocarbon (uHC) emissions from CI engines can be attributed to three different main effects: Injector dripping; local overmixed, non-combustible lean regions; and local fuel-rich regions which have insufficient time to mix and fully burn before the end of combustion [202]. The combination of these three effects makes uHC emissions very dependent on the engine design and operating conditions. Consequently, no clear trend can be extracted from various literature data regarding the impact of OME_x addition to diesel fuel. Some authors report uHC emissions to continuously decrease with increasing OME_x content in a blend [26,63,224] and for neat OME_x compared to fossil diesel fuel [152,202]. Others found the exact opposite trend [181], or even a decrease for small OME_x contents in diesel fuel and an increase for neat OME_x [174]. The differences in trend can be attributed to the different impact that OME_x properties have in different engines and operating conditions. The oxygen content in the fuel should reduce uHC emissions from locally rich regions, but might result in more overmixed lean regions. The different volatility of different OME_x should also impact mixture formation. Finally, the high cetane numbers of $OME_{x>2}$ lead to a faster and more complete burn-out, reducing uHC emissions, while the low cetane number of OME_1 likely has the opposite effect. However, the cetane number impact seems to be low [63]. Overall though, uHC emissions are well below current Euro VI legislation thresholds for typical CI engine air-fuel-ratios. As expected, hydrocarbon emissions steeply rise when approaching fuel-rich conditions as for all fuels [202].

Methane emissions make up a large fraction of total hydrocarbon emissions [151], with this fraction barely changing with the fuel-air equivalence ratio [202]. The reason in terms of reaction kinetics for the large amount of methane formation are the methyl end-groups in OME_x. Details are is discussed in Section 3.4. At lean conditions, methane emissions are significantly lower with OME_x than with diesel fuel [63]. But close to stoichiometric operation with OME_x, methane emissions rise and are barely converted in a typical oxidation catalyst due to the high required light-off temperature, leading to rising exhaust hydrocarbon emissions [24,151,152,176,177,202]. As methane is a powerful GHG, this makes operating strategies near stoichiometric conditions challenging.

Even though OME_x are produced from formaldehyde, formaldehyde emissions are lower than for diesel fuel for most load points [24,63,176]. At very low loads, formaldehyde emissions for neat OME_{3-5} are about twice as high as for diesel fuel [63]. However these emissions are expected to be fully converted in the oxidation catalyst, as has also been demonstrated [177]. Yet, this was not the case with an aged DOC in a Euro II passenger car, where a significant increase of formaldehyde emissions was measured compared to diesel fuel even after the DOC [174]. To avoid toxic and carcinogenic formaldehyde emissions with OME_x, as for the operation with diesel fuel, an efficient and up-to-date DOC is necessary.

Different relations between the OME_x chain length and methane as well as formaldehyde emissions are reported. The source of such emissions could be the methoxy chain elements and the methyl end groups of OME_x, respectively, of which the ratio shifts with increasing chain length. While methane emissions are independent of chain length [152,177], formaldehyde emissions were reported to be significantly higher for OME_{3-5} compared to OME_1 in a particular load point [152], and rising with longer chain lengths for OME_{2-5} in another engine with medium load [187,190], but were reported to be similar for different chain length in a different load point [177].

PAH emissions after DOC increase with a blend of OME_{3-5} in diesel fuel compared to the base fuel, but it is assumed this is likely the result of the measured decreased conversion efficiency of the DOC due to lower exhaust gas temperatures in their operating conditions, not a chemical fuel effect [175].

5.6. CO emissions

CO emissions are moderately to strongly reduced with OME_x compared to conventional diesel fuel [26,63,144,152,188,198,202,224]. A very strong reduction by more than 70 % was found for both OME_1 and OME_{3-5} for a heavy duty single cylinder engine in one load point [152]. In a stationary six-cylinder engine, a reduction by 35 % and 65 % compared to diesel fuel was measured for 20 vol% and 50 vol% OME_{2-6}, respectively [198]. The reason for this is likely more complete and faster combustion due to fuel oxygen, as discussed in Section 6.1, leaving less partially oxidized fuel for the burn-out phase. The relative impact of OME_x is higher for higher engine loads and high speeds, where large fuel-rich regions are expected to exist and there is less time for post-oxidation, such that the contribution of the oxygen in the fuel to the full oxidation is high [181,225]. The opposite happens with particularly high OME_1 contents at low load points, where the long ignition delay leads to more non-reactive mixing, which promotes regions too lean to fully burn, finally resulting in CO emissions [26].

Approaching stoichiometric conditions, CO emissions rise very significantly, even up to the point where engine efficiency is significantly affected [202]. In all cases and down to almost stoichiometric conditions, CO is oxidized very effectively in the DOC [24,151,176].

5.7. Future research perspectives

On the fundamental level, tremendous progress has been made over the recent years in understanding the soot reduction potential of oxygenated fuels in general and OME_x in particular. Still, the exact importance of the different impact factors is a topic of ongoing research. A combination of recently developed detailed kinetic reaction mechanisms for OME_x with state-of-the-art soot nucleation and oxidation models under engine-relevant conditions should result in higher completeness of data unachievable by experiments, allowing to significantly improve understanding of the impact of OME_x on soot formation and oxidation. At the same time, more high-fidelity experimental data would help to validate and improve the aforementioned kinetic models, in particular regarding PAH formation rates. Another open research topic is the reduction of PM particle sizes with OME_x. Some studies have hinted that these particles might not originate from combustion soot formation, but, e.g., engine oil and erosion, and investigation of the interaction of such small particles with soot nuclei and soot precursors (or the lack thereof) could lead to interesting insights about why these small particle sizes are less present in case of fossil diesel. However, experiments in OME_x-doped burner-stabilized ethylene flames have shown no significant reduction in nano-particle formation, while formation of larger soot particles was heavily suppressed with OME_x addition as expected [226]. Further research under engine-relevant conditions is required to improve the understanding of the formation of the smallest particles in OME_x combustion. As discussed above, if the fuel or fuel blend used in vehicle operation is not known beforehand, fuel sensors to distinguish between different OME_x blend ratios are required to allow for flexible operation depending on future OME_x availability. Typical measurement methods based on the permittivity, as used for ethanol-gasoline-blends, are not as suitable for OME_x blends, as the dielectric constants of OME_x and diesel fuel are much closer to each other. Closed-loop control via exhaust gas sensors might be possible, but this will require further testing.

On the engine application side, OME_x allow for novel combinations of operating and aftertreatment strategies which are not possible with fossil diesel. Optimization of the full parameter range of possible fuel blends, different engine operating modes and aftertreatment systems regarding engine performance, emissions, costs and climate impact is an incredibly challenging research task. As some existing studies already showed, significant potential could likely still be leveraged here by deviating further from existing well-known diesel-fueled CI engine approaches. Additionally, most research on state-of-the-art engines was

performed with light vehicles engines. However current trends hint at the fact that application of e-fuels such as OME_x would be more likely in heavy-duty applications. Gathering field data with state-of-the-art heavy duty engines, e.g., in trucks, could be helpful to highlight the potential of OME_x also for these applications.

6. Production costs, efficiency, and market perspectives

The reduction of GHG to reduce global warming becomes even more complex and challenging if economic and social boundary conditions need to be considered. This chapter focuses on the different aspects of the market potential of oxymethylene ethers. Production efficiencies are discussed in Section 6.1. Production cost estimates from literature for various pathways are presented and compared to other fuel candidates in Section 6.2, followed by a discussion on fuel life cycle assessments from well to wheel in Section 6.3, highlighting under which conditions OME_x-based fuels can deliver a net climate benefit. This section closes with a high-level view on policies and market introduction in Section 6.4.

6.1. Production efficiency

As long as the amount of renewable power available for e-fuel production is considered a limiting factor, any increase in production efficiency of a fuel directly relates to a global warming reduction. All e-fuels share the first steps of electrolysis to produce H_2 and, except for carbon-free fuels such as H_2 itself or ammonia, CO_2 capture from air or point sources. Thus, these steps will not be covered in this section to avoid introducing more assumptions and scenarios than necessary. The subsequent chemical processes, on the other hand, show some significant differences, and for OME_x in particular, the choice of production pathway from the wide range discussed above has a significant impact on the overall production efficiency.

In this review, we will give production energy efficiencies collected from literature based on H_2 and CO_2 as reactants and using the reactant and product lower heating values LHV_i per kg of OME_x product

$$\eta = \frac{\mathrm{LHV}_{\mathrm{OME_x}}}{\mathrm{LHV}_{\mathrm{H_2}} + \dot{q}_{in} + \dot{w}_{el} - \mathrm{LHV}_{\mathrm{side}}}. \tag{30}$$

Additionally, $\dot{q}_{in}$ is the net heat demand of production and $\dot{w}_{el}$ is the electrical power demand of production, each for 1 kg of OME_x product. Other authors have denoted such efficiency as plant efficiency or process efficiency. If no comparable efficiency was given in the original work, we have recomputed it based on the published numbers in the original paper and supplemental material. Fig. 19 makes an attempt to visualize the broad range of production efficiencies which have been reported. For comparison, some other prominent e-fuels are also included. Table 3 serves as extended legend for Fig. 19. For each fuel production model, Fig. 19 gives two key values: first, the corresponding energy efficiency calculated as discussed above (lowest bar), and second, a theoretical maximum value based on stoichiometry, i.e., based on a process with no external energy demand and no undesired side product formation (top of the stacked bars). This simplifies Eq. (30) to:

$$\eta_{th,max} = \frac{\mathrm{LHV}_{\mathrm{OME_x}}}{\mathrm{LHV}_{\mathrm{H_2}}}. \tag{31}$$

In addition, the difference between the theoretical efficiency and the practical process efficiency is split into contributions due to undesired side product formation (necessitating additional H_2 input), electrical energy demand, and heat demand. This allows to both investigate differences between different production pathways and fuels, as well as differences between different literature sources for the same fuel production pathway.

It should be noted that an energy-efficiency based comparison as given here based on literature data inherently assumes an equal value of all different energy inputs. Strong arguments can be made against this assumption. E.g., if hydrogen is produced from electrolysis with an efficiency of 80 %, hydrogen energy input should be multiplied by 1.25. Similarly, heat can often be provided using lower exergy sources such as waste heat, while the analysis presented here inherently assumes utilization of electrical power for heating at 100 % efficiency. An exergy-based assessment, as for example done by Burre et al. [56], alleviates this problem, however assigning exergies to educt, product, and heat streams can be challenging. As most literature sources compute energy-based production efficiencies, we will stick to the same metric here despite the shortcomings outlined above.

Focussing on the theoretical maximum efficiencies first, it can be clearly seen that OME_{3-5} produced using the established or the anhydrous pathways **(P6-P18)**, which both rely on partial oxidation of methanol to produce the required formaldehyde, shows clearly inferior values compared to all shown exemplary e-fuel competitors **(P22-P24)**. OME_1, on the other hand, is already competitive even using the established or oxidative pathways **(P1-P3)** due to the more favorable ratio of methanol to formaldehyde. In contrast, using new, reductive or dehydrogenation routes, the theoretical maximum efficiency of production for both OME_1 **(P4-P5)** and OME_{3-5} **(P19-P21)** exceed obtainable values for FT-diesel **(P22)** and methanol **(P23)** significantly. This surprising result stems from the stoichiometric 100 % hydrogen conversion efficiency of the dehydrogenative or reductive formaldehyde production from methanol, if the hydrogen byproduct is rerouted back to methanol production. The resulting very high overall conversion of hydrogen heating value to fuel heating value leads to a very high achievable efficiency showcasing the theoretical potential of OME_x fuels also from a production efficiency point of view.

However, now comparing the currently achievable production efficiencies modeled by the various literature sources, it is also obvious that for all OME_x pathways **(P1-P21)** there are significantly larger gaps to the theoretical values compared to the reference e-fuels **(P22-P24)**. The two main contributors to this difference are side product formation and external heat demand, with electricity demand, mostly for compression, playing a minor role. More surprisingly, at first glance, the established production routes actually outperform the theoretically favored reductive and dehydrogenation routes. The reasons for this and other findings for different pathways will be discussed in more detail in the following.

For OME_1, the two predictions for the established, aqueous pathway by Burre et al. [56] **(P1)** and Schemme et al. [4] **(P2)** agree well, both in terms of resulting efficiency as well as heat demand and loss due to side product formation. The efficiency of the oxidative pathway **(P3)** is slightly higher, mainly because side product formation is significantly reduced due to the one-pot reaction, however the electricity demand goes up due to a refrigeration machine being used in the underlying study for product separation [56]. The efficiency of the reductive and dehydrogenation pathways **(P4-P5)** drops off significantly compared to the former two, mainly because of an enormous heat demand for product separation due to low product yields [56]. For both pathways, equilibrium product yields would reduce heat demand by more than 80 %, putting them significantly ahead of the established pathway **(P1-P2)** [56]. Further catalyst development as well as in-situ H_2 removal in case of the dehydrogenation pathway could help close this gap [56]. Additionally, side products of the dehydrogenation pathway **(P5)** are valuable (MF and DME), and accrediting them as product closes part of the gap to the reductive pathway **(P4)**. Note that in their work, Burre et al. [56] computed exergy efficiencies instead of energy efficiencies and accredited side products, putting the reductive and dehydrogenation pathways **(P4-P5)** ahead of the aqueous and oxidative pathways **(P1-P3)** despite the high heat demand due to the relatively low temperatures of the required heat supply.

Regarding the established, aqueous production pathway for OME_{3-5} **(P6-P10)**, the stark differences between the different predicted efficiencies are immediately recognizable. The results by Voelker et al. [227]

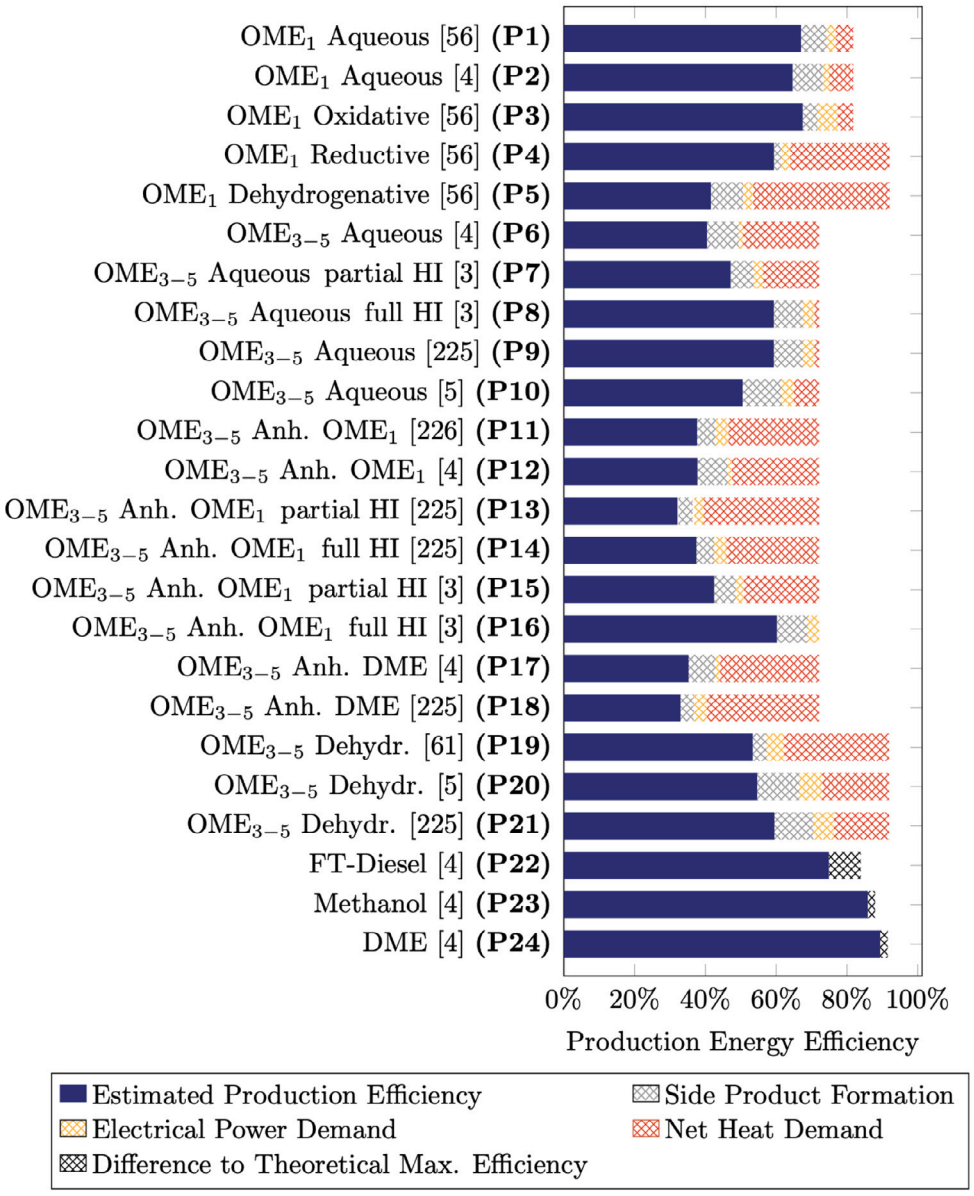

Fig. 19. Estimated OME_x production efficiencies compiled and recomputed from literature compared with some other popular e-fuel candidates (solid bars), as well as break-down of difference to theoretical maximum efficiency (hatched bars). Detailed legend in Table 3.

(P9) are based on the same model as the results by Held et al. [3] **(P8)**, so these two agree well, but differ heavily from the other two results. This has two underlying reasons: first, these process models predict significantly less H_2 consumption per unit mass fuel produced, which means less side products leave the production chain. A major contributor here is the assumption of perfect separation of water in the evaporators utilized to increase the formaldehyde concentration prior to the OME_{3-5} synthesis, while, e.g., in the work of Mantei et al. [5] **(P10)**, a considerable amount of formaldehyde is lost through the waste water stream. Second, there are significant differences in net heat demand. In theory, efficiency values for **(P6, P8-P10)** are based on full heat integration throughout the entire production chain, but the calculations differ both in the heat demand of the individual sub steps as well as the level of detail of the heat integration modeling. With an idealized pinch heat integration throughout the entire production chain, Voelker et al. [227] **(P9)** and Held et al. [3] **(P8)** find a net heat demand of almost zero. If heat integration is only considered within each separate step of methanol production, formaldehyde production, and finally OME_{3-5} synthesis, the overall heat demand increases significantly, and the production efficiency drops by more than 6 % as shown by the corresponding results by Held et al. [3] **(P7)**. With a more realistic heat integration concept with actually modeled heat exchangers, again throughout the entire production chain though, Mantei et al. [5] **(P10)** find a moderate net heat demand. On the other hand, Schemme et al. [4] **(P6)** first of all assume a significantly higher heat demand for the last production step, and on top of that utilize a heat supply on three discrete pressure levels. This limits integration between the sub-processes, resulting in a much higher total net heat demand on a high pressure level and an unused surplus of steam on lower pressure levels.

For the anhydrous OME_{3-5} production pathways **(P11-P18)**, predicted production efficiencies drop by a few percentage points. This is mostly due to the significant heat demand of trioxane production, which can only be partially covered by heat integration of surplus heat from the preceding methanol and formaldehyde production steps, and the significantly reduced heat demand of the final OME_{3-5} synthesis compared to the aqueous pathway **(P6-P10)** discussed above. Additionally, production from DME **(P17-P18)** instead of OME_1 **(P11-P16)** as intermediate is disadvantageous from an energy efficiency perspective,

Table 3
Extended legend for Fig. 19.

Number	Source	Fuel	Production pathway	Heat integration	Comments
(P1)	Burre. [56]	OME_1	Aqueous	Full pinch	Recomputed, org. source uses exergy
(P2)	Schemme [4]	OME_1	Aqueous	Full 3 level steam	–
(P3)	Burre [56]	OME_1	Oxidative	Full pinch	Recomputed, org. source uses exergy
(P4)	Burre [56]	OME_1	Reductive	Full pinch	Recomputed, org. source uses exergy
(P5)	Burre [56]	OME_1	Dehydrogenation	Full pinch	Recomputed, org. source uses exergy, no side prod. credit
(P6)	Schemme [4]	OME_{3-5}	Aqueous	Full 3 level steam	–
(P7)	Held [3]	OME_{3-5}	Aqueous	Sub-process pinch	–
(P8)	Held [3]	OME_{3-5}	Aqueous	Full pinch	–
(P9)	Voelker [227]	OME_{3-5}	Aqueous	Full pinch	identical to (8)
(P10)	Mantei [5]	OME_{3-5}	Aqueous	Detailed HEN model	–
(P11)	Burre [228]	OME_{3-5}	Anhydrous OME_1+TRI	Full pinch	Recomputed, org. source uses exergy
(P12)	Schemme [4]	OME_{3-5}	Anhydrous OME_1+TRI	Full 3 level steam	–
(P13)	Voelker [227]	OME_{3-5}	Anhydrous OME_1+TRI	Sub-process pinch	Recomputed, org. source uses exergy
(P14)	Voelker [227]	OME_{3-5}	Anhydrous OME_1+TRI	Full pinch	Recomputed, org. source uses exergy
(P15)	Held [3]	OME_{3-5}	Anhydrous OME_1+TRI	Sub-process pinch	–
(P16)	Held [3]	OME_{3-5}	Anhydrous OME_1+TRI	Full pinch	–
(P17)	Schemme [4]	OME_{3-5}	Anhydrous DME+TRI	Full 3 level steam	–
(P18)	Voelker [227]	OME_{3-5}	Anhydrous DME+TRI	Full pinch	Recomputed, org. source uses exergy
(P19)	Ouda [60]	OME_{3-5}	Dehydrogenation	Detailed HEN model	H_2 recycled, MeOH prod. efficiency from [4] (23)
(P20)	Mantei [5]	OME_{3-5}	Dehydrogenation	Detailed HEN model	H_2 recycled
(P21)	Voelker [227]	OME_{3-5}	Dehydrogenation	Full pinch	H_2 recycled
(P22)	Schemme [4]	FT-Diesel	–	Full 3 level steam	–
(P23)	Schemme [4]	Methanol	–	Full 3 level steam	–
(P24)	Schemme [4]	DME	–	Full 3 level steam	–

as more energetically costly trioxane is needed. While most of the modeled efficiencies agree well, the results by Held et al. [3] **(P15)** are an outlier. Their calculated heat demand for trioxane production before heat integration with other processes is less than half of what all other studies find, which is surprising because they consider the same distillation-based trioxane production process [229] as all other studies, and the significantly higher energy demand of the latter agrees with the calculations in the original work [230]. Consequently, the results by Held et al. [3] **(P15)** for the anhydrous pathway should be considered an outlier, and thus overall this pathway is significantly behind all other OME_x pathways **(P1-P10, P19-P21)** as well as all other reference e-fuels considered in Fig. 19 **(P22-P24)** in terms of efficiency.

From a stoichiometry point of view, the dehydrogenation method for OME_{3-5} production **(P19-P21)** should deliver promising results as indicated by the very high theoretical maximum efficiency. This is, again, due to the non-oxidative formaldehyde production which allows to recycle the freed hydrogen. This theoretical potential is, however, not fully leveraged yet with currently existing processes, and the practical efficiencies using similar model assumptions are on a similar level (**(P21)** to **(P9)**) only or slightly higher (**(P20)** to **(P10)**) than the efficiencies of the aqueous pathway. While the H_2 demands of Voelker et al. [227] **(P21)** and Mantei et al. [5] **(P20)** seem similar at first glance, this is just the case because two different modeling assumptions cancel each other out. Mantei et al. [5] **(P20)** predict significantly more CO side product formation in the formaldehyde synthesis, but on the other hand assume perfect separation and recycling of H_2, ending up with a similar net H_2 demand as Voelker et al. [227] **(P21)**. Ouda et al. [61] **(P19)** on the other hand aim to achieve an even lower formation of CO, and in this case we apply the assumption of perfect recycling (as their analysis is limited to the reactant methanol) to end up with the numbers presented in Fig. 19. In terms of heat demand, direct comparison is difficult as again different levels of detail in modeling are applied, and in particular different methods are utilized for transporting the produced FA to the OME_{3-5} reactor, resulting in different heat demands for separation. Voelker et al. [227] **(P21)** use an aqueous reaction environment for the OME_{3-5} production step similar to the established, aqueous pathway **(P6-10)**, and can thus utilize water to selectively purge formaldehyde and methanol from the formaldehyde reactor product gas. Ouda et al. [61] **(P19)** and Mantei et al. [5] **(P20)** on the other hand use a dry process with nitrogen as carrier gas. When comparing the numbers given in Fig. 19 with the original sources, note that Ouda et al. [61] give efficiencies based on methanol as reactant, not CO_2 and H_2, and declare the recovered H_2 as product instead of recycling it to reduce the H_2 educt demand in the denominator. Both together lead to significantly, but somewhat misleadingly, higher stated efficiencies in their work.

From this review and discussion of literature studies for OME_x production efficiencies, the following key take-aways can be stated:

1. On a theoretical level based on stoichiometry, OME_x is more than competitive with other e-fuels if the more advanced production pathways avoiding partial oxidation of methanol for formaldehyde production are used.
2. Practical efficiencies with currently existing processes for OME_x production are significantly behind competing e-fuels, necessitating further improvements and research.
3. The latter is particularly true for the advanced processes mentioned in point 1, which are currently even lagging behind the more established, aqueous pathways in terms of achievable efficiencies.
4. Heat integration throughout the entire process chain allows for substantial energy demand reduction. The level of detail used in modeling heat integration significantly impacts the predicted overall efficiencies.

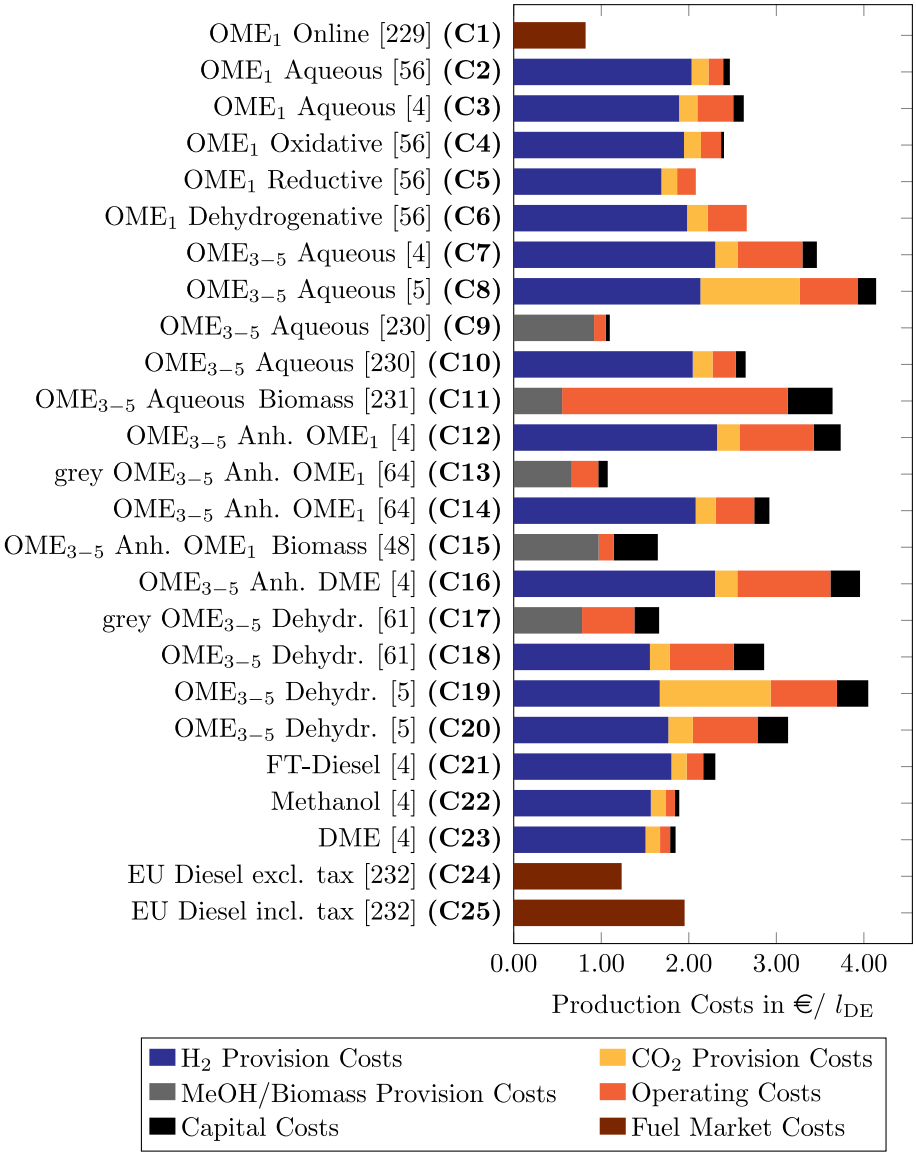

Fig. 20. OME_x production costs compiled and recomputed from literature compared with some other popular e-fuel candidates as well as fossil alternatives. Detailed legend in Table 4.

6.2. Production costs

Cost competitiveness with other propulsion technologies will likely be a major factor in the discussion to introduce an e-fuel such as OME_x into the market. Fig. 20 summarizes production cost predictions from literature per liter diesel equivalent (i.e., on an energy basis), broken down into costs for the reactants H_2 and CO_2 (or methanol in cases where the production chain starts with methanol, or biomass), operational expenses (e.g., heat, electricity), and capital expenses. For comparison, also an EU-average price for fossil diesel with and without taxes, online procurement prices for grey OME_1 as well as production cost predictions for some select other e-fuels are shown. It should be noted that the prices given for diesel **(C24-C25)** and the price for grey OME_1 **(C1)** include an unknown profit margin and, in case of diesel fuel, also shipping and distribution costs, and can therefore not be directly compared to the production costs for the different e-fuels. An extended legend is given in Table 4.

Clearly, for all e-fuels **(C2-C8, C12, C14, C16, C18-C23)**, the costs for H_2 and CO_2 procurement are the major drivers of total product cost. In the studies shown here, assumed baseline prices for green H_2 vary from 4121 to 5000 €/t. All studies except Mantei et al. [5] **(C8, C19)**, who assume 309 €/t for CO_2, use a point source CO_2 price of 70 €/t. Two original works by Schmitz et al. [64] **(C13)** and Ouda et al. [61] **(C17)** calculate OME_{3-5} costs based on grey methanol, using prices of 285 and 336 €/t, respectively. For these two cases, Fig. 20 also additionally presents recomputed values **(C14, C18)** based on the green methanol production cost assessment by Schemme et al. [4] **(C22)**. This corresponds to a green methanol price of 1078 €/t, which is also in the middle of the range between 608 and 1453 €/t given by Hank et al. [235]. In case of the dehydrogenation process **(C18-C20)**, the H_2 product stream was used to reduce the H_2 demand. For the production pathways based on biomass **(C11, C15)**, the raw product costs are significantly lower. However, the process costs increase due to the additional steps of syngas production from biomass. Capital expenses are generally low in comparison to the other expenses.

The price given for grey OME_1 **(C1)** corresponds to online-available prices for OME_1 from China. Interestingly, such fuel could currently be cheaper than fossil diesel **(C24-C25)** if it was taxed less. The same is also true for OME_{3-5} based on grey methanol **(C9,C13)**. However, the climate impact of such fuels would likely be net negative (see

Table 4
Extended legend for Fig. 20.

Number	Source	Fuel	Production pathway	Comments
(C1)	Online [231]	OME_1	Aqueous	Chinese production
(C2)	Burre. [56]	OME_1	Aqueous	Level 3 without misc costs
(C3)	Schemme [4]	OME_1	Aqueous	–
(C4)	Burre [56]	OME_1	Oxidative	Level 3 without misc costs
(C5)	Burre [56]	OME_1	Reductive	Level 2 without misc costs and CAPEX
(C6)	Burre [56]	OME_1	Dehydrogen.	Level 2 without misc costs and CAPEX
(C7)	Schemme [4]	OME_{3-5}	Aqueous	–
(C8)	Mantei [5]	OME_{3-5}	Aqueous	–
(C9)	Tönges [232]	OME_{3-5}	Aqueous	Grey methanol
(C10)	Tönges [232]	OME_{3-5}	Aqueous	Green methanol from (22)
(C11)	Mahbub [233]	OME_{3-5}	Aqueous	Forest residue
(C12)	Schemme [4]	OME_{3-5}	Anhydrous OME_1+TRI	–
(C13)	Schmitz [64]	OME_{3-5}	Anhydrous OME_1+TRI	Grey methanol
(C14)	Schmitz [64]	OME_{3-5}	Anhydrous OME_1+TRI	Green methanol from (22)
(C15)	Damyanov [48]	OME_{3-5}	Anhydrous OME_1+TRI	Full trees
(C16)	Schemme [4]	OME_{3-5}	Anhydrous DME+TRI	–
(C17)	Ouda [60]b	OME_{3-5}	Dehydrogen.	Grey methanol
(C18)	Ouda [61]	OME_{3-5}	Dehydrogen.	Green methanol from (C20), H_2 recycled
(C19)	Mantei [5]	OME_{3-5}	Dehydrogen.	–
(C20)	Mantei [5]	OME_{3-5}	Dehydrogen.	H_2 and CO_2 costs from [4]
(C21)	Schemme [4]	FT-Diesel	–	–
(C22)	Schemme [4]	Methanol	–	–
(C23)	Schemme [4]	DME	–	–
(C24)	EC [234]	Fossil Diesel EU	–	Without tax 2016–2021
(C25)	EC [234]	Fossil Diesel EU	–	With tax 2016–2021

Section 6.3). Any e-fuel produced using green hydrogen is significantly more expensive than fossil diesel fuel as of now.

For OME_1, it can be seen that production based on the reductive route **(C5)** can be competitive with other e-fuels such as Fischer–Tropsch-diesel **(C21)** or DME **(C23)**, with total fuel prices in the range of 2 € per liter diesel equivalent. Here, the reduced hydrogen consumption of this production pathway, as discussed in the previous sections, comes into full effect. Despite a significantly worse energy efficiency, production costs are significantly lower compared to the established, aqueous pathway **(C2-C3)** and the oxidative pathway **(C4)**. For the aqueous pathway, production price predictions by Burre et al. [56] **(C2)** and Schemme et al. [4] **(C3)** agree well at a price of about 2.5 € per liter diesel equivalent. However, note that this is only because a higher assumed price of hydrogen by the former roughly compensates the higher predicted heat demands and thus higher operational expenses by the latter.

As expected, production of green OME_{3-5} **(C7-C8,C10,C12, C14, C16, C17-C20)** is generally more expensive per liter diesel equivalent with a price range between 3 and 4 € per liter diesel equivalent. For the aqueous production pathway, the significant difference between the predictions by Schemme et al. [4] **(C7)** and Mantei et al. [5] **(C8)** are mostly based on the vastly different assumed CO_2 price. The calculations by Tönges et al. [232] **(C9)** for the aqueous pathway are based on grey methanol at 401 €/t, and went into significant detail regarding the underlying plant process model. Different water separation and formaldehyde production pathways lead to a relatively low overall spread of the production costs of around ±10% around the mean [232]. It should be pointed out that their resulting prices would be competitive with diesel fuel in the EU as of today. Utilizing the methanol production calculations by Schemme et al. [4] for green methanol instead, the resulting overall price is still low. The assumed carbon yield is comparatively high, resulting in relatively low raw material costs, and a significant amount of excess steam is assumed to be sold to other processes, resulting in low net operating costs. With an adjusted carbon yield and without selling excess steam, their results move into the range of Schemme et al. [4] **(C7)**. Interestingly, production based on biomass from Mahbub et al. [233] **(C11)** ends up in the same price range as the three previously discussed renewable production routes, indicating that production of syngas from biomass is roughly as expensive as production via electrolysis and CO_2 point capture. For the anhydrous pathways via trioxane, production costs predicted by Schemme et al. [4] **(C12, C16)** are slightly higher due to the higher heat demand as well as higher capital expenses for trioxane production. However, the calculation by Schmitz et al. [64] **(C14)**, extended with the methanol production by Schemme et al. [4], predicts notably lower costs. This is for two reasons: First, the assumed conversion rates from methanol to OME_x product of Schmitz et al. [64] **(C14)** are notably higher, in particular in the formaldehyde production step, leading to lower H_2 and CO_2 procurement costs. Second, and even more importantly, Schmitz et al. [64] **(C14)** do not calculate the heat demand for the trioxane production step, but instead assume similar heat demand to the OME_1 plant. As discussed in Section 6.1 above, this is not a very good approximation, as the heat demand for trioxane formation is significantly higher, and thus Schmitz et al. [64] **(C14)** likely underestimate the total heat demand of the entire production chain significantly despite no assumed heat integration. The most notable outlier of the entire field though is the cost estimate by Damyanov et al. [48] **(C15)** for production from full tree biomass. Their operational expenses are extremely low, despite using the energy-intensive process via trioxane, in comparison with Mahbub et al. [233] **(C11)** who estimate very significant costs for syngas production from biomass. Consequently, the results by Damyanov are questionable.

The dehydrogenation OME_{3-5} pathway **(C17-C20)** shows its potential compared to the other pathways in the cost analysis. The significantly reduced hydrogen demand directly leads to significant overall cost reductions. Again, the values given in the original work by Mantei et al. [5] **(C19)** are based on very high CO_2 costs from DAC. For better comparison, their assessment was recomputed **(C20)** using the H_2 and CO_2 costs for a point source from Schemme et al. [4] **(C22)**, the same that were also used for the recalculated green production assessment from Ouda et al. [61] **(C18)**. Both recalculated values end up at around 3 € per liter diesel equivalent, which is about 15 % cheaper on average compared to the aqueous pathway. **(C20)** with CO_2 from a point source is more than 20 % cheaper than **(C19)** based on DAC, despite slightly higher H_2 costs, showing the significant additional costs of DAC compared to a point source. The remaining difference between **(C18)** and **(C20)** can be mostly attributed to much higher conversion rates for Ouda et al. [61] **(C17-C18)**, as already discussed in Section 6.1. In their work, Ouda et al. [61] also gave significantly lower production costs with a recalculated value around 1.05 € per liter diesel equivalent

for their assessment based on grey methanol if the plant capacity is increased from 35 to 1000 kt/a, as, e.g., used by Schmitz et al. [64] **(C13-C14)**. But, as they do not give further details on the break-down of this price, it was not included in Fig. 20.

As mentioned above, shipping, marketing, and distribution costs as well as profit margins need to be added to the e-fuel production prices given above. In general, ship transport costs are almost negligible for liquid fuels, as for example shown for a hypothetical e-fuel production in Tunisia and subsequent shipping to Europe [236]. This makes the overall e-fuel production location relatively independent of its final destination, underlining the large advantage compared to gaseous fuels and electrical power. Distribution costs and retail margins are typically not public information. Numbers for petrol fuel published by the Australian government might give an indication for other markets as well though: they declared local wholesale costs plus retail margin to have been around 26 % compared to the overall fuel price before taxes in 2019 [237].

Overall, to summarize:

1. OME_x production from grey methanol is cost-competitive with fossil diesel if tax incentives are given (note that distribution costs and profit margin need to be added to the e-fuel prices for comparison with the given diesel fuel numbers).
2. For green OME_x, costs are mainly driven by H_2 (making up between around 60 % and 80 % of total cost).
3. CO_2 price impact on total fuel cost is comparably small for CO_2 from a point source, but can become a relevant cost factor for DAC.
4. Operational costs (mostly heat and electricity demand) differ significantly from pathway to pathway and can play a deciding factor, as they are generally higher for OME_x than for other e-fuels. The latter is due to production steps involving significant heat and/or compression demand.
5. Capital costs are overall low compared to operational expenses.
6. Pathways with reduced hydrogen consumption might not yet fully live up to their potential in terms of energy efficiency, as discussed in Section 6.1, but they already show promising cost advantages. Despite that, the higher TRL of the aqueous pathways might give them the overall edge for any near-term large-scale production plant development.
7. With current technology, production costs for OME_x span between 2 and 4 € per liter diesel equivalent. The difference of OME_{3-5} in particular to other e-fuels such as Fischer–Tropsch-diesel and DME needs to be compensated by their comparably advantageous fuel properties. These fuel properties and their impacts are discussed in Sections 4 and 5.

6.3. Life-cycle assessments

Determining the total life-cycle impact of a fuel is challenging, in particular, when very different propulsion systems are compared because in that case, vehicle production and end-of-life emissions need to be considered as well. The comparison of OME_x with other propulsion systems such as BEV is therefore omitted here, and the focus lies on a well-to-wheel comparison with the baseline of fossil diesel fuel.

Fig. 21 shows GW impact in gram $CO_2-eq.$ per kilometer driven for a CI-engine vehicle with a reference emission of 209 g/km under diesel operation taken from Hank et al. [238]. Table 5 gives more details about the data in Fig. 21. All data from different literature sources has been recalculated to gram CO_2-eq per kilometer driven using the same vehicle as Hank et al. [238] for better comparability. All bars start in the negative due to credited CO_2 utilization, either from air or from a point source. This CO_2 is released again either as purge stream during production or during fuel combustion. Thus, the brown parts of the bars represent the tank-to-wheel emissions, while the other three parts combined make up the well-to-tank emissions. A relative decrease of fuel consumption by 2 % with neat OME_x due to increased engine efficiency is assumed following the original work, otherwise fuel consumption was converted using the fuel's lower heating values. The CO_2 tailpipe emissions are slightly higher with OME_{3-5} and slightly lower for OME_1 in comparison with diesel fuel due to the fuel's molecular composition in combination with the lower heating values.

Scenarios **(L2-L4, L6-L11)** assume fully renewable provision of electrical power (mainly for electrolysis), representing a desirable best-case production setup. If CO_2 is provided by a point source **(L2-L4, L6, L8, L9-L11)** or direct air capture (DAC) with a low carbon footprint **(L7)**, then neat OME_x allows for significant well-to-wheel global warming potential reductions, ranging from −78 % to −95 % compared to the fossil diesel reference depending on the scenario and production pathway. In these scenarios, the GW impact due to hydrogen production is roughly of the same order as the GW impact of the subsequent liquid fuel production, which includes side product combustion and heat as well as electricity demands. The choice of production pathway does not make a significant difference in terms of carbon footprint, see **(L2-L3)** and **(L4, L6)**. If H_2 and CO_2 are provided almost burden-free, the reduced demand in case of the reductive pathway makes less of a difference in GW impact. However, the impact on cost can be significant, as shown in Section 6.2. For all scenarios discussed above, the assumptions in the original works regarding the GW impact of the supplied renewable electricity is responsible for the majority of the differences.

Production from biomass **(L5)** ends up in the same ball park as production as e-fuel using fully renewable power with a GW impact reduction of −85 % for the scenario based on forest residue [233] shown here. In this case, the H_2 bar corresponds to provision of biomass, and it was assumed that all CO_2 released during combustion of the resulting fuel was previously extracted from air by the trees. Together with the results from Section 6.2, this once again underlines the similar potential of biomass-based production, which could supplement e-fuel production to increase the amount of available fuel.

Scenarios **(L9-L10)** show the GW impact of a blend of 35 vol% OME_1 in diesel fuel [239]. Such blend composition was chosen because it gives a very good compromise between heating value of the fuel and soot reduction [26]. With such a blend, a GW impact reduction of 28 % can be achieved, while at the same time significantly reducing soot as well as nitric oxide emissions. This value is lower than the volumetric OME_1 content mostly due to the reduced LHV of OME_1 compared to diesel fuel, i.e., OME_1 only contributes around 25 % of the total LHV of the fuel blend. With OME_{3-5} and the same blending ratio, a similar GW impact reduction can be achieved **(L11)** [227]. Note that the original work by Deutz et al. [239] showed a slightly lower potential GW impact reduction due to a lower assumed carbon footprint of diesel production compared to the values used in this work from Hank et al. [238].

Finally, scenarios **(L12-L14)** were included to showcase how e-fuel production consists of a chain of sub-processes, all of which have to be based on dominantly renewable power supply to deliver a reasonable net carbon footprint reduction compared to the reference of fossil diesel. In particular, even relatively small fractions of non-renewable power in the electricity mix have a massive impact. Mantei et al. [5] **(L12-L13)** use a German grid mix from 2018 and Hank et al. [238] **(L14)** add a further 40 % fully renewable power to such a grid mix, resulting in about 500 g/kWh and 350 g/kWh GW impact burden, respectively. It is immediately obvious how such produced fuel would still be significantly worse in terms of GW impact compared to fossil diesel fuel. In fact, for a high carbon footprint of the available electricity, production of OME_x based on fossil pathways, i.e., grey methanol, becomes favorable compared to e-fuel production based on electrolysis. However, such fuel is also still significantly worse in terms of GW impact than fossil diesel (around 350 g/km), so that grey methanol-based production would only make sense on a very short time scale to ramp up industrial production already while green hydrogen supply is still low. The break point for electricity carbon footprint from which e-fuel OME_x would deliver a net climate benefit compared to fossil

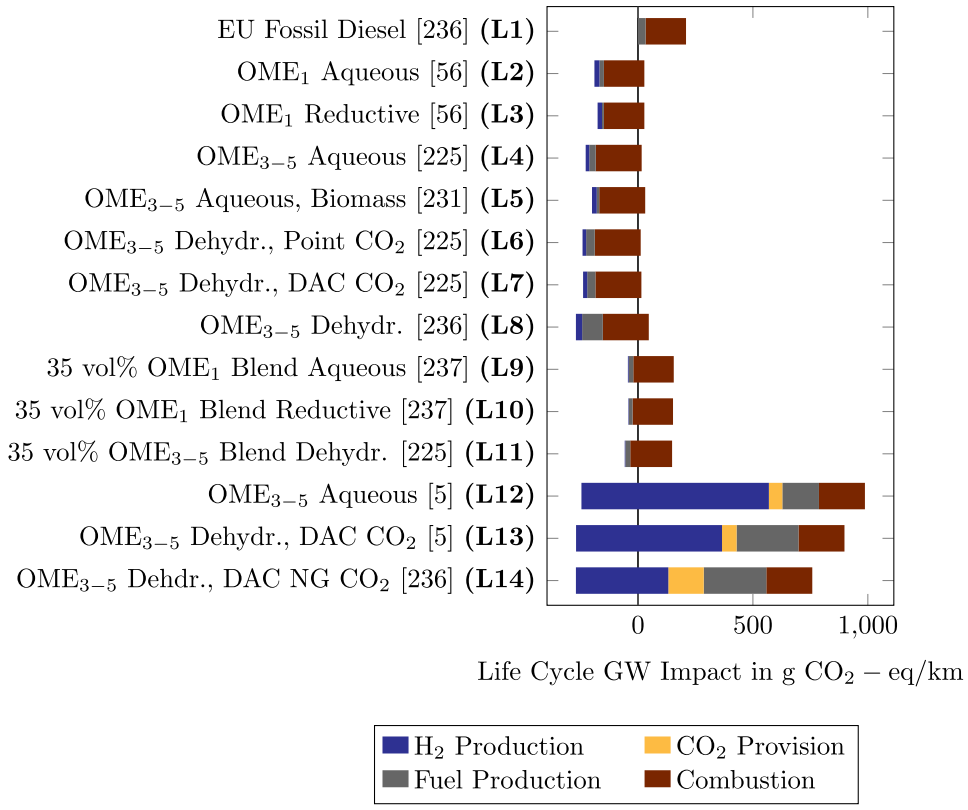

Fig. 21. OME_x well-to-wheel global warming impact compiled from literature, recomputed to the same vehicle, as well as fossil diesel as reference. **(L12-L14)** are not solely based on renewable electricity. Detailed legend in Table 5.

Table 5
Extended legend for Fig. 21.

Number	Source	Fuel	Production pathway	Comments
(L1)	Hank [238]	Fossil Diesel	–	–
(L2)	Burre [56]	OME_1	Aqueous	Onshore wind, point source
(L3)	Burre [56]	OME_1	Reductive	Onshore wind, point source
(L4)	Voelker [227]	OME_{3-5}	Aqueous	EU wind
(L5)	Mahbub [233]	OME_{3-5}	Aqueous	From forest residue
(L6)	Voelker [227]	OME_{3-5}	Dehydrogenation	EU wind, ammonia plant
(L7)	Voelker [227]	OME_{3-5}	Dehydrogenation	EU wind, DAC
(L8)	Hank [238]	OME_{3-5}	Dehydrogenation	Hydro + renewables, biomethane plant incl. avoided burden
(L9)	Deutz [239]	35 vol% OME_1	Aqueous	EU wind, biogas plant
(L10)	Deutz [239]	35 vol% OME_1	Reductive	EU wind, biogas plant
(L11)	Voelker [227]	35 vol% OME_{3-5}	Dehydrogenation	EU wind, ammonia plant
(L12)	Mantei [5]	OME_{3-5}	Aqueous	German grid 2018, DAC
(L13)	Mantei [5]	OME_{3-5}	Dehydrogenation	German grid 2018, DAC
(L14)	Hank [238]	OME_{3-5}	Dehydrogenation	2018 grid + renewables, DAC natural gas

diesel on a well-to-wheel assessment is at around 90–140 g/kWh for OME_{3-5} [5,227,238] and around 120–200 g/kWh for OME_1 [56,239].

If DAC is used for CO_2 provision and heat demand is covered by natural gas **(L14)** instead of fully renewable power **(L8)**, well-to-wheel GW impact rises by 114 g $CO_{2,eq}$/km [238]. For the synthesis steps, covering the heat demand by natural gas increases GW impact by 104 g $CO_{2,eq}$/km compared to an electricity-based heat supply based on a dominantly renewable grid [238]. The sum of these two contributions would exceed current well-to-wheel emissions of fossil diesel, emphasizing that utilization of green hydrogen alone does not automatically lead to a green fuel.

Finally, as production of large quantities of e-fuels will likely be concentrated in regions with high renewable power potential, transport of e-fuels to the final customer over long distances might be required. For example, supply of Central Europe with e-fuels from the Middle East and North Africa region would result in additional shipping emissions not included in the assessments above. However, energy consumption for shipping liquid fuels, and thus also corresponding CO_2 emissions, are almost negligible in comparison to the fuel's heating value [240].

6.4. Policies and market introduction

Technological solutions for defossilization in transport, heating, cooking, and industrial applications also need to take energy availability, cost, and infrastructure into account, which might require different measures in order to accelerate the transition to CO_2 neutrality. Recent

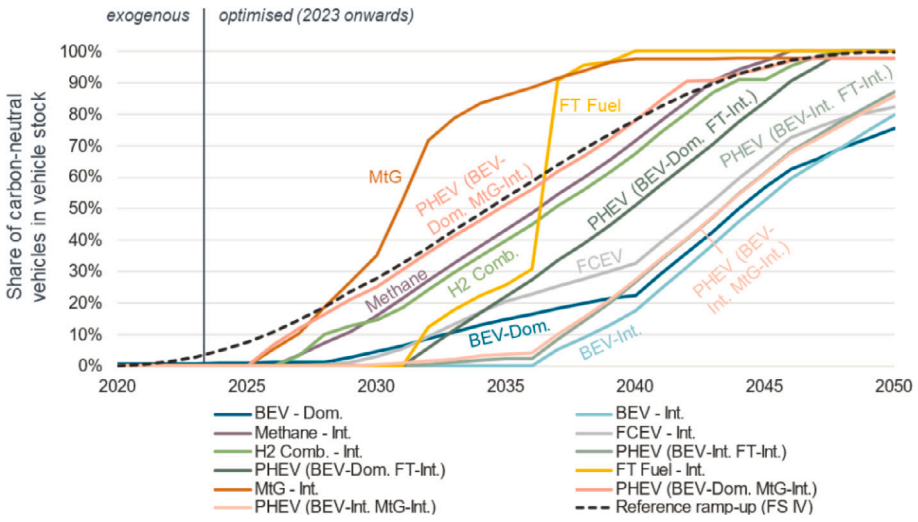

Fig. 22. GHG-neutral vehicle ramp-up for various single technology powertrain solutions presented by FVV [243]. Abbreviations: "BEV" - Battery Electric Vehicles, "PHEV" - Plug-in Hybrid Electric Vehicles, "FT" - Fischer–Tropsch, "MtG" - Methanol to Gasoline, "FCEV" - Fuel Cell Electric Vehicle, "H2 Comb." - Hydrogen ICE. "Dom." corresponds to domestic energy sourcing, "Int." to international energy sourcing. "FS IV" refers to the underlying FVV Fuels Study IV [242].

studies for transport applications [241–243] have shown that low carbon fuels are key for defossilizing the fleet of vehicles in service (currently around 1.3 billion globally), which are dominating the CO_2-emissions in transport. Those vehicles, which typically have a lifetime of 15–20 years, will still emit CO_2 for a long time even if the sale of ICE-powered vehicles would be stopped immediately. As a recent study [243] has shown, the rate of defossilization on the basis of life-cycle-GHG emissions is a function of how quickly CO_2-neutral powertrain solutions can be introduced into the transport sector. This exemplary study focused on the European transport sector, where the results were derived mostly from German references. Regional differences in Europe were not examined. Fig. 22 shows the share of carbon-neutral vehicles in the European fleet, taking into account the rate of introduction of carbon-neutral powertrain technologies and energy sources. In 2020, essentially all vehicles were powered by fossil-based products that need to be replaced, as these vehicles will remain on the road for some time. It can be seen that methanol-based fuels like MtG (Methanol-to-Gasoline) have the potential to reduce CO_2-emissions significantly earlier than electrified solutions, since they would already have an effect in the existing vehicle fleet. For diesel applications, methanol-based fuels like DME or OME_x had not been considered. However, it can be assumed that they would also support a faster rate of defossilization in transport and beyond.

As already indicated, the speed of bringing CO_2-neutral fuels to the market has to be increased in order to achieve carbon neutrality early while electrified solutions just slowly penetrate the vehicle stock. However, in order to accelerate fuel-production and market introduction, the regulatory boundary conditions, standards, and policies need to be in place in order to guarantee investment security. On a high level, e-fuels have the significant advantage of comparably cheap and simple energy storage and transport compared to electricity. Current energy-importing countries will likely still import energy also in the long term, e.g., for Germany, imports of around 25 % of the total energy demand are still expected in a fully climate neutral scenario in 2045 [244]. For central Europe, import of hydrogen or synthetic fuels from MENA (Middle East and North Africa) or other regions with significant resources of renewable energy is a likely and possible solution to close the gap between energy demand and domestic production, even though cost competitiveness with local production relies on relatively cheap transport [245]. Allocation of the imported chemical energy carriers to the different applications in industry and transportation, in competition with direct electrification using domestic renewable power, will be a challenging task, and e-fuels such as OME_x can potentially make very important contributions both for the existing fleet and new vehicles. Introducing new fuels like OME_x can be quite challenging, and many other promising fuels never made it to the market. Existing standards for Diesel-like fuels (i.e., EN590 in Europe for Diesel) do not comply with new fuels such as neat OME_x. This is particularly true for the volatile OME_1. Therefore, new fuel standards have to be developed, which usually is very time consuming. For DME and OME_x, technical specifications have been developed globally in recent years. But before those fuels can be sold or used in new vehicles, they have to be included in relevant regulations so that they can become legal products in the relevant regions. In Europe, for example, they would need to be part of the RED (renewable energy directive), the AFID (alternative fuels infrastructure directive), the CVD (clean vehicles directive) and they have to be included in the type approval for vehicles. These processes are very complex and require a good understanding of the relevant steps. An overview of the complex regulation network, which needs to be considered, was discussed by Grüniger et al. [246]. The major roadblock, however, for opening up the renewable fuel market are the CO_2 regulations, which are mostly tank-to-wheel-based, meaning that the vehicle-CO_2 emissions themselves need to be reduced independent of how the energy carrier was produced (fossil or renewable). Although it has been well accepted that sustainable fuels are required for defossilizing the transport sector, fuel producers are hesitating to invest because their perspective of having a profitable business when CO_2-reduction from renewable fuels is not counted is very poor. In recent years, crediting mechanisms have been discussed allowing the car manufacturers to subsidize renewable fuel production [247]. However, the European commission stated that such a system would counteract the CO_2-saving measures and create a significant administrative overhead, and thereby did not recommend to adopt these proposed amendments to the standards. Recently, discussions in European authorities, who originally had decided to phase out ICE-powered cars beyond 2035 by restricting the Tank-to-Wheel-CO_2-Output, have started to allow ICE-powered vehicles beyond 2035 if they are fueled by carbon-neutral RFNBO (renewable fuels of non-biological origin) fuels. Consultations on how those RFNBOs are defined and what a technical implementation could look like are ongoing. Synthetic fuels like renewable OME_x, DME, or methanol would be ideal candidates for those applications and could play a major role.

On the commercial vehicle side, the phase-out of conventional diesel engines will likely be significantly later with, e.g., an alliance of truck makers consisting of Daimler, Scania, MAN, Volvo, DAF, Iveco and Ford, announcing a target of 2040 for fossil-free commercial

trucks [248]. Full electrification of these vehicles will remain challenging, and both hydrogen and renewable fuels will likely play a role [249]. This includes a chance for $OME_{x\geq 2}$, potentially both as blend component in conventional diesel fuel to already reduce pollutant and CO_2 emissions on the road to 2040, and as a neat fuel for long-range commercial CI engines from 2040 onwards. As the introduction of pure electrification for heavy-duty vehicles is more challenging, synthetic fuel solutions are a very reasonable option, especially for long-haul applications. This is currently being discussed in the political debate on future CO_2 regulations for heavy-duty vehicles, for example in Europe.

Other potential markets for OME_x include stationary diesel engines, e.g., for backup power production, and ship engines. In particular for the latter, solutions to decarbonization are further away from market readiness, and considering the long service time of most vessels, a retrofit of an existing engine during a scheduled major overhaul might be an attractive option. Again, a seamless transition between fossil and green fuel is possible, and significant pollutant emission reduction can be achieved on the way.

7. Conclusions

Only few e-fuels have acquired as much research attention as oxymethylene ethers, and this review attempts to provide a thorough, compact and consolidated overview and assessment of recent research progress in all steps along the life cycle of OME_x, ranging from production to application. Also possible future research directions have been provided at the end of each of the major sections of this review.

In Section 2, the various production pathways and their individual advantages in terms of production efficiencies and costs were discussed. In particular, the life cycle assessments summarized and compared in Section 6.3 showed first that OME_x have significant potential to reduce the climate impact of road transport, if produced under the right circumstances, i.e., using predominantly renewable energy, and second that it is also competitive to other e-fuels if advanced, more efficient production pathways are utilized. This underlined the necessity to focus research on these production pathways, and quickly bring them to higher technology readiness levels for large scale production. Section 3 showed that, over the recent years, tremendous progress was made in understanding the combustion reaction kinetics of OME_x, allowing for high-fidelity simulations necessary to further our understanding of the combustion processes. However, a lack of reduced but still accurate kinetic mechanisms for OME_x and blends of it with, e.g., fossil diesel is currently limiting the possibilities for CFD-based parameter studies to optimize engine geometries and controls for full utilization of the potential of OME_x. The challenges for engine combustion associated with the fuel properties of OME_x were discussed in Section 4. Particular attention was also paid to the material compatibility, which remains a challenge for retrofitting existing engines to be compatible with OME_x fuels, also showcasing that appropriate materials for sealing and tubing exist. Finally, in Section 5, the vast amount of literature data regarding engine performance and emissions was reviewed and compared in an attempt to both highlight the potential of OME_x as well as to investigate which changes to engines must or should be made to utilize this potential. Additionally, especially the super-linear soot reduction of OME_x in fuel blends was discussed in detail. It was shown that this soot reduction potential can be utilized to also drastically reduce nitric oxide emissions, but this requires knowledge of the OME_x content in the fuel and based on this, appropriate changes to the engine control system. With neat OME_x, PM emissions significantly below Euro VI and even below the discussed Euro VII limits can be achieved without aftertreatment, and in combination with a state-of-the-art SCR NO_x emissions can be reduced by more than an order of magnitude compared to Euro VI legislation to almost the detection limit.

OME_x, with the exception of the volatile OME_1, can be regarded as promising blend components when the material compatibility of the engine and engine components is ensured. In Section 4.1.9 we have established that appropriate materials exist. If suitably designed, future diesel vehicles could run on increasing shares of OME_x with minor changes to engine control parameters such as injection duration, timing, and EGR rate relative to conventional diesel fuel. However, potential savings from a simplified exhaust aftertreatment system made possible by OME_x emission reduction can only be realized if the minimum OME_x blend fraction is known during vehicle design. However, smaller savings due to, e.g., less demand for SCR aftertreatment can also be achieved if the share of OME_x changes throughout the vehicle life time, as long as it is known during operation. In any case, possible savings in the aftertreatment system are likely offset by increased fuel costs. For existing vehicles, a retro-fit of sealing and fuel piping materials is also possible. This might enable older vehicles to meet today's more stringent pollutant emission standards, while at the same time reducing well-to-wheel CO_2 emissions, if OME_x is utilized in the fuel. This might also increase the life time of current vehicles as vehicle owners living or working in low emission zones are not forced to switch to a newer model, reducing the global warming impact of new vehicle production. To fully leverage the soot and nitric oxide emission reduction potential lined out in Sections 5.3 and 5.4, knowledge of the OME_x content in the fuel and, based on this, appropriate changes to the engine control system are required.

We have also shown in Section 6.3 that OME_x produced using renewable energy throughout the entire production chain can achieve significant reductions of well-to-wheel green house gas emissions by more than 90 % compared to a fossil diesel base case. From a GWP perspective, such an e-fuel is thus more than capable of achieving the desired reduction in well-to-wheel CO_2 emissions to reach current climate change prevention goals. As showcased in Sections 6.1 and 6.2, in particular the advanced production pathways for OME_x can also be competitive in terms of production efficiency compared to other e-fuel candidates if the advanced production pathways are utilized and the net heat demand can be efficiently covered. For the latter, e.g., usage of low-exergy waste heat from other industrial processes would be desirable to reduce the demand of high-exergy H_2 or water for heat generation. Even without such measures, high energetic production efficiencies of up to around 60 % are estimated in the literature. In terms of production costs, OME_x are more expensive than other e-fuels such as methanol, DME, or FT-diesel, with costs between around 2 and 4 € per liter diesel equivalent. However, they also have significant application advantages compared to them, such as massive soot reduction compared to FT-diesel and advantageous liquid fuel properties compared to DME and methanol such as lubricity, handling, and toxicity.

The simultaneous reduction of pollutant emissions and GHG envisioned for different applications in the mobility sector requires a range of technological solutions to find a good compromise providing GHG reduction with minimum social challenges and costs. Several sustainable forms of energy including electricity, hydrogen, but also synthetic fuels such as OME_x could be valid alternatives. In order to evaluate their impact on GHG reduction, they need to be compared on a cradle-to-grave basis. At present, particularly in the transportation sector, solutions are compared on a tailpipe basis (tank-to-wheel), which does not consider the large scale environmental impacts, for instance in terms of carbon emissions, associated with well-to-wheel part of the energy and the difference in vehicle production. Appropriate regulation (i.e., including emissions trading in the transport sector) would be helpful globally and could minimize the cost of the required transition to a carbon-neutral society. In addition to electrification, especially for the defossilization of the existing fleet in the transportation sector, carbon neutral fuels, such as OME_x, are needed. The different technologies are not in competition with each other, but are rather complementary to provide efficient, cost-effective solutions in a timely manner. However, to enable these technologies for any of the potential applications discussed in the preceding Section 6, the numerous remaining research questions lined out in this review will have to be addressed.

CRediT authorship contribution statement

Heinz Pitsch: Writing – review & editing, Writing – original draft, Methodology, Investigation, Conceptualization. **Dominik Goeb:** Writing – review & editing, Writing – original draft, Methodology, Investigation, Conceptualization. **Liming Cai:** Writing – review & editing, Writing – original draft, Methodology, Investigation, Conceptualization. **Werner Willems:** Writing – review & editing, Writing – original draft, Methodology, Investigation, Conceptualization.

Declaration of competing interest

The authors declare the following financial interests/personal relationships which may be considered as potential competing interests: Werner Willems reports financial support was provided by Ford-Werke GmbH.

Data availability

Data will be made available on request.

Acknowledgments

This work was funded by the Deutsche Forschungsgemeinschaft, Germany (DFG, German Research Foundation) under Germany's Excellence Strategy - Cluster of Excellence 2186 "The Fuel Science Center" - ID: 390919832.

References

[1] International Energy Agency. Tracking transport 2020. 2020, URL https://www.iea.org/reports/tracking-transport-2020.
[2] International Energy Agency. Fuel consumption of cars and vans. 2020, URL https://www.iea.org/reports/fuel-consumption-of-cars-and-vans.
[3] Held M, Tönges Y, Pélerin D, Härtl M, Wachtmeister G, Burger J. On the energetic efficiency of producing polyoxymethylene dimethyl ethers from CO_2 using electrical energy. Energy Environ Sci 2019;12(3):1019–34.
[4] Schemme S, Breuer JL, Köller M, Meschede S, Walman F, Samsun RC, et al. H_2-based synthetic fuels: A techno-economic comparison of alcohol, ether and hydrocarbon production. Int J Hydrogen Energy 2020;45(8):5395–414.
[5] Mantei F, Ali RE, Baensch C, Voelker S, Haltenort P, Burger J, et al. Techno-economic assessment and carbon footprint of processes for the large-scale production of oxymethylene dimethyl ethers from carbon dioxide and hydrogen. Sustain Energy Fuels 2022.
[6] Peters JF, Baumann M, Zimmermann B, Braun J, Weil M. The environmental impact of Li-Ion batteries and the role of key parameters–A review. Renew Sustain Energy Rev 2017;67:491–506.
[7] Andwari AM, Pesiridis A, Rajoo S, Martinez-Botas R, Esfahanian V. A review of battery electric vehicle technology and readiness levels. Renew Sustain Energy Rev 2017;78:414–30.
[8] Yilmaz M, Krein PT. Review of battery charger topologies, charging power levels, and infrastructure for plug-in electric and hybrid vehicles. IEEE Trans Power Electron 2012;28(5):2151–69.
[9] Den Boer E, Aarnink S, Kleiner F, Pagenkopf J. Zero emissions trucks: An overview of state-of-the-art technologies and their potential. CE Delft, German Aerospace Center (DLR), International Council on Clean Transportation (ICCT); 2013.
[10] Mareev I, Becker J, Sauer DU. Battery dimensioning and life cycle costs analysis for a heavy-duty truck considering the requirements of long-haul transportation. Energies 2018;11(1):55.
[11] de Tena DL, Pregger T. Impact of electric vehicles on a future renewable energy-based power system in Europe with a focus on Germany. Int J Energy Res 2018;42(8):2670–85.
[12] Agarwal AK, Gupta JG, Dhar A. Potential and challenges for large-scale application of biodiesel in automotive sector. Prog Energy Combust Sci 2017;61:113–49.
[13] Wiebe K, Croppenstedt A, Raney T, Skoet J, Zurek M, Tschirley J. Biofuels: Prospects risks and opportunities. State Food Agric 2008;55–71.
[14] Eisentraut A. Sustainable production of second-generation biofuels: Potential and perspectives in major economies and developing countries. International Energy Agency; 2010.
[15] Oguchi M, Fuse M. Regional and longitudinal estimation of product lifespan distribution: A case study for automobiles and a simplified estimation method. Environ Sci Technol 2015;49(3):1738–43.
[16] Bothe D, Steinfort T. Cradle-to-grave-lebenszyklusanalyse im mobilitätssektor. metastudie zur CO_2-bilanz alternativer fahrzeugantriebe. Tech. rep., Forschungsvereinigung Verbrennungskraftmaschinen e. V. Frankfurt a. M; 2020.
[17] Frank J, Brown T, Ha H, Slade D, Haverly M, Malmsheimer R. Quantifying and comparing the cumulative greenhouse gas emissions and financial viability of heavy-duty transportation pathways for the Northeastern United States. Fuel 2022;323:124243.
[18] Westbrook CK, Pitz WJ, Curran HJ. Chemical kinetic modeling study of the effects of oxygenated hydrocarbons on soot emissions from diesel engines. J Phys Chem A 2006;110(21):6912–22.
[19] Leitner W, Klankermayer J, Pischinger S, Pitsch H, Kohse-Höinghaus K. Advanced biofuels and beyond: Chemistry solutions for propulsion and production. Angew Chem Int Ed 2017;56(20):5412–52.
[20] Weaver Jr FL, Hough AR, Highman B, Fairhall LT. The toxicity of methylal. Br J Ind Med 1951;8(4):279.
[21] Natarajan M, Frame EA, Naegeli DW, Asmus T, Clark W, Garbak J, et al. Oxygenates for advanced petroleum-based diesel fuels: Part 1. Screening and selection methodology for the oxygenates. SAE Trans 2001;2221–45.
[22] Delfort B, Durand I, Jaecker-Voirol A, Lacôme T, Paillé F, Montagne X. Oxygenated compounds and diesel engine pollutant emissions performances of new generation of products. SAE Trans 2002;1871–80.
[23] Tree DR, Svensson KI. Soot processes in compression ignition engines. Progress Energy Combus Sci 2007;33(3):272–309.
[24] Härtl M, Seidenspinner P, Jacob E, Wachtmeister G. Oxygenate screening on a heavy-duty diesel engine and emission characteristics of highly oxygenated oxymethylene ether OME1. Fuel 2015;153:328–35.
[25] Lautenschütz L, Oestreich D, Seidenspinner P, Arnold U, Dinjus E, Sauer J. Physico-chemical properties and fuel characteristics of oxymethylene dialkyl ethers. Fuel 2016;173:129–37.
[26] Omari A, Heuser B, Pischinger S. Potential of oxymethylenether-diesel blends for ultra-low emission engines. Fuel 2017;209:232–7.
[27] Schröder J, Görsch K. Storage stability and material compatibility of poly (oxymethylene) dimethyl ether diesel fuel. Energy Fuels 2019;34(1):450–9.
[28] Romano U, Terzoni G, Ancillotti F, Giavazzi F. Extenders for gasoil for automotive use. 1985, WO1986003511A1.
[29] Moulton DS, Naegeli DW. Diesel fuel having improved qualities and method of forming. 1998, US5746785A.
[30] Fleisch TH, Sills RA. Large-scale gas conversion through oxygenates: Beyond GTL-FT. In: Studies in surface science and catalysis, vol. 147, Elsevier; 2004, p. 31–6.
[31] Liu Y, Tian J, Song Z, Li F, Zhou W, Lin Q. Spray characteristics of diesel, biodiesel, polyoxymethylene dimethyl ethers blends and prediction of spray tip penetration using artificial neural network. Phys Fluids 2022;34(1).
[32] German Federal Ministry of Education and Research. Kopernikus power–to–X–project. 2020, URL https://www.kopernikus-projekte.de/en/projects/p2x.
[33] German Federal Ministry of Education and Research. Namosyn. 2020, URL http://namosyn.de/.
[34] Azizi Z, Rezaeimanesh M, Tohidian T, Rahimpour MR. Dimethyl ether: A review of technologies and production challenges. Chem Eng Process: Process Intensif 2014;82:150–72.
[35] Semelsberger TA, Borup RL, Greene HL. Dimethyl ether (DME) as an alternative fuel. J Power Sources 2006;156(2):497–511.
[36] Bartholet DL, Arellano-Treviño MA, Chan FL, Lucas S, Zhu J, John PCS, et al. Property predictions demonstrate that structural diversity can improve the performance of polyoxymethylene ethers as potential bio-based diesel fuels. Fuel 2021;295.
[37] Lucas SP, Chan FL, Fioroni GM, Foust TD, Gilbert A, Luecke J, et al. Fuel properties of oxymethylene ethers with terminating groups from methyl to butyl. Energy Fuels 2022.
[38] Arellano-Trevino MA, Bartholet D, To AT, Bartling AW, Baddour FG, Alleman TL, et al. Synthesis of butyl-exchanged polyoxymethylene ethers as renewable diesel blendstocks with improved fuel properties. ACS Sustain Chem Eng 2021;9(18):6266–73.
[39] Arellano-Treviño MA, Alleman TL, Brim R, To AT, Zhu J, McEnally CS, et al. Blended fuel property analysis of butyl-exchanged polyoxymethylene ethers as renewable diesel blendstocks. Fuel 2022;322:124220.
[40] European Council. Technology readiness levels. 2022, URL https://ec.europa.eu/research/participants/data/ref/h2020/wp/2014_2015/annexes/h2020-wp1415-annex-g-trl_en.pdf.
[41] Peters R. Identification and thermodynamic analysis of reaction pathways of methylal and OME-n formation. Energy 2017;138:1221–46.
[42] Hackbarth K, Haltenort P, Arnold U, Sauer J. Recent progress in the production, application and evaluation of oxymethylene ethers. Chem Ingenieur Tech 2018;90(10):1520–8.
[43] ICIS chemical business 2017–2018: Chemical profile special. 2018.
[44] Verhelst S, Turner JW, Sileghem L, Vancoillie J. Methanol as a fuel for internal combustion engines. Prog Energy Combust Sci 2019;70:43–88.
[45] Bozzano G, Manenti F. Efficient methanol synthesis: Perspectives, technologies and optimization strategies. Progress Energy Combust Sci 2016;56:71–105.

[46] Wu J, Zhu H, Wu Z, Qin Z, Yan L, Du B, et al. High Si/Al ratio HZSM-5 zeolite: An efficient catalyst for the synthesis of polyoxymethylene dimethyl ethers from dimethoxymethane and trioxymethylene. Green Chem 2015;17(4):2353–7.

[47] Zhang X, Kumar A, Arnold U, Sauer J. Biomass-derived oxymethylene ethers as diesel additives: A thermodynamic analysis. Energy Procedia 2014;61:1921–4.

[48] Damyanov A, Hofmann P, Geringer B, Schwaiger N, Pichler T, Siebenhofer M. Biogenous ethers: Production and operation in a diesel engine. Automot Eng Technol 2018;3(1):69–82.

[49] Baranowski CJ, Bahmanpour AM, Kröcher O. Catalytic synthesis of polyoxymethylene dimethyl ethers (OME): A review. Appl Catal B 2017;217:407–20.

[50] Banivaheb S, Pitter S, Delgado KH, Rubin M, Sauer J, Dittmeyer R. Recent progress in direct DME synthesis and potential of bifunctional catalysts. Chem Ing Tech 2022;94(3):240–55.

[51] Reuss G, Disteldorf W, Gamer A, Hilt A. Formaldehyde. In: Ullmann's encyclopedia of industrial chemistry. Wiley-VCH; 2012.

[52] Drunsel J-O, Renner M, Hasse H. Experimental study and model of reaction kinetics of heterogeneously catalyzed methylal synthesis. Chem Eng Res Des 2012;90(5):696–703.

[53] Schmitz N, Burger J, Hasse H. Reaction kinetics of the formation of poly (oxymethylene) dimethyl ethers from formaldehyde and methanol in aqueous solutions. Ind Eng Chem Res 2015;54(50):12553–60.

[54] Schmitz N, Homberg F, Berje J, Burger J, Hasse H. Chemical equilibrium of the synthesis of poly (oxymethylene) dimethyl ethers from formaldehyde and methanol in aqueous solutions. Ind Eng Chem Res 2015;54(25):6409–17.

[55] Ouda M, Yarce G, White R, Hadrich M, Himmel D, Schaadt A, et al. Poly (oxymethylene) dimethyl ether synthesis–A combined chemical equilibrium investigation towards an increasingly efficient and potentially sustainable synthetic route. React Chem Eng 2017;2(1):50–9.

[56] Burre J, Bongartz D, Deutz S, Mebrahtu C, Osterthun O, Sun R, et al. Comparing pathways for electricity-based production of dimethoxymethane as a sustainable fuel. Energy Environ Sci 2021.

[57] Thavornprasert K-a, Capron M, Jalowiecki-Duhamel L, Dumeignil F. One-pot 1 1-dimethoxymethane synthesis from methanol: A promising pathway over bifunctional catalysts. Catal Sci Technol 2016;6(4):958–70.

[58] Thenert K, Beydoun K, Wiesenthal J, Leitner W, Klankermayer J. Ruthenium-catalyzed synthesis of dialkoxymethane ethers utilizing carbon dioxide and molecular hydrogen. Angew Chem 2016;128(40):12454–7.

[59] Schieweck BG, Klankermayer J. Tailor-made molecular cobalt catalyst system for the selective transformation of carbon dioxide to dialkoxymethane ethers. Angew Chem Int Ed 2017;56(36):10854–7.

[60] Ouda M, Mantei FK, Elmehlawy M, White RJ, Klein H, Fateen S-EK. Describing oxymethylene ether synthesis based on the application of non-stoichiomsetric Gibbs minimisation. React Chem Eng 2018;3(3):277–92.

[61] Ouda M, Mantei F, Hesterwerth K, Bargiacchi E, Klein H, White RJ. A hybrid description and evaluation of oxymethylene dimethyl ethers synthesis based on the endothermic dehydrogenation of methanol. React Chem Eng 2018;3(5):676–95.

[62] Sun R, Mebrahtu C, Hofmann JP, Bongartz D, Burre J, Gierlich CH, et al. Hydrogen-efficient non-oxidative transformation of methanol into dimethoxymethane over a tailored bifunctional Cu catalyst. Sustain Energy Fuels 2021;5(1):117–26.

[63] Omari A, Heuser B, Pischinger S, Rüdinger C. Potential of long-chain oxymethylene ether and oxymethylene ether-diesel blends for ultra-low emission engines. Appl Energy 2019;239:1242–9.

[64] Schmitz N, Burger J, Ströfer E, Hasse H. From methanol to the oxygenated diesel fuel poly (oxymethylene) dimethyl ether: An assessment of the production costs. Fuel 2016;185:67–72.

[65] Burger J, Siegert M, Ströfer E, Hasse H. Poly (oxymethylene) dimethyl ethers as components of tailored diesel fuel: Properties, synthesis and purification concepts. Fuel 2010;89(11):3315–9.

[66] Arvidson M, Fakley M, Spencer M. Lithium halide-assisted formation of polyoxymethylene dimethyl ethers from dimethoxymethane and formaldehyde. J Mol Catal 1987;41(3):391–3.

[67] Haltenort P, Hackbarth K, Oestreich D, Lautenschütz L, Arnold U, Sauer J. Heterogeneously catalyzed synthesis of oxymethylene dimethyl ethers (OME) from dimethyl ether and trioxane. Catal Commun 2018;109:80–4.

[68] Breitkreuz CF, Hevert N, Schmitz N, Burger J, Hasse H. Synthesis of methylal and poly (oxymethylene) dimethyl ethers from dimethyl ether and trioxane. Ind Eng Chem Res 2022.

[69] Vermeire FH, Carstensen H-H, Herbinet O, Battin-Leclerc F, Marin GB, Van Geem KM. Experimental and modeling study of the pyrolysis and combustion of dimethoxymethane. Combust Flame 2018;190:270–83.

[70] He T, Wang Z, You X, Liu H, Wang Y, Li X, et al. A chemical kinetic mechanism for the low- and intermediate-temperature combustion of Polyoxymethylene Dimethyl Ether 3 (PODE3). Fuel 2018;212:223–35.

[71] Jacobs S, Döntgen M, Alquaity A, Kopp W, Kröger L, Burke U, et al. Detailed kinetic modeling of dimethoxymethane. Part II: Experimental and theoretical study of the kinetics and reaction mechanism. Combust Flame 2019;205:522–33.

[72] Peukert S, Sela P, Nativel D, Herzler J, Fikri M, Schulz C. Direct measurement of high-temperature rate constants of the thermal decomposition of dimethoxymethane. a shock tube and modeling study, the Journal of Physical Chemistry A 2018;122:7559–71.

[73] Golka L, Weber I, Olzmann M. Pyrolysis of dimethoxymethane and the reaction of dimethoxymethane with h atoms: A shock-tube/ARAS/TOF-MS and modeling study. Proceedings of the Combustion Institute 2019;37:179–87.

[74] Golka L, Gratzfeld D, Weber I, Olzmann M. Temperature- and pressure-dependent kinetics of the competing C–o bond fission reactions of dimethoxymethane. Phys Chem Chem Phys 2020;22:5523–30.

[75] Li N, Sun W, Liu S, Qin X, Zhao Y, Wei Y, et al. A comprehensive experimental and kinetic modeling study of dimethoxymethane combustion. Combust Flame 2021;233.

[76] Sun W, Wang G, Li S, Zhang R, Yang B, Yang J, et al. Speciation and the laminar burning velocities of poly (oxymethylene) dimethyl ether 3 (POMDME3) flames: An experimental and modeling study. Proceedings of the Combustion Institute 2017;36(1):1269–78.

[77] Cai L, Jacobs S, Langer R, vom Lehn F, Heufer KA, Pitsch H. Auto-ignition of oxymethylene ethers (OMEn. n=2–4) as promising synthetic e-fuels from renewable electricity: shock tube experiments and automatic mechanism generation, Fuel 2020;264.

[78] Burke S, Burke U, McDonagh R, Mathieu O, Osario I, Keesee C, et al. An experimental and modeling study of propene oxidation. Part 2: Ignition delay time and flame speed measurements, Combustion and Flame 2015;162:296–314.

[79] Daly CA, Simmie JM, Dagaut P, Cathonnet M. Oxidation of dimethoxymethane in a jet-stirred reactor. Combustion and flame 2001;125(3):1106–17.

[80] Dias V, Lories X, Vandooren J. Lean and rich premixed dimethoxymethane/oxygen/argon flames: Experimental and modeling. Combust. Sci. Technol. 2010;182(4–6):350–64.

[81] Marrodán L, Royo E, Millera A, Bilbao R, Alzueta M. High pressure oxidation of dimethoxymethane. Energy Fuels 2015;29:3507–17.

[82] Marrodán L, Monge F, Millera Á, Bilbao R, Alzueta MU. Dimethoxymethane oxidation in a flow reactor. Combustion Science and Technology 2016;188(4–5):719–29.

[83] Kopp W, Kröger L, Döntgen M, Jacobs S, Burke U, Curran H, et al. Detailed kinetic modeling of dimethoxymethane. Part I: *Ab initio* thermochemistry and kinetics predictions for key reactions, Combustion and Flame 2018;189:433–42.

[84] Al-Otaibi JS, Abdel-Rahman MA, Almuqrin AH, El-Gogary TM, Mahmoud MA, El-Nahas AM. Thermo-kinetic theoretical studies on pyrolysis of dimethoxymethane fuel additive. Fuel 2021;290.

[85] Döntgen M, Fuller M, Peukert S, Nativel D, Schulz C, Heufer K, et al. Shock tube study of the pyrolysis kinetics of Di- and trimethoxy methane. Combust Flame 2022;112186:242.

[86] Shrestha K, Krishna P, Eckart S, Elbaz A, Giri B, Fritsche C, et al. A comprehensive kinetic model for dimethyl ether and dimethoxymethane oxidation and NO_x interaction utilizing experimental laminar flame speed measurements at elevated pressure and temperature. Combust Flame 2020;218:57–74.

[87] Curran H, Gaffuri P, Pitz W, Westbrook C. A comprehensive modeling study of *n*-heptane oxidation. Combust Flame 1998;114:149–77.

[88] Westbrook C, Pitz W, Herbinet O, Curran H, Silke E. A comprehensive detailed chemical kinetic reaction mechanism for combustion of *n*-alkane hydrocarbons from *n*-octane to *n*-hexadecane. Combust Flame 2009;156:181–99.

[89] Sarathy S, Westbrook C, Mehl M, Pitz W, Togbé C, Dagaut P, et al. Comprehensive chemical kinetic modeling of the oxidation of 2-methylalkanes from C_7 to C_{20}. Combust Flame 2011;158:2338–57.

[90] Drost S, Schießl R, Werler M, Sommerer J, Maas U. Ignition delay times of polyoxymethylene dimethyl ether fuels (OME_2 and OME_3) and air: Measurements in a rapid compression machine. Fuel 2019;258.

[91] Cai L, Pitsch H. Mechanism optimization based on reaction rate rules. Combust Flame 2014;161:405–15.

[92] Cai L, Pitsch H. Optimized chemical mechanism for combustion of gasoline surrogate fuels. Combust Flame 2015;162(5):1623–37.

[93] Kathrotia T, Oßwald P, Nauman C, Richter S, Köhler M. Combustion kinetics of alternative jet fuels. Part-II: Reaction model for fuel surrogate. Fuel 2021;302:120736.

[94] De Ras K, Kusenberg M, Vanhove G, Fenard Y, Eschenbacher A, Varghese R, et al. A detailed experimental and kinetic modeling study on pyrolysis and oxidation of oxymethylene ether-2 (OME-2). Combust Flame 2022;238.

[95] Vandewiele N, Van Geem K, Reyniers M-F, Marin G. Genesys: Kinetic model construction using chemo-informatics. Chem Eng J 2012;207–208:526–38.

[96] Shrestha KP, Eckart S, Drost S, Fritsche C, Schießl R, Seidel L, et al. A comprehensive kinetic modeling of oxymethylene ethers (omen, n=1–3) oxidation-laminar flame speed and ignition delay time measurements. Combust Flame 2022;246:112426.

[97] Fenard Y, Vanhove G. A mini-review on the advances in the kinetic understanding of the combustion of linear and cyclic oxymethylene ethers. Energy Fuels 2021;35(18):14325–42.

[98] De Ras K, Kusenberg M, Thybaut JW, Van Geem KM. Unraveling the carbene chemistry of oxymethylene ethers: Experimental investigation and kinetic modeling of the high-temperature pyrolysis of ome-2. Proc Combust Inst 2023;39(1):125–33.

[99] Zhong X, Wang H, Zuo Q, Zheng Z, Wang J, Yin W, et al. Experimental and kinetic modeling studies of polyoxymethylene dimethyl ether (PODE) pyrolysis in jet stirred reactor. J Anal Appl Pyrolysis 2021;159:105332.

[100] He T, Liu H-Y, Wang Y, Wang B, Liu H, Wang Z. Development of surrogate model for oxygenated wide-distillation fuel with polyoxymethylene dimethyl ether. SAE Int J Fuels Lubr 2017;10(3).

[101] Ren S, Wang Z, Li B, Liu H, Wang J. Development of a reduced polyoxymethylene dimethyl ethers (PODEn) mechanism for engine applications. Fuel 2019;238:208–24.

[102] Huang H, Chen Y, Zhu J, Chen Y, Lv D, Zhu Z, et al. Construction of a reduced $PODE_3$/nature gas dual-fuel mechanism under enginelike conditions. Energy Fuels 2019;33(4):3504–17.

[103] Lin Q, Tay KL, Zhou D, Yang W. Development of a compact and robust polyoxymethylene dimethyl ether 3 reaction mechanism for internal combustion engines. Energy Convers Manage 2019;185:35–43.

[104] Jing Z, Zhang C, Cai P, Li Y, Wang J. Construction of a reduced diesel/polyoxymethylene dimethyl ether 3 ($PODE_3$) reaction mechanism for combustion and emission analysis. Energy Fuels 2021;35(5):4437–46.

[105] Niu B, Jia M, Chang Y, Duan H, Dong X, Wang P. Construction of reduced oxidation mechanisms of polyoxymethylene dimethyl ethers (PODE1–6) with consistent structure using decoupling methodology and reaction rate rule. Combust Flame 2021;232.

[106] Bai J, Geeson R, Mosbach FFS, Akroyd J, Bringley E, Kraft M. Automated calibration of a poly(oxymethylene) dimethyl ether oxidation mechanism using the knowledge graph technology. J Chem Inf Model 2021;61:1701–17.

[107] Pepiot P, Pitsch H. A chemical lumping method for the reduction of large chemical kinetic mechanisms. Combust Theory Model 2008;12:1089–108.

[108] Russi T, Packard A, Feeley R, Frenklach M. Sensitivity analysis of uncertainty in model prediction. J Phys Chem A 2008;112:2579–88.

[109] Herzler J, Fikri M, Schulz C. High-pressure shock-tube study of the ignition and product formation of fuel-rich dimethoxymethane (DMM)/air and CH_4/DMM/air mixtures. Combust Flame 2020;216:293–9.

[110] Eckart S, Cai L, Fritsche C, vom Lehn F, Pitsch H, Krause H. Laminar burning velocities, CO, and NO_x emissions of premixed polyoxymethylene dimethyl ether flames. Fuel 2021;293.

[111] Sun W, Yang B, Hansen N, Moshammer K. The influence of dimethoxy methane (DMM)/dimethyl carbonate (DMC) addition on a premixed ethane/oxygen/argon flame. Proc Combust Inst 2017;36:449–57.

[112] Sinha A, Thomson M. The chemical structures of opposed flow diffusion flames of C3 oxygenated hydrocarbons (isopropanol, dimethoxy methane, and dimethyl carbonate) and their mixtures. Combust Flame 2004;136(4):548–56.

[113] Sun W, Tao T, Lailliau M, Hansen N, Yang B, Dagaut P. Exploration of the oxidation chemistry of dimethoxymethane: Jet-stirred reactor experiments and kinetic modeling. Combust Flame 2018;193:491–501.

[114] Gao Z, Hu E, Xu Z, Yin G, Huang Z. Low to intermediate temperature oxidation studies of dimethoxymethane/n-heptane blends in a jet-stirred reactor. Combust Flame 2019;207:20–35.

[115] Li Z, Liu P, Chu C, Chung S, Roberts W. Incipient sooting tendency of oxygenated fuels doped in ethylene counterflow diffusion flames. Combust Flame 2022;244.

[116] Nativel D, Herzler J, Krzywdziak S, Peukert S, Fikri M, Schulz C. Shock-tube study of the influence of oxygenated additives on benzene pyrolysis: Measurement of optical densities, soot inception times and comparison with simulations. Combust Flame 2022;243.

[117] Ngũgĩ JM, Richter S, Braun-Unkhoff M, Naumann C, Riedel U. A study on fundamental combustion properties of oxymethylene ether-1, the primary reference fuel 90, and their blend: Experiments and modeling. Combust Flame 2022;243:111996.

[118] vom Lehn F, Cai L, Cáceres B, Pitsch H. Exploring the fuel structure dependence of laminar burning velocity: A machine learning based group contribution approach. Combust Flame 2021;232.

[119] Qiu Z, Zhong A, Huang Z, Han D. An experimental and modeling study on polyoxymethylene dimethyl ether 3 (PODE3) oxidation in a jet stirred reactor. Fund Res 2022;2(5):738–47.

[120] Gaiser N, Bierkandt T, Oßwald P, Zinsmeister J, Kathrotia T, Shaqiri S, et al. Oxidation of oxymethylene ether (OME0–5): An experimental systematic study by mass spectrometry and photoelectron photoion coincidence spectroscopy. Fuel 2022;313.

[121] Gaiser N, Zhang H, Bierkandt T, Schmitt S, Zinsmeister J, Kathrotia T, et al. Investigation of the combustion chemistry in laminar, low-pressure oxymethylene ether flames (OME0–4). Combust Flame 2022;243.

[122] De Ras K, Panaget T, Fenard Y, Aerssens J, Pillier L, Thybaut JW, et al. An experimental and kinetic modeling study on the low-temperature oxidation of oxymethylene ether-2 (OME-2) by means of stabilized cool flames. Combust Flame 2023;253:112792.

[123] Cai L, Ramalingam A, Minwegen H, Heufer K, Pitsch H. Impact of exhaust gas recirculation on ignition delay times of gasoline fuel: An experimental and modeling study. Proc Combust Inst 2019;37:639–47.

[124] Hu E, Gao Z, Liu Y, Yin G, Huang Z. Experimental and modeling study on ignition delay times of dimethoxy methane/n-heptane blends. Fuel 2017;189:350–7.

[125] Zhang H, Kaczmarek D, Rudolph C, Schmitt S, Gaiser N, Oßwald P, et al. Dimethyl ether (DME) and dimethoxymethane (DMM) as reaction enhancers for methane: Combining flame experiments with model-assisted exploration of a polygeneration process. Combust Flame 2022;237.

[126] Richter S, Kathrotia T, Braun-Unkhoff M, Naumann C, Köhler M. Influence of oxymethylene ethers (OME_n) in mixtures with a diesel surrogate. Energies 2021;14:7848.

[127] Schemme S. Techno-ökonomische bewertung von verfahren zur herstellung von kraftstoffen aus H_2 und CO_2 [Ph.D. thesis], RWTH Aachen University; 2020.

[128] Kraftstoffe – Dieselkraftstoff – Anforderungen und Prüfverfahren; Deutsche Fassung. 2017, DIN EN 590.

[129] Daubert T, Danner R. Physical and thermodynamic properties of pure chemicals: Data compilation. Hemisphere Publishing Corporation; 2000.

[130] Lide DR, editor. CRC handbook of chemistry and physics. Cambridge Umiversity Press; 2004.

[131] Lapuerta M, Sánchez-Valdepeñas J, Sukjit E. Effect of ambient humidity and hygroscopy on the lubricity of diesel fuels. Wear 2014;309(1–2):200–7.

[132] Lapuerta M, Villajos M, Agudelo JR, Boehman AL. Key properties and blending strategies of hydrotreated vegetable oil as biofuel for diesel engines. Fuel Process Technol 2011;92(12):2406–11.

[133] Chau VT, Chinda C, Preechar K, Sato S, Kosaka H. Optical study on combustion characteristics of hydrotreated vegetable oil and blends under simulated CI engine conditions and various EGR. J Mech Sci Technol 2017;31(9):4521–31.

[134] Lacey P, Naegeli D, De La Cruz J, Whalen M, Manson R. Lubricity of volatile fuels for compression ignition engines. SAE Trans 2000;980–8.

[135] Lumpp B, Rothe D, Pastötter C, Lämmermann R, Jacob E. Oxymethylene ethers as diesel fuel additives of the future. MTZ Worldwide 2011;72(3):34–8.

[136] Deutsch D, Oestreich D, Lautenschütz L, Haltenort P, Arnold U, Sauer J. High purity oligomeric oxymethylene ethers as diesel fuels. Chem Ing Tech 2017;89(4):486–9.

[137] Aatola H, Larmi M, Sarjovaara T, Mikkonen S. Hydrotreated vegetable oil (hvo) as a renewable diesel fuel: Trade-off between no, particulate emission, and fuel consumption of a heavy duty engine. SAE Int J Engines 2009;1(1):1251–62.

[138] Cheng Q, Tuomo H, Kaario O, Martti L. HVO, RME, and diesel fuel combustion in an optically accessible compression ignition engine. Energy Fuels 2019;33(3):2489–501.

[139] Boyd RH. Some physical properties of polyoxymethylene dimethyl ethers. J Polym Sci 1961;50(153):133–41.

[140] Agarwal AK. Biofuels (alcohols and biodiesel) applications as fuels for internal combustion engines. Progress Energy Combust Sci 2007;33(3):233–71.

[141] Yanowitz J, Ratcliff MA, McCormick RL, Taylor JD, Murphy MJ. Compendium of experimental cetane numbers. Tech. rep., Golden, CO (United States): National Renewable Energy Lab.(NREL); 2017.

[142] Fleisch T, McCarthy C, Basu A, Udovich C, Charbonneau P, Slodowske W, et al. A new clean diesel technology: Demonstration of ULEV emissions on a Navistar diesel engine fueled with dimethyl ether. SAE Trans 1995;42–53.

[143] Teng H, McCandless JC, Schneyer JB. Compression ignition delay (physical+ chemical) of dimethyl ether–an alternative fuel for compression-ignition engines. SAE Trans 2003;377–89.

[144] Pellegrini L, Marchionna M, Patrini R, Beatrice C, Del Giacomo N, Guido C. Combustion behaviour and emission performance of neat and blended polyoxymethylene dimethyl ethers in a light-duty diesel engine. Tech. rep., SAE technical paper, 2012.

[145] Kook S, Pickett LM. Liquid length and vapor penetration of conventional, Fischer–Tropsch, coal-derived, and surrogate fuel sprays at high-temperature and high-pressure ambient conditions. Fuel 2012;93:539–48.

[146] Kim D, Martz J, Violi A. Effects of fuel physical properties on direct injection spray and ignition behavior. Fuel 2016;180:481–96.

[147] Vertin KD, Ohi JM, Naegeli DW, Childress KH, Hagen GP, McCarthy CI, et al. Methylal and methylal-diesel blended fuels for use in compression-ignition engines. Tech. rep. SAE technical paper, 1999.

[148] McCandless JC, Li S. Development of a novel fuel injection system (NFIS) for dimethyl ether-and other clean alternative fuels. Tech. rep. SAE technical paper, 1997.

[149] Wang X, Huang Z, Kuti OA, Zhang W, Nishida K. Experimental and analytical study on biodiesel and diesel spray characteristics under ultra-high injection pressure. Int J Heat Fluid Flow 2010;31(4):659–66.

[150] Barbour R, Rickeard D, Elliott N. Understanding diesel lubricity. SAE Trans 2000;1556–66.

[151] Härtl M, Gaukel K, Pélerin D, Wachtmeister G. Oxymethylene ether as potentially CO_2-neutral fuel for clean diesel engines part 1: Engine testing. MTZ Worldwide 2017;78(2):52–9.

[152] Pélerin D, Gaukel K, Härtl M, Jacob E, Wachtmeister G. Potentials to simplify the engine system using the alternative diesel fuels oxymethylene ether OME1 and OME3–6 on a heavy-duty engine. Fuel 2020;259.

[153] Wang D, Zhu G, Li Z, Xia C. Polyoxymethylene dimethyl ethers as clean diesel additives: Fuel freezing and prediction. Fuel 2019;237:833–9.

[154] Xing-Cai L, Jian-Guang Y, Wu-Gao Z, Zhen H. Effect of cetane number improver on heat release rate and emissions of high speed diesel engine fueled with ethanol–diesel blend fuel. Fuel 2004;83(14–15):2013–20.

[155] Goeb D, Davidovic M, Cai L, Pancharia P, Bode M, Jacobs S, et al. Oxymethylene ether – n-dodecane blend spray combustion: Experimental study and large-eddy simulations. Proc Combust Inst 2021;38(2):3417–25.
[156] Wallington TJ, Hurley MD, Ball JC, Straccia AM, Platz J, Christensen LK, et al. Atmospheric chemistry of dimethoxymethane (CH3OCH2OCH3): Kinetics and mechanism of its reaction with oh radicals and fate of the alkoxy radicals CH3OCHO (·) OCH3 and CH3OCH2OCH2O (·). J Phys Chem A 1997;101(29):5302–8.
[157] Rösel G, Avolio G, Grimm J, Kastner O, Swigon T, Weisse M. System approach for future diesel blends with sustainable fuels. In: Internationaler motorenkongress 2019. Springer; 2019, p. 299–311.
[158] Kane RD, Maldonado JG, Klein LJ. Stress corrosion cracking in fuel ethanol: a newly recognized phenomenon. In: CORROSiON 2004. OnePetro; 2004, NACE–04543.
[159] Uchida T, Kurita Y, Kubo M. The dipole moments and the structure of polyoxymethylene dimethyl ethers. J Polym Sci 1956;19(92):365–72.
[160] Yang Z, Ren C, Jiang S, Xin Y, Hu Y, Liu Z. Theoretical predictions of compatibility of polyoxymethylene dimethyl ethers with diesel fuels and diesel additives. Fuel 2022;307.
[161] Yu M, Chen C, Jiang X. Understanding the miscibility of polyoxymethylene dimethyl ethers (omen) and diesel blend using molecular dynamics simulation. Fuel 2022;323.
[162] Breitkreuz CF, Holzer A, Fuchs T, Günthner M, Hasse H. Miscibility in systems containing (poly (oxymethylene) ethers (OME)+ hydrocarbons+ water). Fuel 2023;338.
[163] Bode M, Kaya Y, Reddeman A, Goeb D, Kirsch V, Kneer R, et al. Experimental and numerical spray investigations of synthetic fuels for sustainable CI engines. In: THIESEL 2018. Valencia; 2018.
[164] Saha A, Grenga T, Deshmukh AY, Hinrichs J, Bode M, Pitsch H. Numerical modeling of single droplet flash boiling behavior of e-fuels considering internal and external vaporization. Fuel 2022;308.
[165] Li D, Gao Y, Liu S, Ma Z, Wei Y. Effect of polyoxymethylene dimethyl ethers addition on spray and atomization characteristics using a common rail diesel injection system. Fuel 2016;186:235–47.
[166] Ottenwaelder T, Pischinger S. Effects of biofuels on the mixture formation and ignition process in diesel-like jets. Tech. rep., SAE technical paper, 2017.
[167] Goeb D, Bode M, Davidovic M, Cai L, Ottenwälder T, Jacobs S, et al. High-fidelity simulations and experiments of oxymethylene ether spray ignition. In: Proceedings of the European Combustion Meeting, vol. 2019, 2019.
[168] Ottenwälder TS. Optische Untersuchung der dieselmotorischen Verbrennung mit Biokraftstoffen [Ph.D. thesis, Dissertation], Rheinisch-Westfälische Technische Hochschule Aachen; 2019, (2019).
[169] Pastor JV, García-Oliver JM, Micó C, García-Carrero AA, Gómez A. Experimental study of the effect of hydrotreated vegetable oil and oxymethylene ethers on main spray and combustion characteristics under engine combustion network spray a conditions. Appl Sci 2020;10(16):5460.
[170] Liu J, Feng L, Wang H, Zheng Z, Chen B, Zhang D, et al. Spray characteristics of gasoline/PODE and diesel/PODE blends in a constant volume chamber. Appl Therm Eng 2019;159.
[171] Pastor JV, García-Oliver JM, Micó C, García-Carrero AA. An experimental study with renewable fuels using ecn spray a and d nozzles. Int J Engine Res 2022;23(10):1748–59.
[172] Saupe C, Atzler F. Potentials of oxymethylene-dimethyl-ether in diesel engine combustion. Automot Engine Technol 2022;7(3–4):331–42.
[173] Liu J, Wang L, Wang P, Sun P, Liu H, Meng Z, et al. An overview of polyoxymethylene dimethyl ethers as alternative fuel for compression ignition engines. Fuel 2022;318.
[174] Pellegrini L, Marchionna M, Patrini R, Florio S. Emission performance of neat and blended polyoxymethylene dimethyl ethers in an old light-duty diesel car. SAE technical paper, 2013.
[175] Pellegrini L, Patrini R, Marchionna M. Effect of POMDME blend on PAH emissions and particulate size distribution from an in-use light-duty diesel engine. Tech. rep. SAE technical paper, 2014.
[176] Münz M, Feiling A, Beidl C, Härtl M, Pélerin D, Wachtmeister G. Oxymethylene ether (OME1) as a synthetic low-emission fuel for DI diesel engines. In: Internationaler motorenkongress 2016. Springer; 2016, p. 537–53.
[177] Pélerin D, Gaukel K, Härtl M, Wachtmeister G. Recent results of the sootless diesel fuel oxymethylene ether. In: Internationaler motorenkongress 2017. Springer; 2017, p. 439–56.
[178] Härtl M, Pélerin D, Dworschak P, Maier T, Stadler A, Blochum S, et al. Potential of the sustainable C1 fuels OME, DMC, and MeFo for particle-free combustion in SI and CI engines. In: Internationaler motorenkongress 2018. Springer; 2018, p. 459–78.
[179] Pastor JV, García-Oliver JM, Micó C, Tejada FJ. Characterization of the oxymethylene ether fuels flame structure for ECN spray A and spray D nozzles. Appl Energy 2023;332.
[180] Parravicini M, Barro C, Boulouchos K. Compensation for the differences in LHV of diesel-OME blends by using injector nozzles with different number of holes: Emissions and combustion. Fuel 2020;259.
[181] Zhu R, Wang X, Miao H, Huang Z, Gao J, Jiang D. Performance and emission characteristics of diesel engines fueled with diesel- dimethoxymethane (DMM) blends. Energy Fuels 2009;23(1):286–93.
[182] Ogawa H, Nabi MN, Minami M, Miyamoto N, Bong-Seock K. Ultra low emissions and high performance diesel combustion with a combination of high EGR, three-way catalyst, and a highly oxygenated fuel, dimethoxy methane (DMM). SAE Trans 2000;1019–27.
[183] Pastor JV, García A, Micó C, Lewiski F. An optical investigation of Fischer–Tropsch diesel and oxymethylene dimethyl ether impact on combustion process for CI engines. Appl Energy 2020;260.
[184] Chen H, Su X, Wang X, Sun F, Zhang P, Geng L, et al. Filtration efficiency and regeneration behavior in a catalytic diesel particulate filter with the use of diesel/polyoxymethylene dimethyl ether mixture. Catalysts 2021;11(12):1425.
[185] Upatnieks A, Mueller CJ. Clean, controlled DI diesel combustion using dilute, cool charge gas and a short-ignition-delay, oxygenated fuel. Tech. rep. SAE technical paper, 2005.
[186] Gaukel K, Dworschak P, Pélerin D, Härtl M, Wachtmeister G. Combustion process optimization for oxymethylene ether fuels in a heavy-duty application. In: Internationaler motorenkongress 2019. Springer; 2019, p. 351–67.
[187] Dworschak P, Berger V, Härtl M, Wachtmeister G. Neat oxymethylene ethers: Combustion performance and emissions of OME 2, OME 3, OME 4 and OME 5 in a single-cylinder diesel engine. Tech. rep. SAE technical paper, 2020.
[188] Huang Z, Ren Y, Jiang D, Liu L, Zeng K, Liu B, et al. Combustion and emission characteristics of a compression ignition engine fuelled with diesel–dimethoxy methane blends. Energy Convers Manag 2006;47(11–12):1402–15.
[189] Barro C, Parravicini M, Boulouchos K. Neat polyoxymethylene dimethyl ether in a diesel engine; part 1: Detailed combustion analysis. Fuel 2019;256.
[190] Dworschak P, Berger V, Härtl M, Wachtmeister G. Oxymethylene ethers: Evaluating the optimum fuel composition from an engine standpoint with respect to emissions and combustion performance. SAE Int J Fuels Lubr 2022;15(04-15-02-0008).
[191] Rösel G, Avolio G, Grimm J, Maiwald O, Kastner O, Brück R. Diesel–e-fuel blends for simultaneous reduction of real driving NOx and CO2 emissions. In: Internationaler motorenkongress 2018. Springer; 2018, p. 501–22.
[192] García-Oliver JM, Novella R, Micó C, De Leon-Ceriani D. Numerical analysis of the combustion process of oxymethylene ethers as low-carbon fuels for compression ignition engines. Int J Engine Res 2022.
[193] Ma Y, Cui L, Ma X, Wang J. Optical study on spray combustion characteristics of PODE/diesel blends in different ambient conditions. Fuel 2020;272.
[194] Cheng A, Dibble RW, Buchholz BA. The effect of oxygenates on diesel engine particulate matter. Tech. rep. SAE technical paper, 2002.
[195] Münz M, Mokros A, Beidl C. OME in the diesel engine–A concept for CO2 neutrality and lowest pollutant emissions. In: Internationaler motorenkongress 2018. Springer; 2018, p. 445–58.
[196] Iannuzzi SE, Barro C, Boulouchos K, Burger J. POMDME-diesel blends: Evaluation of performance and exhaust emissions in a single cylinder heavy-duty diesel engine. Fuel 2017;203:57–67.
[197] Münz M, Mokros A, Beidl C. Analysis of two engine configurations using OME as a potential CO2-neutral and low emission diesel substitute. In: Internationaler motorenkongress 2019. Springer; 2019, p. 369–84.
[198] Popp T, Lechner R, Becker M, Hebauer M, O'Connell N, Brautsch M. Potentials of OME/diesel blends for stationary power production–improving emission characteristics of a diesel CHP unit. Appl Therm Eng 2019;153:483–92.
[199] Chen H, Wang H, Chen Z, Zhao H, Geng L, Gao N, et al. Research progress on the spray, combustion and emission of polyoxymethylene dimethyl ethers as a diesel blend fuel: A review. Fuel 2022;324.
[200] Gelner AD, Beck HA, Pastoetter C, Härtl M, Wachtmeister G. Ultra-low emissions of a heavy-duty engine powered with oxymethylene ethers (OME) under stationary and transient driving conditions. Int J Engine Res 2022;23(5):738–53.
[201] Tan P-Q, Ruan S-S, Hu Z-Y, Lou D-M, Li H. Particle number emissions from a light-duty diesel engine with biodiesel fuels under transient-state operating conditions. Appl Energy 2014;113:22–31.
[202] Barro C, Parravicini M, Boulouchos K, Liati A. Neat polyoxymethylene dimethyl ether in a diesel engine; part 2: Exhaust emission analysis. Fuel 2018;234:1414–21.
[203] Gelner AD, Rothe D, Kykal C, Irwin M, Sommer A, Pastoetter C, et al. Particle emissions of a heavy-duty engine fueled with polyoxymethylene dimethyl ethers (OME). Environ Sci: Atmos 2022;2(2):291–304.
[204] Tian J, Cai Y, Pu X, Gu L, Shi Y, Cui Y, et al. Effect of polyoxymethylene dimethyl ethers on particle properties and diesel particulate filter regeneration. Chem Pap 2019;73(2):455–68.
[205] Yang H, Li X, Wang Y, Mu M, Li X, Kou G. Experimental investigation into the oxidation reactivity and nanostructure of particulate matter from diesel engine fuelled with diesel/polyoxymethylene dimethyl ethers blends. Sci Rep 2016;6(1):1–10.
[206] Yang H, Li X, Wang Y, Mu M, Li X, Kou G, et al. Pyrolysis characteristic analysis of particulate matter from diesel engine run on diesel/polyoxymethylene dimethyl ethers blends based on nanostructure and thermogravimetry. Aerosol Air Qual Res 2016;16(10):2560–9.

[207] Feiling A, Münz M, Beidl C. Potential of the synthetic fuel OME 1b for the soot-free diesel engine. ATZextra Worldwide 2016;21(11):16–21.
[208] Ferraro F, Russo C, Schmitz R, Hasse C, Sirignano M. Experimental and numerical study on the effect of oxymethylene ether-3 (OME3) on soot particle formation. Fuel 2021;286.
[209] Schmitz R, Russo C, Ferraro F, Apicella B, Hasse C, Sirignano M. Effect of oxymethylene ether-2-3-4 (OME2-4) on soot particle formation and chemical features. Fuel 2022;324.
[210] Zheng M, Reader GT, Hawley JG. Diesel engine exhaust gas recirculation – A review on advanced and novel concepts. Energy Convers Manag 2004;45(6):883–900.
[211] Hong KS, Lee KS, Song S, Chun KM, Chung D, Min S. Parametric study on particle size and SOF effects on EGR cooler fouling. Atmos Environ 2011;45(32):5677–83.
[212] Miyamoto N, Ogawa H, Arima T, Miyakawa K. Improvement of diesel combustion and emissions with addition of various oxygenated agents to diesel fuels. Tech. rep. SAE technical paper, 1996.
[213] Choi C-Y, Reitz RD. An experimental study on the effects of oxygenated fuel blends and multiple injection strategies on DI diesel engine emissions. Fuel 1999;78(11):1303–17.
[214] Mueller CJ, Martin GC. Effects of oxygenated compounds on combustion and soot evolution in a DI diesel engine: Broadband natural luminosity imaging. SAE Trans 2002;518–37.
[215] Mueller CJ, Pitz WJ, Pickett LM, Martin GC, Siebers DL, Westbrook CK. Effects of oxygenates on soot processes in DI diesel engines: Experiments and numerical simulations. SAE Trans 2003;964–82.
[216] Curran HJ, Fisher EM, Glaude P-A, Marinov NM, Pitz W, Westbrook C, et al. Detailed chemical kinetic modeling of diesel combustion with oxygenated fuels. Sae Trans 2001;514–21.
[217] M.A. González D, Piel W, Asmus T, Clark W, Garbak J, Liney E, et al. Oxygenates screening for advanced petroleum-based diesel fuels: Part 2, the effect of oxygenate blending compounds on exhaust emissions. SAE Trans 2001;2246–55.
[218] García-Oliver JM, Novella R, Micó C, Bin-Khalid U. A numerical investigation of the performance of oxymethylene ethers blended with fossil diesel to reduce soot emissions in compression ignition engines. Fuel 2022;324.
[219] Janssen A, Kremer F, Pischinger S, Reddemann M, Kneer R, Hottenbach P, et al. Potential of tailor-made fuels for diesel combustion engines. In: 3rd TMFB international workshop. 2010.
[220] Frenklach M. Kinetics and mechanism of soot formation in hydrocarbon flames. Tech. rep. NASA final technical report, 1990.
[221] Mira D, Pérez-Sánchez EJ, Surapaneni A, Benajes J, García-Oliver JM, Pastor JM, et al. LES study on spray combustion with renewable fuels under ECN spray-A conditions. In: Internal combustion engine division fall technical conference, vol. 85512, American Society of Mechanical Engineers; 2021, V001T06A004.
[222] Arias S, Agudelo JR, Ramos A, Lapuerta M. Emissions from a Euro 6 engine using polyoxymethylene dimethyl ethers: Chemical effects vs mapping strategy. Fuel 2023;335.
[223] Kastner O, Avolio G, Rösel G. Ome–diesel blends für niedrigere well-to-wheel co 2 emissionen in pkw motoren. In: Zukünftige Kraftstoffe. Springer; 2019, p. 929–41.
[224] Wei Y, Zhang Y, Zhu Z, Zhu X, Gu H, Liu S. Effect of PODE on emission characteristics of a china VI heavy-duty diesel engine. Appl Sci 2022;12(3):1108.
[225] Liu H, Wang Z, Wang J, He X, Zheng Y, Tang Q, et al. Performance, combustion and emission characteristics of a diesel engine fueled with polyoxymethylene dimethyl ethers (PODE3-4)/diesel blends. Energy 2015;88:793–800.
[226] Ferraro F, Schmitz R, Sirignano M, Hasse C. Particle formation in oxymethylene ethers (OME_n, n=2-4)/ethylene premixed flames. 2022, arXiv preprint arXiv:2204.10733.
[227] Voelker S, Deutz S, Burre J, Bongartz D, Omari A, Lehrheuer B, et al. Blend for all or pure for few? Well-to-wheel life cycle assessment of blending electricity-based OME 3–5 with fossil diesel. Sustain Energy Fuels 2022;6(8):1959–73.
[228] Burre J, Bongartz D, Mitsos A. Production of oxymethylene dimethyl ethers from hydrogen and carbon dioxide – Part ii: Modeling and analysis for OME3–5. Ind Eng Chem Res 2019;58(14):5567–78.
[229] Grützner T, Hasse H, Lang N, Siegert M, Ströfer E. Development of a new industrial process for trioxane production. Chem Eng Sci 2007;62(18–20):5613–20.
[230] Grützner T. Entwicklung eines destillationsbasierten verfahrens zur herstellung von trioxan [Ph.D. thesis], University of Stuttgart; 2007.
[231] Echemi. Dimethoxymethane price and market analysis. 2022, URL https://www.echemi.com/productsInformation/temppid160628000900-dimethoxymethane.html.
[232] Tönges Y, Dieterich V, Fendt S, Spliethoff H, Burger J. Techno-economic analysis of large scale production of poly (oxymethylene) dimethyl ether fuels from methanol in water-tolerant processes. Fuels 2023;4(1):1–18.
[233] Mahbub N, Oyedun AO, Zhang H, Kumar A, Poganietz W-R. A life cycle sustainability assessment (LCSA) of oxymethylene ether as a diesel additive produced from forest biomass. Int J Life Cycle Assess 2019;24(5):881–99.
[234] European Council. Oil bulletin prices history. 2022, URL http://ec.europa.eu/energy/observatory/reports/Oil_Bulletin_Prices_History.xlsx.
[235] Hank C, Gelpke S, Schnabl A, White RJ, Full J, Wiebe N, et al. Economics & carbon dioxide avoidance cost of methanol production based on renewable hydrogen and recycled carbon dioxide–power-to-methanol. Sustain Energy Fuels 2018;2(6):1244–61.
[236] Terrapon-Pfaff J, Prantner M, Zelt O, Missaoui R, Ghezal A, Toumi M. Study on the opportunities of power-to-x in Tunisia. Tech. rep., Deutsche Gesellschaft fürInternationale Zusammenarbeit (GIZ) GmbH; 2021.
[237] Gargett D. Impact of COVID-19 on petrol prices in Australia. Tech. rep., Bureau of Infrastructure and Transport Research Economics; 2020.
[238] Hank C, Lazar L, Mantei F, Ouda M, White R, Smolinka T, et al. Comparative well-to-wheel life cycle assessment of OME 3-5 synfuel production via the power-to-liquid pathway. Sustain Energy Fuels 2019;3(11):3219–33.
[239] Deutz S, Bongartz D, Heuser B, Kätelhön A, Langenhorst LS, Omari A, et al. Cleaner production of cleaner fuels: Wind-to-wheel - environmental assessment of CO2-based oxymethylene ether as a drop-in fuel. Energy Environ Sci 2018;11(2):331–43.
[240] Hank C, Sternberg A, Köppel N, Holst M, Smolinka T, Schaadt A, et al. Energy efficiency and economic assessment of imported energy carriers based on renewable electricity. Sustain Energy Fuels 2020;4(5):2256–73.
[241] Kramer U, Ortloff F, Stollenwerk S. Defossilisierung des Transportsektors: Optionen und Voraussetzungen in Deutschland. FVV; 2018.
[242] Kramer U, Bothe D, Gatzen C, Reger M, Lothmann M, Dünnebeil F, Biemann K, Liebich A, Dittrich M, Limberger S, Rosental M, Frölich T. Future fuels: FVV fuels study IV - The transformation of mobility to the GHG-neutral post-fossil age. FVV; 2021.
[243] Kramer U, Bothe D, Gatzen C, Pfannenschmidt A, Baum C, Schrogl F, Mahmood O. Future fuels: FVV fuel study iVb - transformation of mobility to the GHG-neutral post-fossil age. FVV; 2022.
[244] Prognos, Öko-Institut and Wuppertal Institut. Towards a climate-neutral Germany by 2045. How Germany can reach its climate targets before 2050, stiftung klimaneutralität, agora energiewende and agora verkehrswende. 2021.
[245] Lux B, Gegenheimer J, Franke K, Sensfuß F, Pfluger B. Supply curves of electricity-based gaseous fuels in the MENA region. Comput Ind Eng 2021;162:107647.
[246] Grüninger M, Toedter O, Koch T. Gesetzliche Rahmenbedingungen für moderne Antriebe mit Verbrennungsmotor. MTZ - Motortechnische Zeitschrift 2023;84(5):30–7. http://dx.doi.org/10.1007/s35146-023-1468-z.
[247] Bothe D, Zähringer M, Bauer J, Sieberg C, Korbmacher F. Crediting system for renewable fuels in EU emission standards for road transport: report for the German Federal Ministry for Economic Affairs and Energy (BMWi). Frontier Economics Ltd; 2020.
[248] Rockström J, Henriksson H, Edenhofer O, Daum M, Lundstedt M, Marx G, Trostmann A, Wolters H, Yenigün H. The transition to zero-emission road freight transport. 2020, URL https://www.acea.auto/files/acea-pik-joint-statement-the-transition-to-zero-emission-road-freight-trans.pdf.
[249] Perner J, Unteutsch M, Loevenich A. The future cost of electricity-based synthetic fuels. Agora Verkehrswende, Agora Energiewende Front Econ 2018.

Prof. Heinz Pitsch is a Professor at RWTH Aachen University and has been the Director of the Institute for Combustion Technology at RWTH Aachen University since 2010. He has been Assistant and Associate Professor at Stanford University from 2003–2013 after receiving his Ph.D. from RWTH Aachen University in 1998 and holding post-doctoral positions at the University of California, San Diego and Stanford University. His main research interests are in the fields of combustion theory, combustion chemistry, turbulence, and multi-phase flows with application to technical combustion systems. Prof. Pitsch has published over 200 papers in archival journals, he is presently the chair of the German Section of the Combustion Institute and co-Editor-in-Chief of the journal Applications in Energy and Combustion Science. He is a Fellow of the American Physical Society and of the Combustion Institute, and has received several prestigious awards, such as the Advanced Grant of the European Research Council and the International Award of the Japanese Combustion Society.